

**PHYSICO-CHEMICAL CHARACTERIZATION OF
BRANCHED-CHAIN GLYCOLIPIDS FOR
DRUG DELIVERY SYSTEM**

NORAINI BINTI AHMAD

**FACULTY OF SCIENCE
UNIVERSITY OF MALAYA
KUALA LUMPUR**

2012

**PHYSICO-CHEMICAL CHARACTERIZATION OF
BRANCHED-CHAIN GLYCOLIPIDS FOR
DRUG DELIVERY SYSTEM**

NORAINI BINTI AHMAD

**THESIS SUBMITTED IN FULFILMENT OF
THE REQUIREMENTS FOR THE DEGREE OF
DOCTOR OF PHILOSOPHY**

**DEPARTMENT OF CHEMISTRY
FACULTY OF SCIENCE
UNIVERSITY OF MALAYA
KUALA LUMPUR**

2012

UNIVERSITI MALAYA

ORIGINAL LITERARY WORK DECLARATION

Name of Candidate: NORAINI BINTI AHMAD (I.C/Passport No: 800710-01-5852)

Registration/Matric No: SHC 080039

Name of Degree: DOCTOR OF PHILOSOPHY

Title of Project Paper/Research Report/Dissertation/Thesis ("this Work"):

PHYSICO-CHEMICAL CHARACTERIZATION OF BRANCHED-CHAIN GLYCOLIPIDS FOR
DRUG DELIVERY SYSTEM

Field of Study: PHYSICAL CHEMISTRY

I do solemnly and sincerely declare that:

- (1) I am the sole author/writer of this Work;
- (2) This Work is original;
- (3) Any use of any work in which copyright exists was done by way of fair dealing and for permitted purposes and any excerpt or extract from, or reference to or reproduction of any copyright work has been disclosed expressly and sufficiently and the title of the Work and its authorship have been acknowledged in this Work;
- (4) I do not have any actual knowledge nor do I ought reasonably to know that the making of this work constitutes an infringement of any copyright work;
- (5) I hereby assign all and every rights in the copyright to this Work to the University of Malaya ("UM"), who henceforth shall be owner of the copyright in this Work and that any reproduction or use in any form or by any means whatsoever is prohibited without the written consent of UM having been first had and obtained;
- (6) I am fully aware that if in the course of making this Work I have infringed any copyright whether intentionally or otherwise, I may be subject to legal action or any other action as may be determined by UM.

Candidate's Signature

Date 8 AUGUST 2012

Subscribed and solemnly declared before,

Witness's Signature

Date 8 AUGUST 2012

Name: PROF. DR. RAUZH HASHIM

Designation: LECTURER

ABSTRACT

Natural and synthetic glycolipid biosurfactants have drawn much attention due to their nonionic and biodegradable properties. In addition, synthetic branched-chain glycolipids have become of great interest in biomimicking research, since they provide a suitable alternative for natural glycolipids, which are difficult to extract from natural resources. Two new synthetic branched-chain glycolipids are presented here, namely 2-hexyldecyl- β (/ α)-D-glucoside (2-HDG) and 2-hexyldecyl- β (/ α)-D-maltoside (2-HDM), whose structures are closely mimicking the natural glyceroglycolipids. Their amphiphilic characteristic gives rich phase behaviour in dry form and in dispersions. 2-HDG form a columnar liquid crystalline phase thermotropically, whereas in a binary aqueous system, 2-HDG form inverted hexagonal liquid crystalline dispersions (hexosomes). On the other hand, 2-HDM form a lamellar liquid crystalline phase (smectic A) and multilamellar vesicles were observed in aqueous media. Moreover, 2-HDM mixed with SDS or AOT induced the formation of more stable unilamellar vesicles. Further studies were conducted to investigate the effect of incorporating these novel branched-chain glycolipids into the reference nano-emulsions of water/Cremophor[®] EL/medium chain triglyceride system. We found the different head groups of the Guerbet glycolipids affected the stability of the nano-emulsions differently. The presence of 2-HDG enhanced nano-emulsion stability by reducing the oil droplet size, whereas the 2-HDM slightly improved the properties of the reference nano-emulsion in terms of droplet size and storage time stability. These nano-emulsions have been proven capable of encapsulating ketoprofen showing a relatively fast release of drug. Thus, both branched-chain glycolipids not only provided alternative nonionic surfactants with rich phase behaviour and versatile nano-structures, but also could be used as new drug carrier systems in the future and are also suitable as nano-emulsion stabilizing agents.

ABSTRAK

Biosurfaktan glikolipid semulajadi dan sintetik telah menarik banyak perhatian disebabkan oleh sifat mereka yang bukan-ionik dan mudah dibiodegradasikan. Di samping itu, glikolipid rantaian bercabang sintetik telah menjadi kepentingan besar dalam penyelidikan biomimik, kerana mereka menyediakan alternatif yang sesuai untuk glikolipid semulajadi, yang sukar diekstrak daripada sumber asli. Dua glikolipid rantaian bercabang sintetik baru diperkenalkan di sini, iaitu 2-heksildesil- β (/α)-D-glukosida (2-HDG) dan 2-heksildesil- β (/α)-D-maltosida (2-HDM), yang mana struktur mereka hampir menyerupai glisero-glikolipid semulajadi. Ciri amfifilik mereka memberikan kepelbagaian fasa tingkah laku dalam keadaan kering dan serakan (larutan). 2-HDG membentuk fasa hablur cecair kolumnar secara termotropik, manakala dalam sistem akueus binari, 2-HDG membentuk serakan hablur cecair heksagon terbalik (heksosom). Sebaliknya, 2-HDM membentuk fasa hablur cecair lamelar (smektik A) dan vesikel berbilang-lamelar telah diperhatikan di dalam media akueus. Selain itu, 2-HDM bercampur dengan SDS atau AOT mendorong pembentukan vesikel satu-lamelar yang lebih stabil. Kajian selanjutnya telah dijalankan untuk mengkaji kesan menggabungkan glikolipid rantaian bercabang baru ini dengan sistem nano-emulsi rujukan iaitu air/Cremophor[®] EL/trigliserida rantaian sederhana. Kami mendapati kumpulan kepala glikolipid Guerbet yang berbeza memberi kesan kepada kestabilan nano-emulsi yang berbeza. Kehadiran 2-HDG meningkatkan kestabilan nano-emulsi dengan mengurangkan saiz titisan minyak, manakala 2-HDM menambah-baik sedikit sifat-sifat nano-emulsi rujukan dari segi saiz titisan dan kestabilan masa simpanan.

Nano-emulsi ini telah terbukti mampu memerangkap (mengkapsulkan) ketoprofen yang menunjukkan kadar pelepasan obat yang agak cepat. Oleh itu, kedua-dua glikolipid rantaian bercabang ini bukan sahaja menyediakan alternatif kepada surfaktan bukan-ionik dengan kepelbagaian fasa tingkah laku dan struktur-nano serba-boleh, malahan boleh juga digunakan sebagai sistem penghantar obat yang baru di masa depan dan juga sesuai sebagai ajen penstabil nano-emulsi.

ACKNOWLEDGEMENTS

I wish to express my appreciation of the many people and affiliations that have made this thesis possible.

My sincere gratitude goes to my immediate supervisors, Prof. Dr. Rauzah Hashim and Dr. Hairul Anuar Tajuddin, for their invaluable guidance, enlightening discussions, supervision and patience throughout the course of this research. I am also grateful to Prof. Dr. Conxita Solans Marsà and Dr. Jordi Esquena Moret for their kind guidance and brilliant discussions during my attachment at the Instituto de Química Avanzada de Cataluña (IQAC), Consejo Superior de Investigaciones Científicas (CSIC), Barcelona, Spain.

I was given invaluable guidance on research methodologies and operation of instruments during my attachment at IQAC-CSIC. For this, I thank Dr. Roland Ramsch, Dr. Meritxell Llinàs and Ms. María Martínez. My gratitude also extends to all members of the Fundamental Science of Self-Assembly group especially Dr. Karem J. Sabah and Ms. Noor Idayu Mat Zahid, for their encouragement and assistance throughout the research.

The Ministry of Higher Education Malaysia (MOHE) has provided generous financial support under the SLAI Fellowship for my PhD studies at the University of Malaya and Overseas Research Programme (my attachment at IQAC-CSIC). I gratefully acknowledge this. Similarly, I am grateful for the financial support by the Integrating Nanomaterials in Formulations (InForm) Grant – European Union FP7 (Researcher Exchange Programme), High Impact Research Grant – Fundamental Science of Self-Assembly (UM.C/625/1/HIR/MOHE/05) and Postgraduate Research Fund (PS242/2009A).

My heartfelt appreciation goes out to all lecturers and staff in the Department of Chemistry, the Faculty of Science as well as the University of Malaya management for their diligent dedication and support.

Last but not least, my deepest gratitude goes to my family and my in-laws especially my mother Hjh. Siti Zaliha Hassan, my father Hj. Ahmad Abdul Rahim and my mother in-law Hjh. Hamidah Dasuki for encouraging and inspiring me all these years. My beloved husband Mohd Syahkirin Mahpot has always been there for me throughout this research project. He has been caring, supportive and encouraging. To him, I express my deepest love and appreciation. To our children, Amirul Afif, Amirul Amin and Amirah Hanis, thank you for being my inspiration throughout this time.

TABLE OF CONTENTS

ABSTRACT	ii
ABSTRAK	iii
ACKNOWLEDGEMENTS	v
TABLE OF CONTENTS	vii
LIST OF FIGURES	xiii
LIST OF SCHEMES	xvii
LIST OF TABLES	xviii
LIST OF ABBREVIATIONS	xx

CHAPTER 1: INTRODUCTION AND LITERATURE REVIEW

1.1 INTRODUCTION	1
1.2 REVIEW ON SURFACTANT	3
1.2.1 Aggregation Behaviour of Surfactants	8
1.2.2 Packing Parameter	11
1.2.3 Hydrophilic-Lipophilic Balance (HLB)	14
1.2.4 Application of Surfactants	16
1.3 REVIEW ON LIQUID CRYSTALS	17
1.3.1 Application of Liquid Crystals	23
1.3.2 Glycolipids Liquid Crystal	24
1.4 REVIEW ON HEXOSOMES	26
1.4.1 Formation of Hexosomes	26
1.4.2 Hexosome Stability	29
1.4.3 Application of Hexosomes	30

1.5	REVIEW ON VESICLES	31
1.5.1	Formation of Vesicles	31
1.5.2	Formation of Mixed Vesicles	34
1.5.3	Vesicle Stability	34
1.5.4	Application of Vesicles	36
1.6	REVIEW ON NANO-EMULSIONS	37
1.6.1	Formation of Nano-emulsions	37
1.6.2	Nano-emulsion Stability – Destabilization Mechanism	40
1.6.3	Nano-emulsion for Drug Delivery System	43
1.6.4	Proposed Nano-emulsion System	44
1.7	RESEARCH OUTLINE	45
1.7.1	Objectives of the Research	45
1.7.2	Organization of Research	45
CHAPTER 2: SYNTHESIS OF BRANCHED-CHAIN GLYCOLIPIDS		
2.1	INTRODUCTION	47
2.2	MATERIALS	49
2.3	SYNTHESIS METHODS	50
2.3.1	Peracetylation: Synthesis of $\beta(\alpha)$ -D-maltose octaacetate (3)	52
2.3.2	Glycosidation: Synthesis of 2-hexyldecyl- $\beta(\alpha)$ -D-glucose tetraacetate (1)	52
2.3.3	Glycosidation: Synthesis of 2-hexyldecyl- $\beta(\alpha)$ -D-maltose heptaacetate (4)	53
2.3.4	Deacetylation: Synthesis of 2-hexyldecyl- $\beta(\alpha)$ -D-glucoside (2)	53
2.3.5	Deacetylation: Synthesis of 2-hexyldecyl- $\beta(\alpha)$ -D-maltoside (5)	54
2.4	INSTRUMENTATIONS	54
2.4.1	Nuclear Magnetic Resonance Spectrophotometer	54
2.4.2	Fourier Transform Infrared Spectrophotometer	54

2.5	RESULTS AND DISCUSSIONS	55
2.5.1	¹ H-NMR Data of 2-hexyldecyl- β (/ α)-D-glucose tetraacetate and 2-hexyldecyl- β (/ α)-D-maltose heptaacetate	55
2.5.2	¹ H-NMR and FTIR Data of 2-hexyldecyl- β (/ α)-D-glucoside and 2-hexyldecyl- β (/ α)-D-maltoside	56
2.5.3	Percentage of Yield of 2-HDG and 2-HDM	58
2.6	CONCLUSIONS	59

CHAPTER 3: PHYSICO-CHEMICAL CHARACTERIZATION OF BRANCHED-CHAIN GLYCOLIPIDS

3.1	INTRODUCTION	60
3.2	MATERIALS	61
3.3	METHODOLOGY	61
3.3.1	Samples Preparation for TGA	61
3.3.2	Samples Preparation for DSC	62
3.3.3	Thermotropic and Lyotropic Determination by Optical Polarizing Microscope (OPM)	62
3.3.4	Liquid Crystalline Pattern by Small- and Wide-Angle X-Rays Scattering (SWAXS)	64
3.4	INSTRUMENTATIONS	65
3.4.1	Thermogravimetric Analyzer (TGA)	65
3.4.2	Differential Scanning Calorimeter (DSC)	65
3.4.3	Optical Polarizing Microscope (OPM)	67
3.4.4	Small- and Wide-Angle X-Ray Scattering (SWAXS)	68

3.5	RESULTS AND DISCUSSIONS	70
3.5.1	Thermogravimetric Analysis	70
3.5.2	Differential Scanning Calorimetry	71
3.5.3	Thermotropic Behaviour of Branched-Chain Glycolipids	73
3.5.4	Lyotropic Behaviour of Branched-Chain Glycolipids	76
3.5.5	SAXS Results of Dried Branched-Chain Glycolipids	77
3.5.6	SAXS Results of Hydrated Branched-Chain Glycolipids	80
3.6	CONCLUSIONS	82

**CHAPTER 4: BINARY PHASE BEHAVIOUR OF BRANCHED-CHAIN
GLYCOLIPIDS/WATER SYSTEM TOWARDS FORMATION
OF HEXOSOMES AND VESICLES**

4.1	INTRODUCTION	83
4.2	MATERIALS	84
4.3	METHODOLOGY	85
4.3.1	Samples Preparation for Critical Aggregation Concentration (CAC) Determination	85
4.3.2	Preparation of Glycolipids/Water System	85
4.3.3	Preparation of Hexosomes	86
4.3.4	Preparation of Vesicles	86
4.4	INSTRUMENTATIONS	87
4.4.1	Tensiometer	87
4.4.2	3D-Photon Correlation Spectrometer (3D-PCS)	88
4.4.3	Nano-Zetasizer	89
4.4.4	Cryogenic Transmission Electron Microscopy (Cryo-TEM)	90

4.5	RESULTS AND DISCUSSIONS	92
4.5.1	Critical Aggregation Concentration (CAC)	92
4.5.2	Binary Phase Behaviour of 2-HDG/Water and 2-HDM/Water Systems	94
4.5.3	Hexosomes Formation from 2-HDG	97
4.5.4	Vesicles Formation from 2-HDM	102
4.5.5	Effect of Adding Anionic Surfactant to 2-HDM Vesicles	104
4.6	CONCLUSIONS	107

**CHAPTER 5: INFLUENCE OF BRANCHED-CHAIN GLYCOLIPIDS ON
TERNARY NANO-EMULSION AS DRUG DELIVERY
SYSTEMS**

5.1	INTRODUCTION	108
5.2	MATERIALS	109
5.3	METHODOLOGY	110
5.3.1	Preparation of Nano-emulsions	110
5.3.2	Incorporation of Drug into Nano-emulsions	111
5.3.3	<i>In-Vitro</i> Drug Release Experiment	112
5.4	INSTRUMENTATIONS	113
5.4.1	3D-Photon Correlation Spectrometer (3D-PCS)	113
5.4.2	Cryogenic Transmission Electron Microscopy (Cryo-TEM)	113
5.4.3	Stability Analyzer	114
5.4.4	High-Pressure Liquid Chromatography (HPLC)	115
5.5	RESULTS AND DISCUSSIONS	116
5.5.1	Formation of Nano-emulsion	116
5.5.2	Nano-emulsion Stability – Dynamic Light Scattering	121
5.5.3	Nano-emulsion Stability – Light Backscattering	127

5.5.4	Nano-emulsion Characterization	130
5.5.5	Drug Delivery Study	133
5.5.5.1	Drug Incorporated-Nano-emulsion	133
5.5.5.2	<i>In-Vitro</i> Drug Release Study	133
5.6	CONCLUSIONS	136

CHAPTER 6: CONCLUSIONS

6.1	CONCLUSIONS	138
6.2	MOTIVATION FOR FUTURE WORK	141

REFERENCES	143
-------------------	-----

APPENDICES

<i>APPENDIX 1</i>	155
--------------------------	-----

(A)	¹H-NMR Spectra	155
-----	----------------------------------	-----

(B)	FTIR Spectra	157
-----	---------------------	-----

<i>APPENDIX 2</i>	159
--------------------------	-----

(A)	PHD PUBLICATIONS	159
-----	-------------------------	-----

	Journal Articles	159
--	-------------------------	-----

	Proceeding Papers	159
--	--------------------------	-----

(B)	PROCEEDINGS OF CONFERENCE/SEMINAR/WORKSHOP	160
-----	---	-----

(C)	RESEARCH GRANT	164
-----	-----------------------	-----

(D)	AWARD	164
-----	--------------	-----

(E)	ATTACHMENTS	164
-----	--------------------	-----

LIST OF FIGURES

CHAPTER 1

Figure 1.1: Chemical structures of (a) 2-hexyldecyl- β / α -D-glucoside ($M_r = 404.58$ g/mol) and (b) 2-hexyldecyl- β / α -D-maltoside ($M_r = 566.73$ g/mol).	2
Figure 1.2: Illustration of a surfactant molecule which consists of a polar head group and a non-polar hydrocarbon tail.	3
Figure 1.3: Examples of anionic surfactants.	5
Figure 1.4: Examples of cationic surfactants.	5
Figure 1.5: Examples of nonionic surfactants.	7
Figure 1.6: Example of zwitterionic surfactant.	7
Figure 1.7: The CMC determinations of surfactants in aqueous medium.	8
Figure 1.8: Typical aggregate morphologies into which surfactants self-assemble in aqueous solution.	10
Figure 1.9: Different ordering of molecules in some thermotropic liquid crystals.	18
Figure 1.10: Typical textures of liquid crystalline phases (adopted from [27]).	20
Figure 1.11: Generic phase behaviour of lyotropic liquid crystalline phases (adapted from [37]).	22
Figure 1.12: Example of hexosomes formation from branched-chain glucosides.	28
Figure 1.13: Example of vesicles formation from branched-chain maltosides.	31
Figure 1.14: A schematic diagram of oil-in-water (O/W) nano-emulsion.	38
Figure 1.15: A schematic diagram of water-in-oil (W/O) nano-emulsion.	38
Figure 1.16: Nano-emulsion formation by PIT emulsification method.	39
Figure 1.17: Nano-emulsion formation by PIC emulsification method.	39
Figure 1.18: A schematic diagram of nano-emulsion breakdown/destabilization mechanisms.	42

CHAPTER 2

- Figure 2.1:** Chemical structures of (a) monogalactosyl diacylglycerol (MGDG) and (b) digalactosyl diacylglycerol (DGDG). 47
- Figure 2.2:** Chemical structures of (a) 2-hexyldecyl- β / α -D-glucoside (2-HDG) and (b) 2-hexyldecyl- β / α -D-maltoside (2-HDM). 48

CHAPTER 3

- Figure 3.1:** Sample preparation for thermotropic study. 63
- Figure 3.2:** Contact penetration technique for lyotropic study. 64
- Figure 3.3:** A schematic diagram of a heat flux differential scanning calorimeter. 66
- Figure 3.4:** Sample observation under optical polarizing microscope. 68
- Figure 3.5:** A schematic diagram of the (a) X-ray scattering measurement and (b) Bragg's Law. 69
- Figure 3.6:** TGA thermogram of 2-hexyldecyl- β / α -D-glucoside (2-HDG) and 2-hexyldecyl- β / α -D-maltoside (2-HDM). 70
- Figure 3.7:** DSC thermograms of (a) 2-HDG and (b) 2-HDM upon heating and cooling (two cycles). 72
- Figure 3.8:** Optical polarizing micrographs of phase transitions of the 2-HDG upon heating. The texture corresponds to those of a columnar phase. 74
- Figure 3.9:** Optical polarizing micrographs of phase transitions of the 2-HDG upon cooling. The focal conic texture corresponds to the columnar phase. 74
- Figure 3.10:** Optical polarizing micrographs of phase transitions of the 2-HDM upon heating. The texture corresponds to those of a smectic A phase. 75
- Figure 3.11:** Optical polarizing micrographs of phase transitions of the 2-HDM upon cooling. The fan-shaped texture corresponds to those of a smectic A phase. 75
- Figure 3.12:** Optical polarized micrographs of the contact penetration experiment for 2-HDG. (L = isotropic phase and H_{II} = inverted hexagonal phase). 76
- Figure 3.13:** Optical polarized micrographs of the contact penetration experiment for 2-HDM. (L = isotropic phase, L_{α} = lamellar phase and SmA = smectic A phase). 77

Figure 3.14: SAXS spectrum of dried 2-HDG at 25.0 °C.	78
Figure 3.15: SAXS spectrum of dried 2-HDM at 25.0 °C.	79
Figure 3.16: SAXS spectrum of hydrated 5.0 wt% 2-HDG at 25.0 °C.	80
Figure 3.17: SAXS spectrum of hydrated 5.0 wt% 2-HDM at 25.0 °C.	81

CHAPTER 4

Figure 4.1: A schematic diagram of Wilhelmy plate method used for measuring the surface tension of the solution.	87
Figure 4.2: A schematic diagram of a conventional photon correlation spectrometer.	88
Figure 4.3: A schematic diagram of the Nano-Zetasizer setup for zeta potential measurement.	89
Figure 4.4: A schematic diagram of a transmission electron microscope (TEM). The electron beam is highlighted in yellow while electron-optical lenses are depicted in grey.	91
Figure 4.5: Surface tension profiles of (a) 2-HDG and (b) 2-HDM alone and mixed with SDS or AOT as a function of log concentration at 25.0 °C.	93
Figure 4.6: Pseudo-binary phase diagram of (a) 2-HDG/water and (b) 2-HDM/water systems as a function of temperature. One-phase region of isotropic phase (grey) and two-phase region of (a) an inverted hexagonal liquid crystalline phase and (b) lamellar liquid crystalline phase dispersed in water (white).	95
Figure 4.7: An example of 2-HDG hexosomes sample.	97
Figure 4.8: Static light scattering of 2-HDG hexosomes and MALLS (multi-angle laser light scattering) measurements.	99
Figure 4.9: Radius distribution of hexosome dispersion with 0.50 wt% of 2-HDG in water obtained by a Contin data analysis of dynamic light scattering results.	100
Figure 4.10: Cryo-TEM micrograph of hexosomes dispersion with 0.50 wt% of 2-HDG in water. Hexosomes are visible as dark grey hexagonal or spherical-shaped particles.	100
Figure 4.11: An example of 2-HDM vesicles sample.	102

Figure 4.12: Cryo-TEM micrograph of 0.50 wt% of 2-HDM dispersion. Multilamellar vesicles (MLVs) with polydisperse nature can be observed.	103
Figure 4.13: Radius distribution of 1.0 wt% of 2-HDM/AOT dispersion in water. Two main populations were observed at 80 and 25 nm.	104
Figure 4.14: Cryo-TEM micrographs of 1.0 wt% of 2-HDM/AOT dispersions. Spherical unilamellar vesicles were observed, indicating that AOT induced the formation of small and large unilamellar vesicles.	105
Figure 4.15: Radius distribution of 1.0 wt% of 2-HDM/SDS dispersion in water. Main population was observed at 40 nm.	105
Figure 4.16: Cryo-TEM micrographs of 1.0 wt% of 2-HDM/SDS dispersions. SDS induced the formation of small unilamellar vesicles.	106

CHAPTER 5

Figure 5.1: Low-energy emulsification method: Phase Inversion Composition (PIC).	110
Figure 5.2: Chemical structure of Ketoprofen.	111
Figure 5.3: <i>In-vitro</i> drug release experiment (dialysis bag method).	112
Figure 5.4: Turbiscan operating principle.	114
Figure 5.5: A schematic diagram of HPLC setup for drug release experiment.	115
Figure 5.6: Pseudo-ternary phase diagram of water/Crem EL/MCT oil at 25.0 °C.	117
Figure 5.7: Comparison of nano-emulsion droplets radii between water/Crem EL/2-HDG/MCT oil to the reference system of water/Crem EL/MCT oil as a function of Crem EL/2-HDG ratios at 25.0 °C. Water content was fixed at 90 wt%, whereas the oil/surfactant ratio was selected at 40/60.	120
Figure 5.8: Comparison of nano-emulsion droplets radii between water/Crem EL/2-HDM/MCT oil to the reference system of water/Crem EL/MCT oil as a function of Crem EL/2-HDM ratios at 25.0 °C. Water content was fixed at 90 wt%, whereas the oil/surfactant ratio was selected at 40/60.	120
Figure 5.9: Nano-emulsions physical appearance of Crem EL only (1A-1D), 85/15 of Crem EL/2-HDG (2A-2D) and 85/15 of Crem EL/2-HDM (3A-3D) at 1 day, 1 week and 1 month of storage time in water bath at 25.0 °C and 37.0 °C. Refer to Table 5.2 for the nano-emulsion compositions.	123

- Figure 5.10:** Nano-emulsion droplet radius (nm) of (a) Crem EL only (1A-1D), (b) 85/15 of Crem EL/2-HDG (2A-2D) and (c) 85/15 of Crem EL/2-HDM (3A-3D) as a function of storage time and temperatures of 25.0 °C and 37.0 °C. Preparation temperatures are 25.0 °C (A, B) and 70.0 °C (C, D). Refer to Table 5.2 for the nano-emulsion compositions. 125
- Figure 5.11:** Back Scattering (%) of (a) Water/Crem EL/MCT oil, (b) Water/Crem EL/2-HDG/MCT oil and (c) Water/Crem EL/2-HDM/MCT oil nano-emulsions as a function of sample height (mm) at 25.0 °C. Data are given for different period of time up to 24 h. Water content was fixed at 90 wt%, whereas oil/surfactant ratio was 40/60 and Crem EL/Glycolipid ratio was 85/15. 128
- Figure 5.12:** Backscattering (%) at a fixed sample height (1000 nm) of Crem EL (1A), Crem EL/2-HDG (2A) and Crem EL/2-HDM (3A) nano-emulsions as a function of measurement time. 129
- Figure 5.13:** Nano-emulsion samples of (a) Water/Crem EL/MCT oil, (b) Water/Crem EL/2-HDG/MCT oil and (c) Water/Crem EL/2-HDM/MCT oil after 24 h measurements. Water content was fixed to 90 wt%, whereas oil/surfactant ratio was 40/60 and Crem EL/Glycolipid ratio was 85/15. 130
- Figure 5.14:** Nano-emulsion droplets size images under cryo-TEM of ternary (a) Water/Crem EL/MCT oil (b) Water/Crem EL/2-HDG/MCT oil and (c) Water/Crem EL/2-HDM/MCT oil at 25.0 °C. 132
- Figure 5.15:** Release profile of KT from the MCT oil solution and from the three nano-emulsions: water/Crem EL/MCT oil, water/Crem EL/2-HDG/MCT oil and water/Crem EL/2-HDM/MCT oil as a function of time at 25.0 °C. The nano-emulsion composition was 90 wt% water content, whereas O/S and Crem EL/Glycolipid ratios of 40/60 and 85/15 respectively. 134

LIST OF SCHEMES

CHAPTER 2

- Scheme 2.1:** 2-hexyldecyl- β (/ α)-D-glucoside (2-HDG) was produced from glycosidation between Guerbet alcohol and protected sugars. The acetyl groups were cleared away by deacetylation under basic condition. 50
- Scheme 2.2:** 2-hexyldecyl- β (/ α)-D-maltoside (2-HDM) was produced from glycosidation between Guerbet alcohol and protected sugars. The acetyl groups were cleared away by deacetylation under basic condition. 51

LIST OF TABLES

CHAPTER 1

Table 1.1: Relationship between the shape of surfactant monomers and preferred aggregate morphology.	13
Table 1.2: HLB values and their general areas of application.	14

CHAPTER 2

Table 2.1: Percentage of yield of 2-hexyldecyl- β (/ α)-D-glucosides (2-HDG).	58
Table 2.2: Percentage of yield of 2-hexyldecyl- β (/ α)-D-maltosides (2-HDM).	58

CHAPTER 3

Table 3.1: The overall DSC results for 2-HDG and 2-HDM.	73
Table 3.2: d-spacing and lattice spacing (nm) of dried 2-HDG and 2-HDM obtained by SAXS experiments at 25.0 °C.	79
Table 3.3: d-spacing and lattice spacing (nm) of hydrated 5.0 wt% 2-HDG and 2-HDM obtained by SAXS experiments.	81

CHAPTER 4

Table 4.1: The CAC values of 2-HDG and 2-HDM alone and mixed with SDS or AOT in aqueous solution at 25.0 °C. The 2-HDG or 2-HDM/SDS or AOT ratio was fixed to 10:1.	94
Table 4.2: Static light scattering measurement at different angles.	98

CHAPTER 5

Table 5.1: Summary of different mixing ratios between water/Crem EL/Gly/MCT oil at 25.0 °C. The branched-chain glycolipids used were 2-HDG and 2-HDM.	118
Table 5.2: Lists of nano-emulsion compositions as well as of their preparation and storage temperatures. Water content was fixed to 90 wt%, whereas the oil/surfactant ratio was 40/60 and the Crem EL/Glycolipid ratio was selected to be 85/15.	122
Table 5.3: Amount of ketoprofen (KT) released after 24 h.	135
Table 5.4: Determination Coefficients (R^2) of Weibull Model.	136

LIST OF ABBREVIATIONS

ΔH	Enthalpy change
2D	Two-dimensional
3D	Three-dimensional
2-HDG	2-hexyldecyl- β (/ α)-D-glucoside
2-HDM	2-hexyldecyl- β (/ α)-D-maltoside
AcO	Acetate group
AOT	Aerosol OT/Dioctyl sodium sulfosuccinate
APG	Alkyl polyglucoside
APGs	Alkyl polyglycosides
A.U.	Arbitrary Units
ASs	Anionic Surfactants
CAC	Critical Aggregation Concentration
CD ₃ OD	Perdeuterated methanol
CDCl ₃	Deuterated chloroform
CMC	Critical Micellar Concentration
Col	Columnar
CPC	Cryo Preparation Chamber
Crem EL	Cremophor [®] EL
Cryo-TEM	Cryogenic Transmission Electron Microscopy
CTAB	Cetyl trimethyl ammonium bromide
CVC	Critical Vesicular Concentration
DGDG	Digalactosyl diacylglycerol
DLS	Dynamic Light Scattering
DMSO	Dimethyl sulfoxide
DSC	Differential Scanning Calorimetry
DTAB	Dodecyl trimethyl ammonium bromide
e.g.	Exempli gratia/for example
et al.	et alii/and others
etc	et cetera/and the others
FTIR	Fourier Transform Infrared
Gly	Glycolipids

H _I	Normal hexagonal
H _{II}	Inverted hexagonal
HLB	Hydrophilic-Lipophilic Balance
HPLC	High-Pressure Liquid Chromatography
i.e.	Id est/that is
I _I	Normal discontinuous cubic
I _{II}	Inverted discontinuous cubic
KT	Ketoprofen
L _α	Lamellar
L _I	Normal micellar solution
L _{II}	Inverted micellar solution
LUV	Large Unilamellar Vesicle
M _r	Relative molecular mass
MCT	Medium-chain triglyceride
MGDG	Monogalactosyl diacylglycerol
MLV	Multilamellar Vesicle
n	Director
N	Nematic
N*	Chiral Nematic/Cholesteric
NaCl	Sodium Chloride
NMR	Nuclear Magnetic Resonance
O/S	Oil-Surfactant
O/W	Oil-in-Water
OPM	Optical Polarizing Microscope
P	Packing Parameter
PCS	Photon Correlation Spectrometer
PIC	Phase Inversion Composition
PIT	Phase Inversion Temperature
ppm	Parts per million
R _f	Retention factor
SAXS	Small-Angle X-Ray Scattering
SDS	Sodium dodecyl sulphate

SLS	Static Light Scattering
Sm	Smectic
SmA	Smectic A
SmB	Smectic B
SmC	Smectic C
SUV	Small Unilamellar Vesicle
SWAXS	Small- and Wide-Angle X-Ray Scattering
TGA	Thermogravimetric Analyzer
TLC	Thin Layer Chromatography
Triton X-100	Polyethyleneglycolmono[4-(1,1,3,3-tetramethylbutyl)phenyl] ether
W/O	Water-in-Oil
WAXS	Wide-Angle X-Ray Scattering
V _I	Normal bicontinuous cubic
V _{II}	Inverted bicontinuous cubic

CHAPTER 1:
INTRODUCTION AND LITERATURE REVIEW

1.1 INTRODUCTION

A great deal of attention has been given to the many types of bio-surfactants such as glycolipids and phospholipids in the last decade, particularly for their self-aggregation properties and characterization. Amongst them, glycolipids have been most widely studied because of they are nonionic, non-toxic, biocompatible and biodegradable. Their amphiphilic and amphitropic characteristic can be expected from a hydrophilic group because of the sugar moiety and the lipophilic (hydrophobic) group from the hydrocarbon alkyl chains. The structures result in a range of phase behaviour, such as the formation of different thermotropic liquid crystalline phases in dry form and lyotropic phases when in contact with polar solvents such as water and dimethyl sulfoxide (DMSO).

Glycolipids influence membrane functionality (cell wall stability and transport process) and they exhibit a wide spectrum of practical applications, for example as stabilizer of hydrocarbon foam, cleaning agents, cosmetics emulsifiers and syntheses of nano-structure materials. It is not easy extracting glycolipids from natural sources and totally synthesizing the natural glycolipids. Therefore, continuous study and research into the synthesis and development of synthetic glycolipids are on-going, alongside the structural improvement of glycolipids capabilities. Branched-chain glycolipids are more suitable because they represent a simplified model of the natural ones and are an admissible alternative to natural glycolipids. For this reason, chemists use the simpler synthetic branched-chain glycolipids in formulation and synthesis projects.

In the present study, Guerbet branched-chain glycosides will be characterized in dried and hydrated forms. First of all, two technical grade derivatives with the same chain lengths but different head group polarities will be prepared. The first one is based on glucose; 2-hexyldecyl- β (/ α)-D-glucoside (2-HDG) and the second one is based on maltose; 2-hexyldecyl- β (/ α)-D-maltoside (2-HDM). Their chemical structures are shown in **Figure 1.1**.

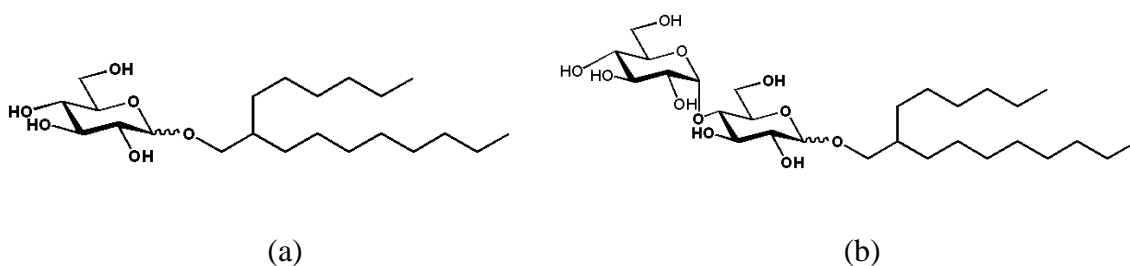


Figure 1.1: Chemical structures of (a) 2-hexyldecyl- β (/ α)-D-glucoside ($M_r = 404.58$ g/mol) and (b) 2-hexyldecyl- β (/ α)-D-maltoside ($M_r = 566.73$ g/mol).

These compounds are both β -dominant ($\sim 90\%$) anomeric mixtures, which are produced without further α - and β -isolation using column chromatography process. Although α/β glycosides anomers are known to give different phase behaviours, a selected composition of anomeric mixture will be indicated, and reused, for economic reasons. A set of fundamental investigations will be conducted for their emulsifying strength that will be the basis of the formulation in binary and ternary phase systems. The investigation will include the measurement of their thermal properties (decomposition and melting temperatures), morphology (thermotropic and lyotropic properties) and critical aggregation concentrations. More information will be derived from the physico-chemical characterizations and binary phase in the formation of glycolipids dispersions and aggregations. In the final part, the influence of glycolipids incorporated in nano-emulsions for drug transportation and delivery will be investigated.

1.2 REVIEW ON SURFACTANT

The word *surfactant* is an abbreviation of surface-active-agent, which is also commonly called a detergent. Surfactants have a dualistic character, having both hydrophilic and hydrophobic moieties in a molecule known as amphiphile. A molecular structure of a surfactant is illustrated in **Figure 1.2**. Self-assembly of the amphiphilic surfactants is a possible way of eliminating the energetically unfavourable contact between the non-polar part and water, while simultaneously retaining the polar part in an aqueous environment [1]. The physical phenomenon responsible for such behaviour is referred to as the hydrophobic effect and arises from a subtle balance between intermolecular energies and entropies [2].

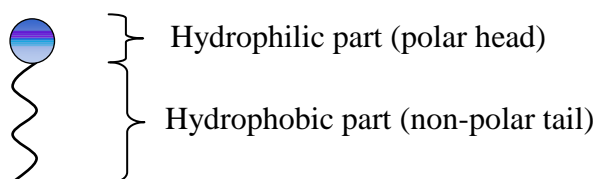


Figure 1.2: Illustration of a surfactant molecule which consists of a polar head group and a non-polar hydrocarbon tail.

Surfactants can occur naturally in biological components of animals and plants, which are called natural surfactants or bio-surfactants. Some examples are phosphatidylcholine, lecithin, sodium cholate and fatty acids such as caprylic acid, capric acid, lauric acid, myristic acid and others [3]. On the other hand, synthetic surfactants are surfactants that can be synthesized in the laboratory such as sodium dodecyl sulphate, decyltrimethyl ammonium bromide and sodium dioctyl sulfosuccinate.

In general, most of these molecules are soluble in water although some of them form colloidal dispersions instead of solutions. For this reason, these surfactants find a wide spectrum of practical applications ranging from chemistry to biology (as membrane mimics) to pharmacy (as drug delivery vesicles) [3-4].

Surfactants are usually classified by the charge type of their polar head group, such as cationic, anionic, nonionic and zwitterionic [4-6]. Generally, in ionic surfactants, the hydrophilic part of the molecule normally exists as a salt form that increases the attraction for aqueous solution. It is sensitive to the presence of other ions in the solution system and to temperature. On the other hand, nonionic surfactants can be classified according to whether the head groups are from an ethylene oxide group or hydroxyl group, by forming a region that is favourable/miscible in water. Besides, nonionic surfactants are also typically insensitive to electrolytes and environmental temperature [7]. The following are brief descriptions of the classes of surfactants according to the charges in their hydrophilic head groups.

Anionic Surfactants

Anionic surfactants are compounds that dissociate in solution into negatively charged ions. Surfactants such as fatty acid behave in a similar way where its carboxylic group (COOH) forms carboxylate (COO⁻) in basic conditions. Some common anionic agents are alkyl benzene sulphonates (RC₆H₄SO₃⁻Na⁺), alkyl phosphates (RPO₄⁻M⁺), alkyl sulphonates (RSO₃⁻M⁺), alkyl sulphates (ROSO₃⁻M⁺) or carboxylates (RCOO⁻M⁺) where R is a hydrocarbon chain or unit [6-7]. Examples include sodium dodecyl sulphate (SDS) and sodium bis (2-ethyl hexyl) sulfosuccinate (AOT).

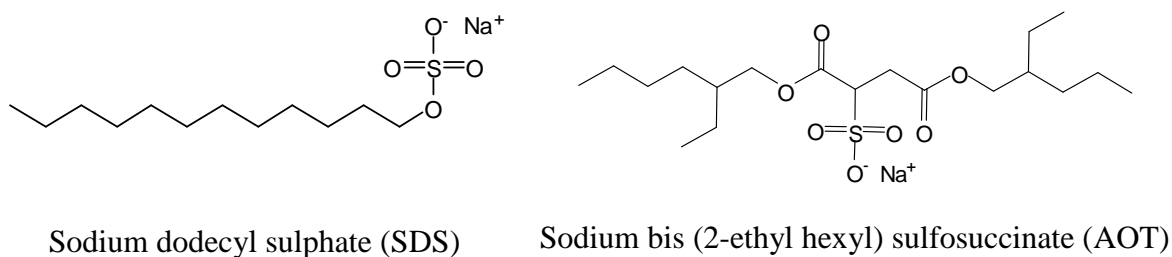


Figure 1.3: Examples of anionic surfactants.

Cationic Surfactants

Cationic surfactants account for not more than 5.0% of the total world production of surfactants [1]. Such compounds possess useful germicidal properties but are unsuitable as detergents. They are more expensive and generally less stable than anionic compounds. The most distinct property that a cationic surfactant has is the positively charged polar head group such as tetra alkyl ammonium halides ($\text{RN}^+(\text{CH}_3)_3\text{Cl}^-$), where R is a hydrocarbon chain or unit. The compounds most often encountered are the quaternary ammonium salts, such as cetyl trimethyl ammonium bromide ($\text{C}_{16}\text{H}_{33}(\text{CH}_3)_3\text{N}^+\text{Br}^-$) and the alkyl pyridinium salts, a commercial example of which is dodecyl pyridinium bromide ($\text{C}_{12}\text{H}_{25}\text{N}^+(\text{C}_5\text{H}_5)\text{Br}^-$) [4,6-7]. Other examples include dihexadecyl dimethyl ammonium acetate and dodecyl trimethyl ammonium bromide (DTAB).

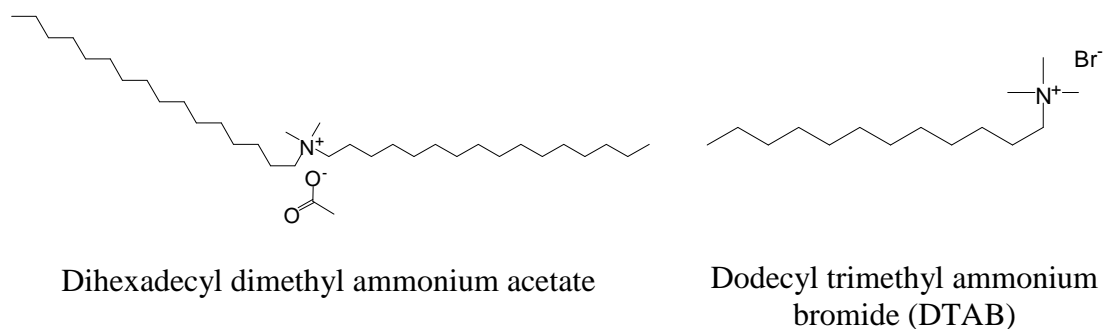


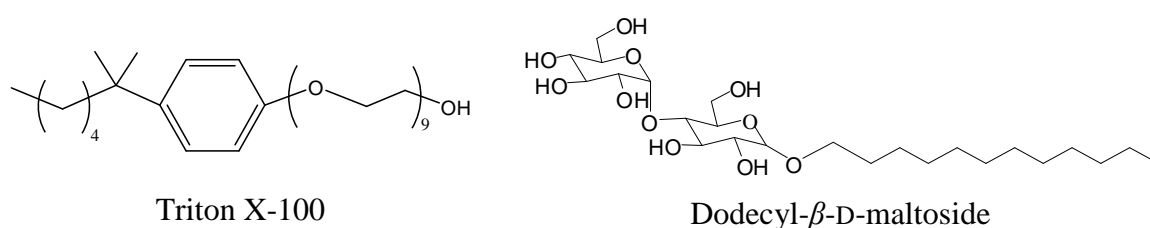
Figure 1.4: Examples of cationic surfactants.

Nonionic Surfactants

Nonionic surfactants cannot dissociate into ions but are solubilized in water due to the presence of polar groups. Examples of nonionic surfactants are the compounds with a general formula of $R(\text{OCH}_2\text{CH}_2)_n\text{OH}$, obtained by condensing an alcohol or a phenol with ethylene oxide [2]. In such substances the R group is hydrophobic whereas the hydroxyl group and the -O- links in the polyethoxyl moiety are water seeking. Consequently, it is possible to obtain the desired balance between hydrophilic and lipophilic properties by adjusting either the value of n or the size of the alkyl group. For example, when R is an alkyl phenol group, an alkyl chain of 8-12 carbons will give a detergent when n is in the order of 10 [3-4]. In practice, a commercial product obtained by polymerization is usually a mixture of several homologues with various numbers of monomer units in the chain. Polyoxyethylene surfactants have widespread use in industrial and domestic cleaners. They are stable in acids and in alkalis, and usually foam less than anionic agents do.

Two other successful ranges of nonionic surfactants are the laurate, palmitate and oleate esters of anhydrosorbitols and the ethylene oxide condensates of these esters. These series are better known under their trade names of “Span” and “Tween” respectively. They may be blended together to produce a wide range of HLB (Hydrophilic-Lipophilic Balance) values suitable for various applications [4].

The polar head group of nonionic compounds does not carry any overall charge. Some common nonionic surfactants are oxyethylene $(-\text{OCH}_2\text{CH}_2)_n-$ and oxyethylene alcohol. Examples are polyethyleneglycolmono[4-(1,1,3,3-tetramethylbutyl)phenyl] ether (Triton X-100) and dodecyl- β -D-maltoside [6-7].

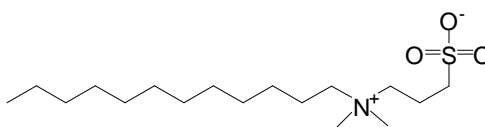


Triton X-100

Dodecyl- β -D-maltoside**Figure 1.5:** Examples of nonionic surfactants.

Zwitterionic Surfactants

As the name implies, this type of surfactants carries both an anionic and a cationic group in the same molecule. One series of zwitterionic surfactant has the general formula $\text{R-NH-CH}_2\text{-CH}_2\text{-COO}^-\text{Na}^+$, where the amino group become positively charged in acid media and the carboxyl group negatively charged in the presence of a base. Sodium n-dodecyl-3-aminopropionate is a representative of this type of compound [4]. Some other common zwitterionic compounds are carboxybetaine ($\text{R}(\text{CH}_3)\text{N}^+\text{CH}_2\text{COO}^-$) and sulphobetaine ($\text{RN}^+(\text{CH}_2)_2\text{CH}_2\text{SO}_3^-$), where R is a hydrocarbon chain [6]. Dodecyl dimethyl propane sultaine is an example of this.



Dodecyl dimethyl propane sultaine

Figure 1.6: Example of zwitterionic surfactant.

1.2.1 Aggregation Behaviour of Surfactants

The solubilization of amphiphilic compounds in an aqueous medium normally results in the formation of more than one type of self-aggregation structures. The type of aggregation the surfactant will form depends on the type of surfactant structures such as its packing parameter [3,12]. Aggregation behaviour of surfactants in aqueous solution is fundamental to understanding the strength of a surfactant that is directly correlated to the volume of hydrophobic-hydrophilic regions. A surfactant can dissolve and form monomers in a very dilute aqueous solution. The aggregation of the surfactant starts to form by increasing the molar of monomers in the solution indicated by “aggregation number, N ” [4-5]. The physical properties of the solution will change in the presence of surfactant aggregation, and the simplest aggregation is normal micelle. Thus, the transition from a monomeric solution to an aggregated form can be seen as a change in the slope of plots against surfactant concentration of many physical properties such as surface tension, electrical conductivity, osmotic pressure, turbidity and light scattering measurements as shown in **Figure 1.7**.

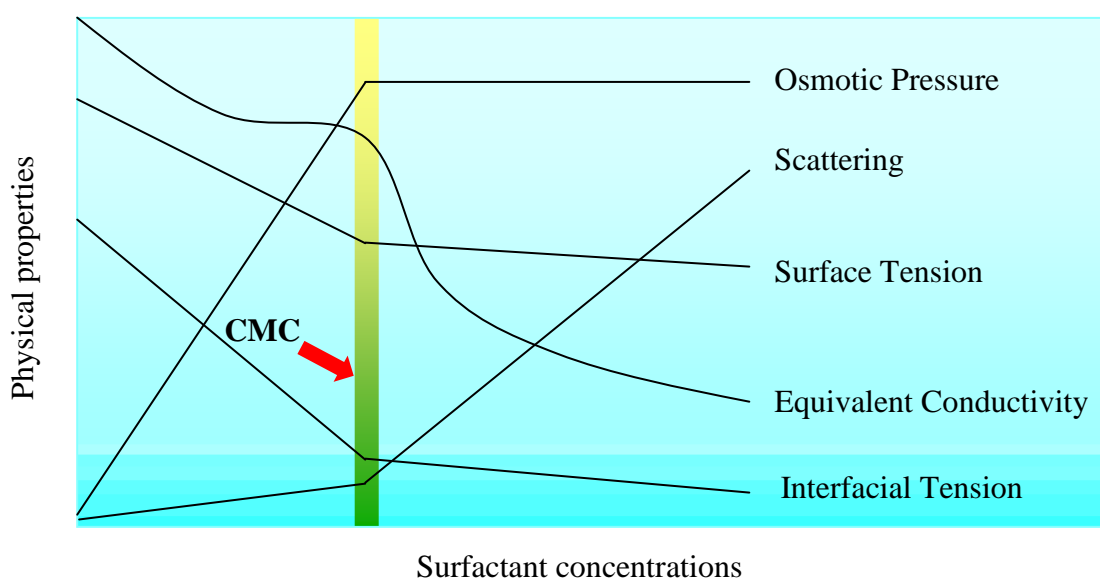


Figure 1.7: The CMC determinations of surfactants in aqueous medium.

The concentration of surfactants at which the physical properties of the solution change and the concentration of micelles becomes suddenly appreciable is referred to as the critical micellar concentration (CMC) or critical aggregation concentration (CAC) [6-7,12-13]. The CMC/CAC value is conveniently determined from a break or deviation of physical properties profiles as a function of surfactant concentration (**Figure 1.7**). In fact, the tendency of amphiphilic molecules to form micelles in an aqueous solution is a consequence of the hydrophobic effect [14-15]. Once the surfactants are aggregates or micelles are formed, further increase of the total surfactant concentration does not change the concentration of the free monomer. The concentration of the free surfactant molecules remains constant after the surfactants are aggregated or micelles are formed.

Some surfactants can be dissolved in non-polar solvents. Similar aggregation can be formed whereby the hydrophilic head groups of the surfactants associate together by allowing the hydrophobic alkyl chain towards the non-polar environment. These can be seen when the surfactant is dissolved in a non-polar solvent such as hexane. The structures formed are called reverse micelles.

Depending on the particular molecular architecture of the surfactant molecule, a variety of microstructures can be formed. They are able to rearrange themselves in response to changing environmental conditions (polar/non-polar solvent) [2]. Possible aggregate structures formed by surfactants are spherical micelles, cylindrical micelles, vesicles, lamellar sheets or other bicontinuous or inverted assembly structures [4,6,13] as shown in **Figure 1.8**.

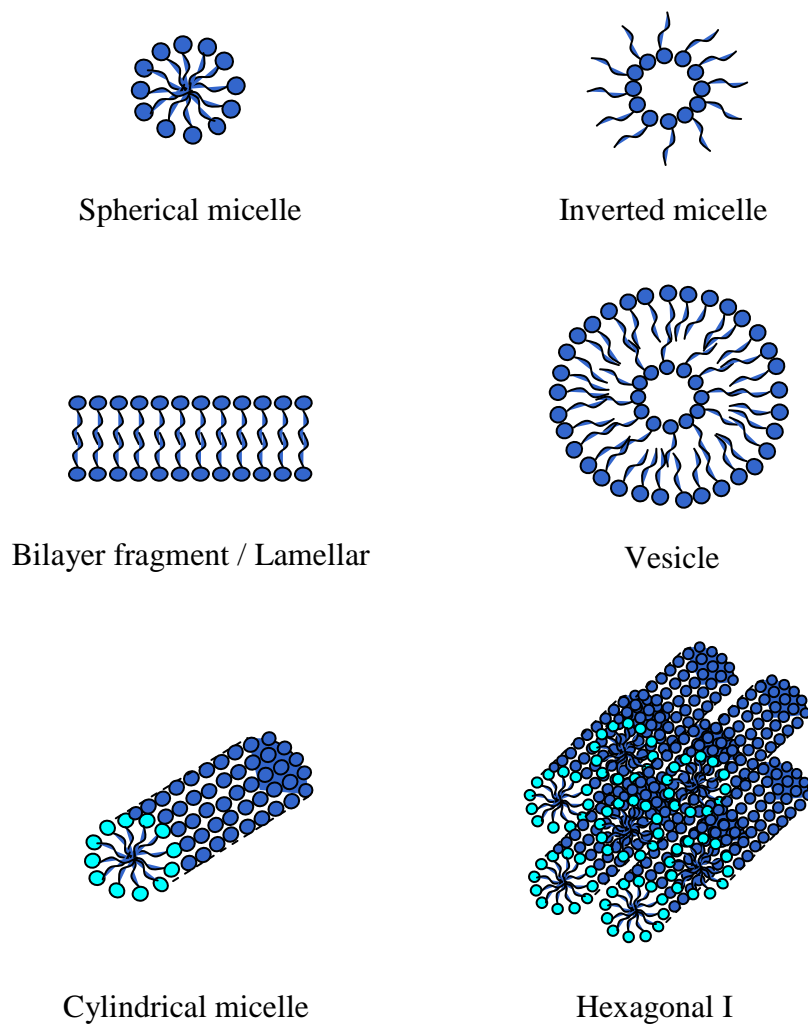


Figure 1.8: Typical aggregate morphologies into which surfactants self-assemble in aqueous solution.

1.2.2 Packing Parameter

Aggregate morphology is determined mainly by a delicate balance between attractive hydrophobic interactions of surfactant alkyl tails and electrostatic repulsions of surfactant head groups. In addition to repulsive interactions of electrostatic origin, repulsions due to hydration of the head groups must be taken into account. An opposing effect is exerted by the interfacial tension that tends to decrease the effective head group area. The molecular architecture of a given surfactant determines the type of aggregate into which a surfactant associates in aqueous solution. Moreover, the formation of self-assembly structure is also influenced by other factors such as pH, temperature, surfactant concentration and electrolytes content. All these factors will cause the modification of surfactant aggregation structure, which is related to its packing parameter. The relationship between the shape of the surfactant monomer and the aggregate morphology can be represented by the packing parameter approach [6-7,12-13]. The packing parameter (P) is calculated from this equation (1.1):

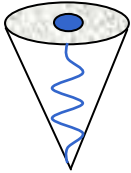
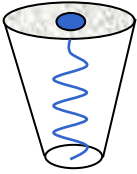
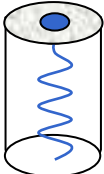
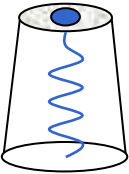
$$P = \frac{v}{a_o l} \quad (1.1)$$

where v is the volume of the hydrophobic part of the surfactant molecule, a_o is the mean cross-sectional (effective) head group surface area and l is the most extended chain length of the hydrocarbon alkyl tail [4-5].

The preferred type of aggregate to be formed is dictated largely by these parameters. For example, increasing v of the surfactant molecule will increase P , hence changing the structure from wedge shape to cylindrical. As a result, a transformation from micellar to lamellar or bilayer structure is more likely to happen. Increase in v can also be achieved by replacing the hydrocarbon chain from a single to a double chain. Similarly, decreasing a_o either by replacing it with a smaller head group or decreasing head group-head group repulsion such as by the addition of salt will have the same effect. For ionic surfactants, a decrease in repulsive head group interactions induced by added salt will decrease a_o , thus increasing P , causing a transition from spherical to cylindrical micelles to vesicles or bilayers [4-6,8,13].

Furthermore, the packing parameter, P of the surfactants determines the morphology of self-assembly structures as shown in **Table 1.1**. Surfactants where $0 < P < 1/3$, will form spherical micelles such as SDS in low salt. If $1/3 < P < 1/2$, cylindrical micelles are formed such as CTAB in high salt and nonionic lipids. On the other hand, surfactants with a P value of around 1, will form planar bilayers and vesicle structures such as sodium dodecanoate-dodecanoic acid and didodecyldimethyl ammonium bromide. Inverted structures, such as reversed micelle and reversed vesicle structures that are formed by polyethylene glycol nonylphenylether (Triton X-100) and dihexadecyl phosphate respectively have a P value greater than 1 [2,4,6-7].

Table 1.1: Relationship between the shape of surfactant monomers and preferred aggregate morphology.

Critical packing shape of the surfactant molecule	Packing parameter	Aggregate morphology
 <p>Cone</p>	$0 < P < 1/3$	Spherical micelles
 <p>Truncated Cone</p>	$1/3 < P < 1/2$	Cylindrical micelles
 <p>Cylinder</p>	~ 1	Planar bilayers, vesicles
 <p>Inverted Truncated Cone or Wedge</p>	> 1	Inverted micelles, inverted hexagonal

1.2.3 Hydrophilic-Lipophilic Balance (HLB)

One of the crucial yardsticks for measuring the magnitude of a surfactant is HLB value. The HLB value is used to determine whether the surfactant is hydrophilic or lipophilic (hydrophobic), in other words, to predict the solubility of surfactants. The scale range of HLB values is from 0 to 20. A HLB value that is approaching 0 corresponds to a completely lipophilic compound, whereas a value approaching 20 indicates an absolutely hydrophilic compound [15-19]. It is usually applied in the formulation of emulsion because the value will predict the type of emulsion that will form. Thus, lipophilic surfactants are deemed suitable for the formation of w/o emulsion, while hydrophilic surfactants are suitable for the formation of o/w emulsion.

In general applications, the HLB system has been found most useful in guiding the formulator in the choice of surfactants most suited for a specific purpose. **Table 1.2** lists the typical HLB values of surfactants broadly used to indicate the suitability of a particular surfactant for a particular application [14,18-19].

Table 1.2: HLB values and their general areas of application.

HLB Value	Application
<3	Surface films
3-6	Water-in-oil emulsifiers
7-9	Wetting agents
8-15	Oil-in-water emulsifiers
12-15	Detergents
15-18	Solubilizers

The HLB system was introduced by Griffin in 1949 [15]. His work was an attempt to identify the optimum nonionic surfactant for the stabilization of emulsion. In the system, Griffin proposed calculating the HLB number of a surfactant from its chemical structure and matching the number with the HLB of the oil phase to be dispersed.

Experimental determination of the HLB number for a given emulsifier is a tedious process. However, this value may be calculated with satisfactory accuracy based on easily determined characteristics of the emulsifier. The following HLB equation was suggested by Griffin for polyhydric alcohol fatty acid esters:

$$HLB = 20 \left(1 - \frac{S}{A} \right) \quad (1.2)$$

where, S is the saponification number of the ester and A is the acid number of the acid.

In certain cases where accurate determination of the saponification number is difficult, the relationship

$$HLB = \frac{(E + P)}{5} \quad (1.3)$$

is used, where E is the weight percent of polyoxyethylene chain and P is the weight percent of polyhydric alcohol (glycerol, sorbitan, etc) in the molecule. When ethylene oxide is the only hydrophilic group present, the equation is reduced to

$$HLB = \frac{E}{5} \quad (1.4)$$

A general HLB formula commonly used for nonionic surfactants [16-17] is

$$HLB = 20 \left(\frac{M_H}{M_H + M_L} \right) \quad (1.5)$$

where M_H is the formula weight of the hydrophilic portion of molecule and M_L is the formula weight of the lipophilic (hydrophobic) portion of the molecule.

1.2.4 Application of Surfactants

Surfactants are often named according to their technological importance in industry such as detergent, emulsifier, dispersant and wetting agent. They are mostly used as detergents, cosmetic additives and for biological functions [2-4,7]. In cosmetics (emulsion formulation), surfactants with high solubility in water will form an oil-in-water emulsion whereas those of high solubility in oil will form a water-in-oil emulsion system [5].

Anionic surfactants such as SDS and dodecyl benzyl sulfonic acid are commonly used as detergents due to their availability and lower price. Fatty acids also have important biological functions and are present in a variety of forms in body tissues and fluids [6-8]. Thus, esterified to glycerol and stored in the cytoplasm of many cells, fatty acids serve as an important source for energy. Possibly even more important is their presence in phospholipids, the major building blocks of most biological membranes. The level of free unesterified fatty acid is generally low in both body fluids and cell membranes, and mostly found associated with albumin or lipoproteins [9-10]. These characteristics have a wide range of practical applications including in encapsulation and control drug delivery [10], the preparation of bactericidal and vaccine formulations [11], as well as in the preparation of cosmetics and pharmaceutical products [12].

1.3 REVIEW ON LIQUID CRYSTALS

Liquid crystalline state was detected more than 100 years ago. A liquid crystal is a state of matter, a phase called mesophases (in between phases). The molecular order is intermediate between a solid crystal and an isotropic liquid [20-21]. Molecules in liquid crystals are in a partially random state of motion and possess some long range ordering in one or two dimensions, orientationally or/and positionally. They possess some properties of solid crystals (e.g. optical birefringence properties) and some of the liquids (e.g. fluidity), resulting in a unique anisotropic behaviour [22].

A liquid crystal compound (or mesogen), may form one liquid crystalline phase or more than one phase (polymorphism). Liquid crystals can be divided into two classes: thermotropic liquid crystals and lyotropic liquid crystals [23]. Liquid crystalline phase driven by temperature is called thermotropic liquid crystals, whereas that which is driven by the concentration of the solution in addition to temperature is called lyotropic liquid crystals [21].

Thermotropic Liquid Crystal

Ordinary thermotropic liquid crystals are usually classified as nematic, cholesteric (chiral nematic), smectic and columnar [21-25] (**Figure 1.9**).

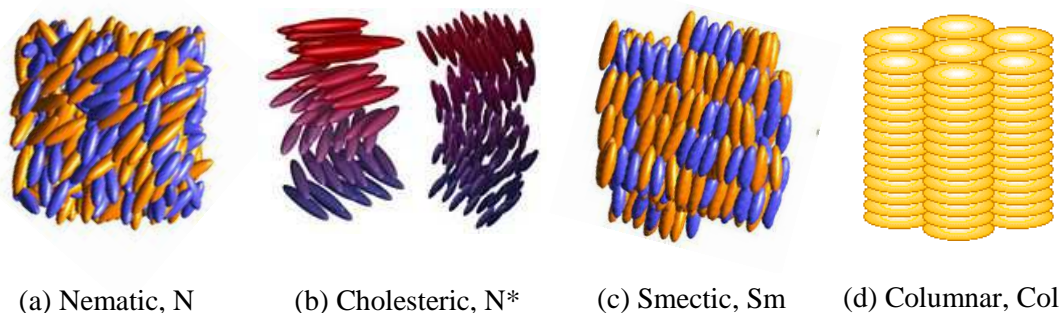


Figure 1.9: Different ordering of molecules in some thermotropic liquid crystals.

The simplest liquid crystal phase is the *nematic phase* (N). Nematic liquid crystals exhibit a long-range orientational order but no positional order. They consist of parallel or nearly parallel elongated molecules, which are mobile in three directions due to lack of a periodic arrangement [21]. The molecules are aligned in a preferred direction called the director, n . In nematic phase the director, n is equivalent to $-n$. Indeed, nematic liquid crystals possess the lowest structural order in thermotropic liquid crystals and they are transformed on heating to isotropic liquid without undergoing a further mesophases transition.

Another special type of nematic phase is called *cholesteric phase* (N^*) or *chiral nematic phase*. The structure can be described as a nematic mesophase twisted about an axis perpendicular to the long axes of the molecules, in which the cholesteric director follows a helical form.

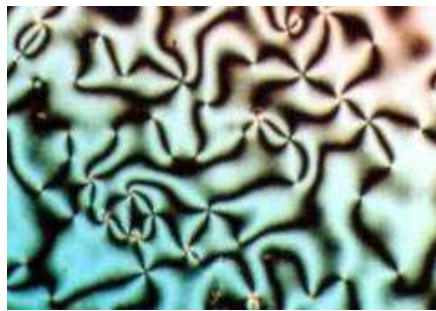
Smectic phases (Sm) are more ordered than nematic and chiral nematic phases since they have some degree of positional order. In *smectic liquid crystals* the elongated molecules are essentially parallel to one another and are arranged in layers with the mean direction of the long axes of the molecules normal to the layers. There are many different types of smectic phases, for example smectic A, smectic B, smectic C and so on [21,25-28]. The molecules in a smectic A phase (SmA) are on average parallel to the layer's normal while the molecules in smectic C phase (SmC) are on average tilted with respect to the layer's normal.

There are other types of thermotropic phases called *frustrated phases* e.g. blue phases, formed by chiral mesogens that pack into 'double-twist' cylinders, in which the orientation of the director varies helically in two different directions. Thus, blue phases are characterized by a frustration between helical ordering and the inability to fill three-dimensional space, which leads to three-dimensional lattices of orientation defects [25].

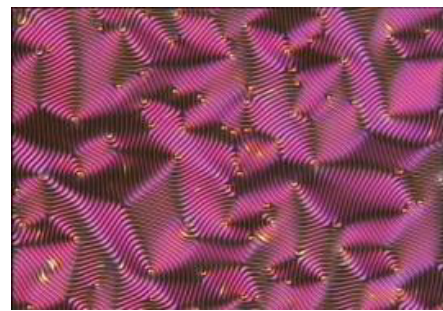
Columnar phases (Col) are formed mainly by discotic mesogens (liquid crystals formed by disk-like molecules that are stacked together into columns). The columnar phase usually forms a hexagonal lattice because this arrangement allows the densest packing of columns. Besides, discotic molecules can form a nematic phase (N_D) just like calamatic mesogens. Accordingly, different packings of these discotic mesogens give rise to different types of columnar phases.

Thermotropic liquid crystalline phases can be identified using many different techniques such as optical polarizing microscopy, miscibility studies, light scattering, X-ray and neutron diffractions, spectroscopic techniques and differential scanning calorimetry [25-26]. However, the most useful but qualitative technique for identification of the liquid crystal phase is optical polarizing microscopy. Liquid crystal phases possess characteristic textures when viewed in polarized light under a

microscope. These textures result from defects in the structures. Defects in liquid crystals can be classified as point, line and wall defects. Disclination is an example of a line defect, which is unique to liquid crystals and it is a discontinuity of orientation of the director. This effect gives typical textures such as schlieren texture of a nematic phase, fingerprint of a cholesteric (chiral nematic) phase, fan-shaped texture of a smectic A phase and focal conic texture of a smectic A phase [27] (**Figure 1.10**).



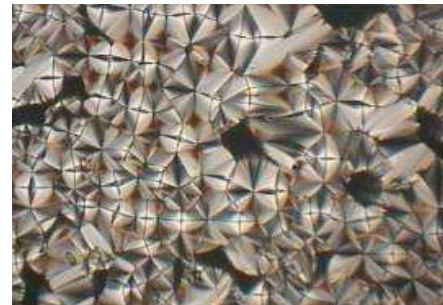
(a) Schlieren texture of a nematic phase



(b) Fingerprint of a cholesteric phase



(c) Fan-shaped texture of a smectic A phase



(d) Focal conic texture of a smectic A phase

Figure 1.10: Typical textures of liquid crystalline phases (adopted from [27]).

Lyotropic Liquid Crystal

Lyotropic liquid crystals are formed when solvents like water or glycerin are added to amphiphilic materials (e.g. surfactants) at a certain composition. Surfactants in dilute aqueous dispersions may assemble into a variety of micellar aggregates above both a critical concentration and temperature, giving rise to different geometrical shapes [29-30]. These are controlled by geometrical constraints and by the interface curvature, which in turn are determined by intra-micellar forces occurring in different planes [31]. However, as the surfactant concentration increases, inter-micellar forces become progressively more important and may cause either change in critical packing parameter (shape transition) or disorder/order transition to liquid crystalline state [32-34].

Many lyotropic phases have been observed and their detailed structures reported for the different surfactant systems [29,35-36], such as the metastable gel phase, which has a lamellar structure with solid-like chains. However, the most commonly observed phases are the fluid lamellar, hexagonal and cubic phases. The generic mesophase behaviour of lyotropic systems [37] is shown in **Figure 1.11**. Their structures can be characterized by an optical polarizing microscope and X-ray diffraction techniques. In brief, in polar solvents (e.g. water) the aggregation of the surfactant can be defined as normal micellar solution (L_I), normal discontinuous cubic (I_I), normal hexagonal (H_I), normal bicontinuous cubic (V_I) and lamellar (L_a), whereas in non-polar solvents (e.g. paraffin) the surfactant aggregates and forms an inverted micellar solution (L_{II}), inverted discontinuous cubic (I_{II}), inverted hexagonal (H_{II}) and inverted bicontinuous cubic (V_{II}).

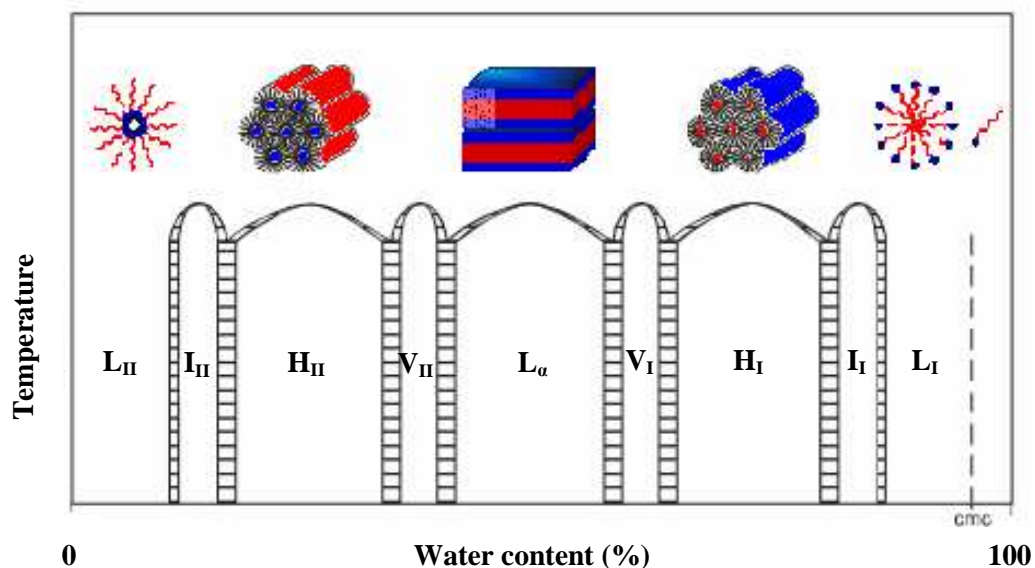


Figure 1.11: Generic phase behaviour of lyotropic liquid crystalline phases (adapted from [37]).

The *lamellar phase* (L_a) is similar to smectic A in the thermotropic system [21-22,29,37]. It consists of a layered arrangement of amphiphilic molecules. The molecular packing in the lamellar structure consists of bilayer, in which two layers are made up of intertwining non-polar chains opposite directed molecules, and where the polar head groups meet it is separated by a layer of water (**Figure 1.11**). The thickness of the layer is generally less than twice the length of the molecules. This arrangement causes the heads of molecules to be in contact with water, while the hydrocarbon chains are separated from the water.

The *hexagonal phases* have a molecular aggregate ordering which corresponds to a hexagonal arrangement. There are two types of hexagonal liquid crystalline phases such as normal hexagonal phase (H_I) and inverted/reversed hexagonal phase (H_{II}) [21-22,29,37]. The normal hexagonal phase consists of micellar cylinders of indefinite length packed in a hexagonal arrangement, whereas the inverted hexagonal phase is basically the same as normal hexagonal phase except the micellar cylinders are inverted with the non-polar chain radiating outwards from the cylinders.

Cubic phases are optically isotropic and very viscous [21-22,29,37]. The high viscosity results from the lack of shear plane within the structure, thus allowing a sliding movement. This phase is based on three cubic lattices: primitive, face-centered and body-centered cubic. It can be classified into four classes subdivided into two sets of structures. The first set is the discontinuous cubic phase (I), while the second set is the bicontinuous cubic phase (V). In the discontinuous cubic phase, the small spherical micelles are packed in cubic lattice, whereas the micelles in the bicontinuous cubic phase are arranged in a 3-D network, in which the single bilayer aggregate has both positive and negative curvatures. When observed by optical polarizing microscopy in cross configuration, the cubic phase has an optically dark texture (lacking in birefringence) and is thus difficult to detect. Both sets exist as normal (I_I, V_I) and inverted/reversed phases (I_{II}, V_{II}).

1.3.1 Application of Liquid Crystals

Lyotropic liquid crystalline phases based on self-assembly of surfactants in aqueous media have been extensively studied not only for their fundamental interest but also for practical applications. Indeed, liquid crystals have interesting applications in various fields such as in detergents and the cosmetics industry [38-39], in pharmacy as vehicles or solubilization media of active compounds, in biology for membrane function, vesicles and in the extraction of peptides and protein [24,40-41], in the food industry [42-44], and in emulsion technology as stabilizers [45-46].

Many kinds of ionic and nonionic surfactants can self-assemble into ordered lyotropic liquid crystal phases at high surfactant concentrations. However, sugar-based surfactants have recently drawn much attention due to their nonionic, less toxic and bio-surfactant properties [47-50], and of these, glycolipids are among the most popular because they can be found in nature [51] or synthesized from cheap natural resources such as alkyl polyglycosides (APGs) [52-54]. Therefore, new mimic branched-chain glycolipids, a kind of interesting sugar-based surfactant have been synthesized and chosen in this particular study.

1.3.2 Glycolipids Liquid Crystal

In recent years, glycolipids have attracted much attention among formulators and researchers as a replacement of the common synthetic surfactants in household products, personal care products and pharmaceutical products, because of the detrimental effects of synthetic surfactants on the environment and humans. Glycolipids have great advantages compared to common surfactants not only because they are nonionic, environmentally friendly and non-toxic in nature as surfactants and emulsifying agents [12,52] but also because they are readily biodegradable and biocompatible [51]. They can be produced at relatively low cost from locally available raw materials such as palm oil and sugar [53-54]. Moreover, compared to other synthetic surfactants, they can self-assemble into different lyotropic liquid crystalline phases that are stabilized by the hydrogen bonding interaction between the sugar moieties [55-56]. The chirality of the sugar moieties also plays an important role in their thermotropic and lyotropic phase behaviours [57].

Glycolipids are classified as *amphiphilic* molecules comprising two different kinds of moieties e.g. polar/non-polar, rigid/flexible, bulky/planar and hydrophobic/hydrophilic, which can self-assemble in various structures. Glycolipids are also referred to as *amphitropic*. These form interesting phase behaviours, namely thermotropic phases in dry/pure form and lyotropic phases when in contact with polar solvents such as water [21,29]. Typical examples of amphitropic materials are mono-alkylated glycolipids (octyl- β -D-glucopyranoside) [54] and branched-chain glycolipids [48-49]. Recently, self-aggregation of branched-chain glycolipids at nanometer scale in diluted aqueous dispersions have been reported [58-59].

In biological sciences, besides solubilization of biological membranes, glycolipids are widely used for the production of lipid-surfactant and protein-surfactant membranes [8,12,24,50]. Moreover, possible biological functions involved in certain glycolipids head groups may make glycolipids particularly attractive as a new type of lipids for liposomal drug delivery systems [6-8,53]. They also exhibit a large spectrum of useful applications, such as a stabilizer of hydrocarbon foam, cleaning agents (e.g. household soaps), cosmetics emulsifiers, and in the synthesis of nano-structure materials [38-39,45,53,57,60].

1.4 REVIEW ON HEXOSOMES

1.4.1 Formation of Hexosomes

The formation of well-defined aggregating states with controllable morphology and structure at the nanometer scale is of technological importance for a wide range of practical applications [61-62]. The self-assembly structure formed depends not only on the type of surfactant used but also on many external factors, such as temperature, composition and solvent [63-64]. Thus, to enlarge the possible applications of self-assembly structures, the liquid crystalline phase such as the inverted hexagonal, H_{II} has to be dispersed into an aqueous media. In order to stabilize the obtained particles against coalescence or coagulation, an appropriate stabilizer, such as Pluronic F127, is used [65-69]. However, this stabilizer may change the internal structure of the dispersed particle, depending on the quantity used.

Previous studies have focused mainly on the self-assembly of an interesting class of amphiphilic lipids such as monoglycerides, phospholipids, urea-based lipids, and glycolipids. These self-assemble spontaneously in water to form various well-ordered inverted-type nanostructures such as a fluid isotropic micellar phase (L_{II}), a lamellar phase (L_{α}), an inverted hexagonal phase (H_{II}), and a discontinuous cubic (V_{II}) liquid crystalline phase [64,69-78]. The important breakthrough in the idea of dispersing the viscous non-lamellar bulk phases to form the hexosomes (aqueous dispersions of a H_{II} phase) and cubosomes (aqueous dispersions of a V_{II} phase) was made more than 18 years ago by Larsson and co-workers [79-80]. The H_{II} and V_{II} systems comprising aqueous nano-channels embedded in continuous hydrophobic matrices, are interesting in both fundamental and applied research [61-62,83-86]. This unique characteristic is fundamental in applications, where the mesophase structure must remain intact in dilute aqueous media (i.e. excess of water). In fact, the preparation of stable colloidal

dispersions of the inverted hexagonal and cubic liquid crystalline phases (hexosomes and cubosomes) has opened exciting new opportunities for applications of lyotropic liquid crystals [65,87-91].

Here, we will discuss further the formation of hexosomes. Hexosome particles show internal arrangements of a hexagonal symmetry (**Figure 1.12**), which is obviously good illustration for the presence of an H_{II} mesophase structure. As the observed hexagonal tubes in the hexosome particles are infinitely long (or limited by the particle size), there is no periodicity in the direction of the cylindrical tube, explaining why only the hexagonal arrangement or parallel lines are observed in Cryo-TEM measurement. For hexosomes, the hexagonal motif is still present in some regions after 40° of tilting. This comes from the fact that hexosomes are not really single crystals because the longitudinal axis of the cylinders is bent and therefore, it is more likely that some crystallographic planes are parallel to the electron beam after a very large tilt. The presence of curved tubes in the hexosome particles is probably associated with the stabilization mechanism of hexosomes. Hexosome stabilization requires that two different surfaces are stabilized. One surface is at the outside of the cylinder tubes which is completely lipophilic and easily stabilized by a surfactant layer, and the second surface is at the end of the tube where both the hydrophilic and lipophilic parts of the molecules are in contact with water. These characteristics give the hexosomes image of hexagonal or close to spherical-shaped particles under Cryo-TEM [89].

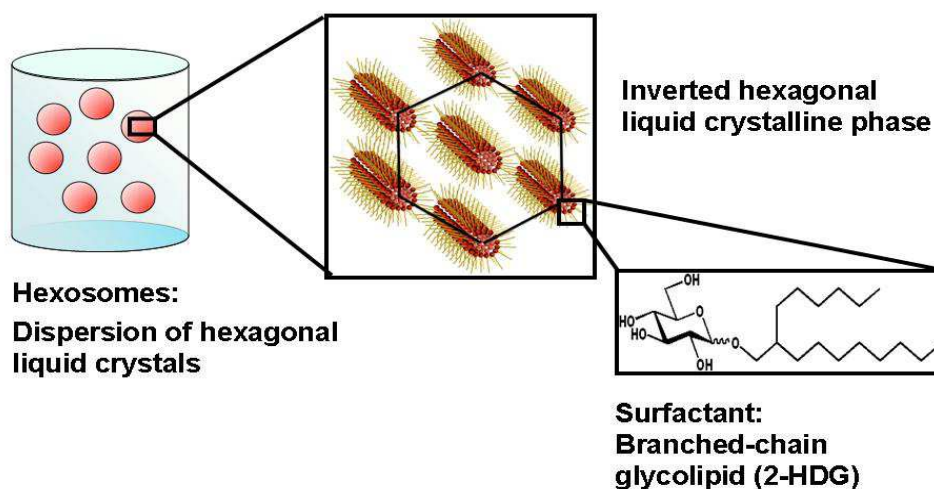


Figure 1.12: Example of hexosomes formation from branched-chain glucosides.

In literature, the following emulsification methods have been introduced for the formation of lipid-based colloidal nanostructured dispersions:

- The application of high-energy input such as ultrasonication, microfluidization, and homogenization [69,80-81].
- A multi-step premixing method including the formation of a dry lipid/stabilizer film and the application of mechanical stirring during the hydration of the dry film. Stable glycolipid cubosome particles were formed [92].
- A dilution process (spontaneous formation) of lipids in the presence of ethanol. A method recently introduced by Spicer et al. for the formation of stable dispersions of submicron-sized cubosomes [93].
- The application of microfluidization followed by heat treatment at 125 °C. A new method proposed for the formation of dispersions (hexosomes and cubosomes) with narrow particle distributions and a good colloidal stability [94].

Specifically, a major issue in the investigation of the morphology and the internal nano-structure of the dispersed soft nano-structured aqueous dispersions is the appropriate choice of analytical methods that allow structural characterization of the system. Different techniques such as small angle X-ray scattering (SAXS) [62,64], cryogenic transmission electron microscopy (Cryo-TEM) [95], atomic force microscopy (AFM) [96], dynamic light scattering (DLS) and ^{13}C NMR [67,97] have been applied.

1.4.2 Hexosome Stability

The stability of the dispersed hexosomes as a function of composition and homogenization time can be evaluated by Stability Analyzer (e.g. LUMiFuge or Turbiscan) tests; indirect determination can also be made by DLS measurements of particle size distributions and Cryo-TEM imaging [87-89].

The stability of nano-structured dispersion upon storage time can be measured by dynamic light scattering (DLS). Here, particle size distribution and polydispersity of hexosomes (H_{II} particles) is monitored and recorded. Thus, the destabilization process can be determined as a function of time. Besides, the hexosomes particles size and images also could be measured and observed by Cryo-TEM. However, this measurement is without the presence of continuous phase. Thus, the size obtained is much smaller compared to the size measured by DLS.

Dispersion stability can be examined using Stability Analyzer measurements. With this instrument, lack of stability (stability to aggregation, particle precipitation and separation) is measured by the extent of centrifugation-induced changes in light transmission as a function of both time and position in the sample tube. With time,

there will be an increase in transmission at the bottom of the tube, indicating loss of stability. The stability analyses of hexosome dispersions by the Stability Analyzer technique can confirm our findings concerning the influence of the quantity of polymer and the length of the homogenization periods.

1.4.3 Application of Hexosomes

Hexosomes as self-assembled nano-objects are candidates for constructing novel composite and matrices mimic biological systems in the formation of new nanoparticulate carriers for delivering active biomolecules such as drugs, peptides and so on [62,87-89]. These biologically relevant phases have been shown as potential drug delivery systems [61-62]. Studies on the applicability of fully hydrated inverted liquid-crystalline phases (H_{II} phase) for accommodation and controlled release of solubilized drugs have been conducted extensively by Boyd and co-workers [62]. There is an increasing interest in utilizing nano-structured aqueous dispersions of non-lamellar phases in various applications due to properties that are identical to those of non-dispersed phases [98-99], the high interfacial area and the capability of solubilizing amphiphilic components [100] and their use as nano-carriers for loading bioactive materials and drugs [101-104].

1.5 REVIEW ON VESICLES

1.5.1 Formation of Vesicles

Phospholipid vesicles (liposomes) were first described in the 1960s by Bangham et al [105]. It has been shown that phospholipids spontaneously form closed structures when hydrated in aqueous solutions. Liposomes are also called natural bio-surfactant vesicles, and can be found in human, animal and plant cells. These liposomes or lipid vesicles, are spherical (**Figure 1.13**) [6-8,78]. Their self-closed structures are composed of curved lipid bilayers, enabling entrapment of the solvent into their interior. Because lipids are both hydrophobic and hydrophilic (amphiphathic) in aqueous medium, their thermodynamic phase properties and self-assembling characteristics evoke entropically driven sequestration of their hydrophobic regions into spherical bilayers. Those layers are referred to as lamellar [1-2,7].

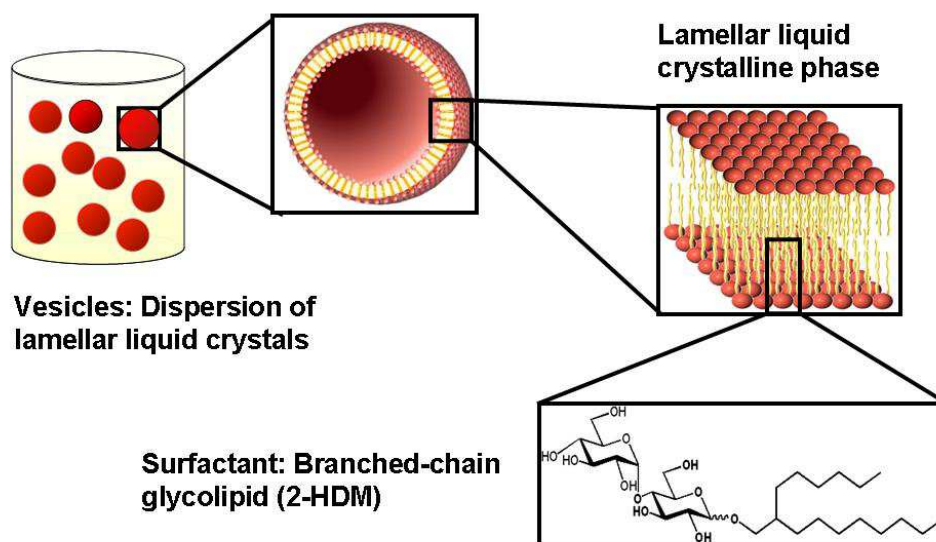


Figure 1.13: Example of vesicles formation from branched-chain maltosides.

Vesicles can be large or small and may be composed of from one to several hundred concentric bilayers. With respect to the size and the number of lamellar, large multilamellar vesicle (MLVs), large and small unilamellar vesicles (LUVs and SUVs) can be distinguished. Vesicles vary in charge and size depending on the method of preparation and the lipids used (MLV size range is 0.1–5.0 μm , SUV size range is 0.02–0.05 μm and LUV size range is from 0.06 μm) [6,8].

The head group charge is important in influencing the preferred structures and structural transition from micelles to vesicles. When the surface charge and the head group repulsion are reduced, the separation of the head group is also reduced and the system will tend to a more lamellar (bilayer) structure [33]. Often, above certain concentrations and under certain experimental conditions such as electrolyte, hydrophobes and pH, these micelles will structurally reorganize to give these vesicles [7]. The concentration at which the appearance of vesicle is detectable is called the critical vesicular concentration (CVC) [6,105].

The dynamics of spontaneous vesicle formation is induced by several factors including the pH of the solution, temperature, electrolyte concentration and mixed charge surfactants. The presence of electrolytes and substrates can modify the surface and packing of surfactants in aggregates, and subsequently induce structural changes such as micelle-to-vesicle, lamellar-to-vesicle and cylindrical micelle-to-vesicle [6-7,105-109].

Vesicles can be prepared in a laboratory using both synthetic and natural surfactants from techniques such as ethanolic injection, thin film hydration, dissolution in electrolyte solution and pH-induced technique. The dynamics and kinetics of vesicle formation have attracted many researchers, especially for pharmaceutical purposes such as drug delivery systems [10-12]. In general, two major methods are used to make

vesicle systems for drug delivery. The first is simple hydration of a lipid followed by high-intensity agitation using sonication or a high-shear impeller. Vesicles are then sized by filtration or extrusion. The second method is emulsion. Phospholipids are first dissolved in an organic solvent (such as methylene chloride) and then added under control to an aqueous medium with vigorous agitation. Subsequently, the organic solvent is removed under reduced pressure. The resulting liposomal dispersion is also sized by filtration or extrusion. In general, the first method yields multilamellar products and the second method yields products with few lamellar [105].

Vesicles can also be prepared by adding an appropriate amount of a salt (NaCl) to a surfactant solution [109]. The formation of vesicles is spontaneous and generally takes place over a period of a few minutes. Furthermore, in some cases, the change of pH of the surfactant solution will also change the counter ions of pH of the surfactant molecules, thus the vesicle can be produced in a certain range of pH of the surfactant solution. The titration of dilute acid to alkaline clear solutions of fatty acids, in the range of $C_8 - C_{18}$, produces a turbid solution indicating the presence of vesicles [110]. For example, alkylphosphoric acid and alkylphosphonic acid have shown similar behaviours with fatty acids where vesicles are formed by varying the pH of the surfactant solutions [111].

1.5.2 Formation of Mixed Vesicles

The stability of a mixed vesicle system can be understood by considering the possibility of a spontaneous curvature of bilayers resulting from asymmetric partitioning of different amphiphiles between two membrane leaflets [112-116]. Analysis of the bending energy of such systems took into account the entropy of mixing in the membrane and an additional interaction between the amphiphiles in the bilayer.

Nevertheless, the growth of vesicle size upon the addition of micelle-forming surfactant is still not very well understood, since simple models predict an opposite behaviour, namely, a decrease in the vesicle size due to added surfactants [112,116]. Indeed, the concentration of surfactant molecules should be higher in the outer leaflet (compared to inner one) of a spherical vesicle since the curvature has the same sign as the spontaneous curvature of the micelle-forming surfactant [117-118]. In some cases, there is an increase of the spontaneous curvature of the bilayer, favouring the formation of vesicles with small radii [4-6,8]. On the other hand, the more common observation of the increase in the vesicle size remains unexplained.

1.5.3 Vesicle Stability

Generally, vesicles are kinetically more stable than micelles. It is very important to be able to control the stability of the vesicles, so that they can be stored for a long period of time. For example, a lipidic vesicle-encapsulated drug for pharmaceutical applications must be stable for at least 18 months to 3 years, besides being stable at room temperature [119].

Stable vesicle suspension can only be obtained using surfactants that form liquid-state bilayers. For example, an ionic surfactant vesicle suspension has been reported to remain stable for two months at room temperature [120]. However, the investigation for stable vesicle dispersion is still difficult. Commonly, the vesicles are polydispersed, non-reproducible and the outcomes depend on the preparation methods and precursor intermediates. Fusion and aggregation of vesicles over time makes the analysis much more difficult.

In solution, vesicles are subjected to instabilities which can lead to shape transformation. Vesicle fusion is common as a result of two vesicles being in contact. Since the membrane is a liquid-like assembly, smaller vesicles can penetrate in and out of larger vesicles without destroying their structures. However, small unilamellar vesicles are more stable than large unilamellar and multilamellar vesicles. The high curvature of the bilayer requires more energy input into the system to form these small unilamellar vesicles [121]. Thus, sonication and vigorous agitation can fulfill this need. Unfortunately, small unilamellar vesicles can only maintain their stability for periods of days or weeks. This stability can be attributed to the existence of inter-vesicular repulsive interactions, which prevent coalescence/coagulation of the vesicles [6,8].

1.5.4 Application of Vesicles

All vesicle structures (MLVs, LUVs and SUVs) have many interesting physical and chemical properties such as osmotic activity, permeability of their membranes to different solutes, solubilizing power and interaction with hydrophilic and hydrophobic solutes or aggregation behaviour that can depend on temperature, chemical composition and surface characteristics of the membrane [6-8]. They provide a number of important advantages over other dispersed systems including high encapsulation of water-soluble drugs, lipid economy, and reproducible drug release rates. For example, vesicle preparation can replace some commercial products containing toxic solubilizing agents, thus providing useful alternative dosage forms for intravenous administration [10-11]. Pharmaceutical researchers use the tools of biophysics in evaluating liposomal dosage forms. Such combination of multidisciplinary activities is reflected in the increasing number of review articles and monographs incorporating both the physics and therapeutic applications of liposomes [12].

1.6 REVIEW ON NANO-EMULSIONS

1.6.1 Formation of Nano-emulsions

Nano-emulsion is a dispersion of two immiscible liquids, usually water and oil, which are generally stabilized by a surfactant. It has droplet radius in the nanometer scale ranging from 20–200 nm. Nano-emulsion is also sometimes referred to as miniemulsion, ultrafine emulsion and submicron emulsion [122]. Due to the small droplet size, nano-emulsion is stable against sedimentation or creaming and visually it appears transparent or translucent bluish [122]. The transparent or translucent bluish property of nano-emulsion is due to Tyndall effect or Tyndall scattering. Tyndall effect is light scattering by particles in a colloid suspension, where the intensity of the scattered light depends on the fourth power of the frequency. As a result, blue light is scattered much more strongly than red. At the same time, the longer wavelength light tends to be transmitted, while the shorter wavelength light is reflected via scattering. This effect is seen when light-scattering particulate-matter is dispersed in an otherwise light-transmitting medium, when the cross-section of an individual particulate is in the range of roughly between 40 and 900 nanometers, i.e., somewhat below or near the wavelength of visible light (400–750 nanometers).

Nano-emulsions can be dispersed in several ways and the most common being oil-in-water (o/w) and water-in-oil (w/o) nano-emulsions (**Figures 1.14** and **1.15**) [39,122]. The type of nano-emulsion dispersion is highly dependent on the nature of surfactant used in the system and nano-emulsion preparation. According to Bancroft's postulate, the phase in which the surfactant is most soluble is the continuous phase [14,17,39,122], meaning hydrophobic surfactants will form w/o emulsions whereas hydrophilic surfactants will form o/w emulsions.

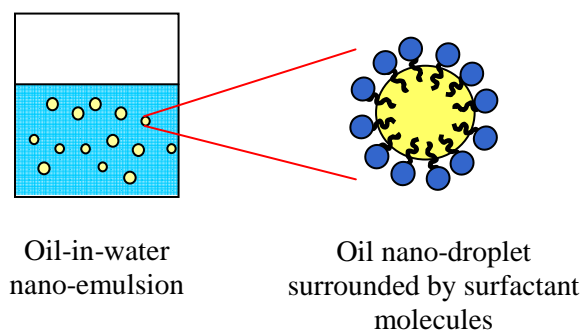


Figure 1.14: A schematic diagram of oil-in-water (O/W) nano-emulsion.

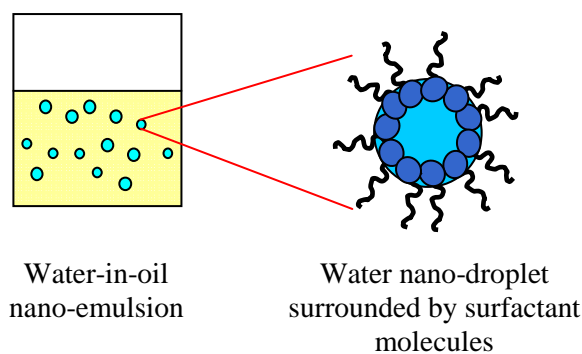


Figure 1.15: A schematic diagram of water-in-oil (W/O) nano-emulsion.

Unlike microemulsions, which are thermodynamically stable and form spontaneously, nano-emulsions being thermodynamically unstable require energy input for their preparation (kinetically stable). Nano-emulsion preparation is usually via two main methodologies – the high-energy input methods (e.g. high pressure homogenization, high shear stirring and ultrasound generator) and the low-energy emulsification methods (e.g. phase inversion temperature (PIT) method introduced by Shinoda et al. [123-124] (**Figure 1.16**) and the phase inversion composition (PIC) method [122,125] (**Figure 1.17**).

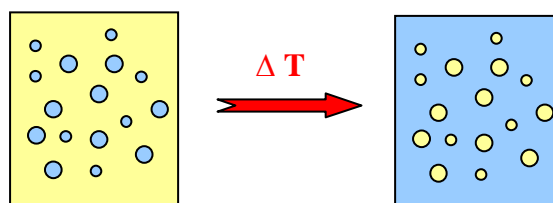


Figure 1.16: Nano-emulsion formation by PIT emulsification method.

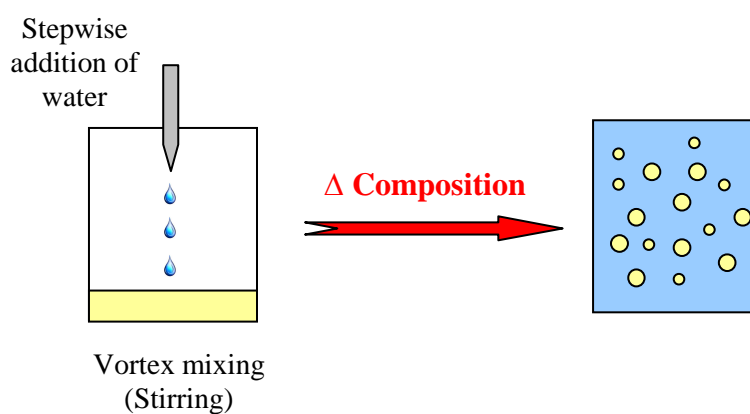


Figure 1.17: Nano-emulsion formation by PIC emulsification method.

In this research, nano-emulsions were prepared by the PIC method. The preparation method involved keeping the temperature constant, but changing the composition during emulsification (e.g. by adding water to an oil-surfactant mixture to obtain an o/w nano-emulsion). After the phase inversion, low polydispersity droplets of oil-in-water or water-in-oil were formed.

1.6.2 Nano-emulsion Stability – Destabilization Mechanism

The main trigger for nano-emulsion breakdown is Ostwald ripening, where molecular diffusion of the disperse phase from the small droplets to the bigger ones takes place as a consequence of the difference in Laplace pressure (i.e. different solubility) of droplets of different sizes. One way to increase the stability of nano-emulsions against Ostwald ripening is by reducing the polydispersity to a minimum and by using oils with very low solubility in the continuous phase [122,126-127]. The long-term stability of nano-emulsions against flocculation or coalescence makes them unique.

Emulsion stability is referred to as the ability of an emulsion to resist change with time. Since the emulsion is thermodynamically unstable, they are expected to undergo destabilization after a period of time leading to a total phase separation. For this reason, an emulsifier is used to increase the stability of the emulsion system. The instability of emulsion discussed is referred to as physical instability such as creaming/sedimentation, flocculation, coalescence, and Ostwald ripening [4,6,14,17-18,39,42,122].

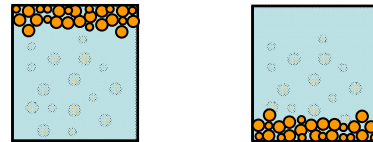
There are four nano-emulsion breakdown/destabilization processes (**Figure 1.18**):

- a) *Creaming/Sedimentation* of emulsion droplets happens due to the density difference between the two phases which are forms of gravitational separation. For example, in the creaming process the oil droplet (o/w emulsion) moves upward to the surface due to its lower density compared to that of water.

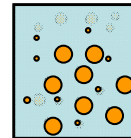
- b) *Ostwald ripening* is a diffusive transfer of disperse phase from smaller droplets to larger ones under the influence of Laplace pressure difference. Ostwald ripening destabilization occurs especially in a polydispersed emulsion facilitated by the presence of micelles in the continuous phase. The micelles solubilize the oil molecules and transport them from one droplet to another. In other words, the micelles enhance Ostwald ripening by increasing the solubility of oil in water, allowing the oil molecules to diffuse from the small droplets to the larger ones.
- c) *Flocculation* is an aggregation process of two or more droplets to form flocs/clumps together. Flocculation only happens after a collision of droplets. After a collision, particles may either move away from one another or form a permanent aggregate. This is highly dependent on the type of interaction (attractive and repulsive) between the droplets. When the attractive force is dominant, collision of droplets will lead to floc formation. The flocculation is a reversible process, since the droplets will re-disperse when subjected to gentle agitation. This flocculation process enhances the gravitational separation rate and is a significant destabilization process in dilute emulsion. It decreases the shelf life of the emulsion.
- d) *Coalescence* is another emulsion destabilization mechanism. Coalescence is a process where two or more droplets merge to form a single larger droplet which is the most thermodynamically stable condition. This process can only happen when the droplets are close together and the interfacial membrane between the droplets is disrupted. In general, the forces acting between the droplets and the resistance of droplets against membrane rupture are the major factors affecting the coalescence process and are important for a concentrated emulsion. The stiffness of the interfacial layer is the key to the droplet coalescence, which

creates an energy barrier that has to be overcome before the thermodynamically stable state is reached. Therefore, it is necessary to introduce a strong interfacial layer to an emulsion in order to enhance the emulsion stability. Coalescence often happens when the droplets are close to one another. At this point, the attractive force is greater than the repulsive force and causes failure of the interfacial layer to protect the droplets. Consequently, the droplets will merge and the energy of the droplet will fall into a deep minimum, which is an irreversible process.

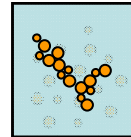
a) Creaming/Sedimentation



b) Ostwald Ripening



c) Flocculation



d) Coalescence

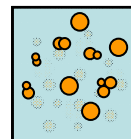


Figure 1.18: A schematic diagram of nano-emulsion breakdown/destabilization mechanisms.

1.6.3 Nano-emulsion for Drug Delivery System

Another interesting group of drug delivery system is nano-emulsion. It is part of a broad class of multiphase colloidal dispersions. Although some lyotropic liquid crystalline phases such as micellar, mesophases and microemulsions may appear to be similar to nano-emulsions in composition and nano-scale structure, such matrices are actually quite different.

Nano-emulsions act as efficient carriers for drugs, facilitating administration by various routes such as parenteral, oral, ocular, pulmonary and transdermal delivery. It has been reported in numerous publications that nano-emulsion effectiveness is directly related to the droplet size [128-134], while other reports have shown no such correlation [135]. Nevertheless, the high interfacial area in nano-emulsions may allow a higher solubilization of drugs with amphiphilic properties, which in turn may favour their absorption in skin and the gastrointestinal tract. The modelling of drug release from delivery systems is important for understanding the transport mechanisms.

Basically, the main mathematical expressions used to describe the kinetics of drug release and the discernment of the release mechanisms are Fick's law, zero order [136-137], first order [138-139], Higuchi law [140-141], Weibull [142-145] and the Korsmeyer-Peppas models [146-149]. On the mechanism of drug release from nano-emulsions however, there is a lack of information on how the experimental results fit these mathematical models. For a better understanding of drug release from nano-emulsions, experimentally released profiles can be compared with those calculated by applying different mathematical expressions.

1.6.4 Proposed Nano-emulsion System

In this research, the reference O/W nano-emulsion system selected to study the effect of the two branched-chain glycolipids surfactants in oil droplet size, long term stability and release properties of a model drug is water/Cremophor[®] EL/medium chain triglyceride (MCT) oil system. There are several reasons for the selection of oil phase and nonionic surfactants. Firstly, the oil phase is a medium-chain triglycerides (MCT) oil, consisting of 6 to 12 carbons fatty acid esters of glycerol. This oil is suitable for pharmaceutical applications. One benefit of the oil is that it helps in burning off excess calories and weight loss in human bodies. Secondly, the main nonionic surfactant is Cremophor[®] EL which is obtained by reacting castor oil with ethylene oxide in a molar ratio of 1:35 and its hydrophilic-lipophilic balance lies between 12 and 14. Likewise, branched-chain glycolipids (2-hexyldecyl- β (/α)-D-glucoside (2-HDG) and 2-hexyldecyl- β (/α)-D-maltoside (2-HDM)) are also nonionic surfactants, acting as the second surfactant in the nano-emulsion formulation. Both of them are biocompatible, easily biodegradable, non-toxic in nature and suitable for cosmetic and pharmaceutical applications.

Sadurni et al. [150] reported nano-emulsion formation in the water/Cremophor[®] EL/MCT oil system at water content above 50% with oil-surfactant ratios between 10/90 and 60/40. These nano-emulsions, whose droplet size is highly dependent on oil-to-surfactant ratio, showed high kinetic stability. The incorporation of a small concentration of the novel glycolipids in nano-emulsions of the reference system is expected to have an influence in their properties. Therefore, this study will contribute to the basic knowledge of nano-emulsions and may allow for expansion on the application field of these novel surfactants.

1.7 RESEARCH OUTLINE

1.7.1 Objectives of the Research

The objectives of this research are to

- synthesis various types of branched-chain glycolipids as a main surfactant in formulation;
- determine the physico-chemical properties of branched-chain glycolipids;
- study the behaviour of different types of branched-chain glycolipids in binary colloidal dispersions in the formation of hexosomes and vesicles;
- formulate and investigate the stability of ternary water/non-ionic surfactant/oil systems (nano-emulsions) from branched-chain glycolipids; and
- evaluate the efficiency of incorporation and release properties of drugs from nano-emulsion systems (drug delivery study).

1.7.2 Organization of Research

Chapter 1 is the *Introduction and Literature Review*. It gives an introduction to the proposed research, literature review of surfactants, liquid crystals, hexosomes, vesicles and nano-emulsions and the research outline (objectives and organization of the research).

Chapter 2 describes the *Synthesis of Branched-Chain Glycolipids*. This chapter explains the synthesis techniques applied in this research. The synthesis procedure comprises three stages: the peracetylation (protection), glycosidation (alkylation) and deacetylation (deprotection) procedures. In this work, two synthetic branched-chain

glycolipids will be synthesized namely 2-hexyldecyl- β (/ α)-D-glucoside (2-HDG) and 2-hexyldecyl- β (/ α)-D-maltoside (2-HDM), which are technical grade (β -dominant anomeric mixtures) as shown previously in **Figure 1.1**.

Chapter 3 describes the *Physico-chemical Characterization of Branched-Chain Glycolipids*. A set of fundamental investigations will be conducted for their emulsifying strength including the measurements of their thermal properties (decomposition and melting temperatures) and morphology (thermotropic and lyotropic properties in dry and hydrated states).

Chapter 4 describes the *Binary Phase Behaviour of Branched-Chain Glycolipids/Water System towards Formation of Hexosomes and Vesicles*. This chapter explains the critical aggregation concentration (CAC), binary phase behaviour of 2-HDG and 2-HDM in aqueous medium and the preparation of hexosomes and vesicles. The stability of hexosomes and vesicles will be tested upon the storage time. The effect of addition of anionic surfactant to the glycolipids vesicles also will be investigated.

Chapter 5 describes the *Influence of Branched-Chain Glycolipids on Ternary Nano-emulsion as Drug Delivery Systems*. The present work investigates the effect of two branched-chain glycolipids in oil droplet size, long term stability and release properties of a model drug from the O/W reference nano-emulsion system of water/Cremophor[®] EL/medium chain triglyceride (MCT) oil. The effect of these glycolipids on the reference O/W nano-emulsion will be studied by partially replacing Cremophor[®] EL with the glycolipids.

Chapter 6 presents *Conclusions*. This chapter summarises all findings, including some motivation for conducting future work involving various types of branched-chain glycolipids.

CHAPTER 2:
SYNTHESIS OF BRANCHED-CHAIN GLYCOLIPIDS

2.1 INTRODUCTION

Natural and synthetic glycolipids bio-surfactants are nonionic, amphiphiles, claimed to be non-toxic and biodegradable [50]. Most of the natural glycolipids such as monogalactosyl diacylglycerol (MGDG) and digalactosyl diacylglycerol (DGDG) (**Figure 2.1**) have branched alkyl group that may consist of up to 24 numbers of carbon [51,53]. The branched structures contribute to the bulkiness of hydrophobic region and a cunning drive force in arranging the molecules within the cell membrane.

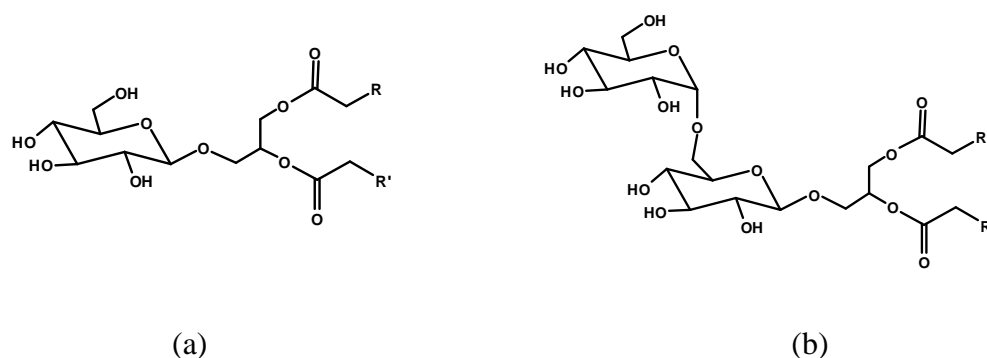


Figure 2.1: Chemical structures of (a) monogalactosyl diacylglycerol (MGDG) and (b) digalactosyl diacylglycerol (DGDG).

Extracting pure natural branched-chain glycolipids is still impracticable for industrial scale. There were also attempts of synthesizing of the inspiring structures, however, total syntheses are rarely achievable. Alternatively, syntheses of mimic structures have taken place to fulfil the demand of similar branched-chain glycolipids. Due to the costly production of pure natural glycolipids and complexity of synthesizing them, different strategies of synthetic substitutes are always been involved [48-49].

It has been very well known acid catalyzed glycosylation between acetal group of a sugar and an alcohol to produce simple glycolipids. Similarly, synthetic glycosides have been produced from Lewis acid glycosylation between sugar and Guerbet alcohols to produce branched alkyl chain glycolipids [49]. The procedure was used in the

preparation of two technical grade branched-chain glycolipids dedicated to their physico-chemical characterizations, binary and ternary phases investigation. Both have the same hydrophobic chain length but different hydrophilic head groups and polarities namely 2-hexyldecyl- β (/ α)-D-glucoside (2-HDG) and 2-hexyldecyl- β (/ α)-D-maltoside (2-HDM) as shown in **Figure 2.2**. They were produced by avoiding the column chromatography step to give β -dominant (~90%) anomeric mixtures.

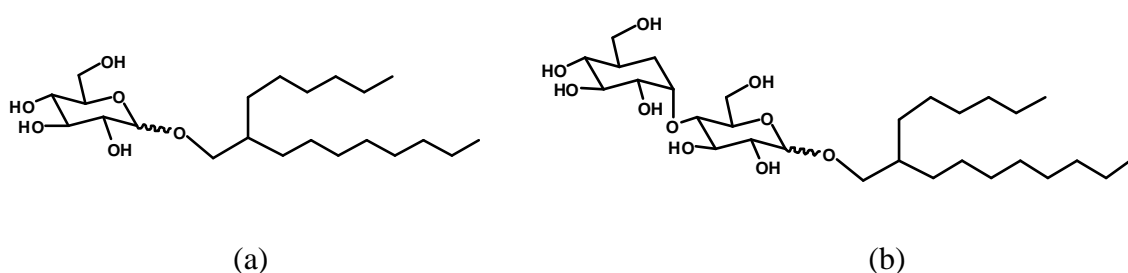


Figure 2.2: Chemical structures of (a) 2-hexyldecyl- β (/ α)-D-glucoside (2-HDG) and (b) 2-hexyldecyl- β (/ α)-D-maltoside (2-HDM).

The syntheses part is comprised of three major stages including peracetylation (protection), glycosidation (alkylation) and deacetylation (deprotection). The synthesis of 2-HDG was only involving two stages; glycosylation and deacetylation procedures because β -D-glucose pentaacetate is commercially available and relatively cheaper than preparation of peracetylated glucose. However, the synthesis of 2-HDM was involving all three major stages because peracetylated maltose is more expensive than the commercial precursor.

In the following part, the chemicals and materials, synthesis procedures and the instruments used will be described. All collected data and spectra from the synthesis works will be further analyzed.

2.2 MATERIALS

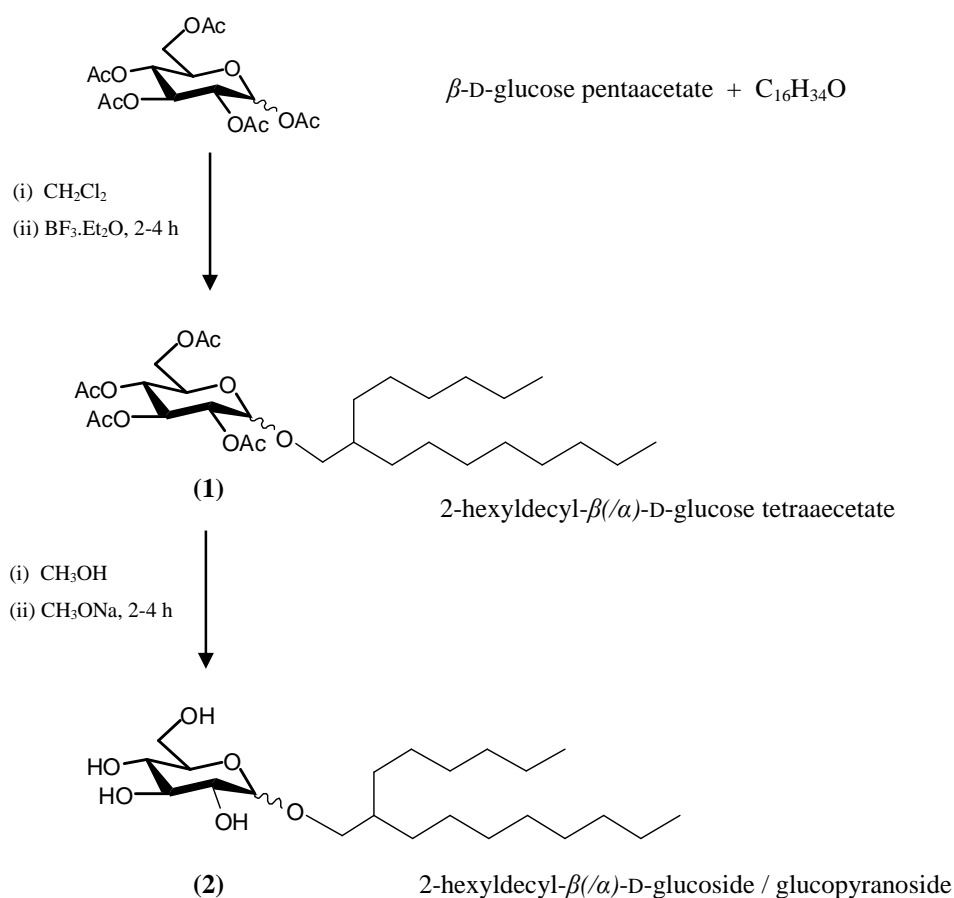
β -D-glucose pentaacetate (98%) and D-maltose monohydrate (90%) were purchased from Sigma-Aldrich. 2-hexyl-1-decanol, the Guerbet alcohol (97%) was purchased from Aldrich. The solvents used in this research were dichloromethane (99.99%), ethyl acetate (99.97%), acetonitrile (99.99%) and hexane (98.11%) were purchased from Fisher Scientific while methanol (99.85%) and 1-butanol (99.5%) were purchased from J. Kollin Chemicals and Merck respectively. Boron trifluoride diethyl etherate (100%) and sodium methoxide (100%) were purchased from Aldrich and Acros Organics respectively. Sodium acetate anhydrous (98%) was purchased from R & M Chemicals. Acetic anhydride (98.5%) and sodium hydrogen carbonate (99.7-100%) were purchased from Merck. Magnesium sulphate anhydrous (99%) was purchased from Acros Organics. Hydrochloric acid (with fuming ~36%) was purchased from Fisher Scientific. All chemicals were used as received. De-ionized water from Elga Labwater-migromeg purified water system was used in the extraction step.

Chloroform-d (99.8 atom %D) and methanol-d₄ (99.8%) were purchased from Aldrich and Merck respectively for NMR analysis.

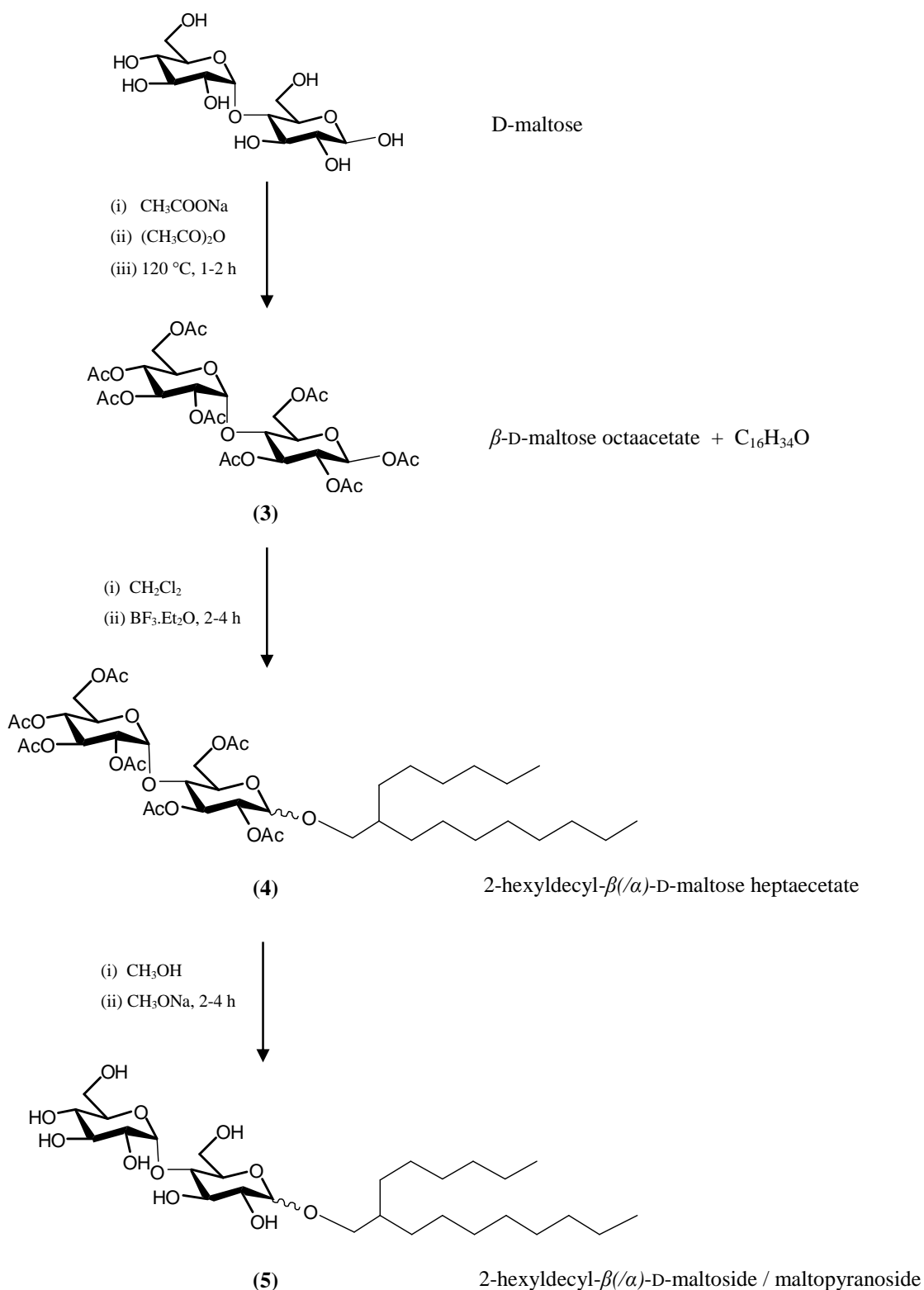
Thin layer chromatography (TLC) was performed on silica gel (Merck GF₂₅₄) coated on aluminium plates. Sulphuric acid (95-97%) and ethanol (95%) were purchased from Riedel-de Haën and J. Kollin Chemicals respectively.

2.3 SYNTHESIS METHODS

2-HDG and 2-HDM have been prepared from glycosidation between Guerbet alcohol and their respective protected sugars as shown in **Schemes 2.1** and **2.2**. 2-HDG was prepared by introducing Guerbet alcohol to protected sugar in the presence of boron trifluoride diethyl etherate. The reaction was completed after 4 hours to produce β -dominant peracetylated glycolipids. The intermediate product was further treated in basic condition by dissolving in methanol and sodium methoxide for another 4 hours. The product was purified by solvent extraction methods. 2-HDM was produced in the similar way but it began with protection procedure of maltose by adding D-maltose to the solution of acetic anhydride and sodium acetate [49].



Scheme 2.1: 2-hexyldecyl- β (/ α)-D-glucoside (2-HDG) was produced from glycosidation between Guerbet alcohol and protected sugars. The acetyl groups were cleared away by deacetylation under basic condition.



Scheme 2.2: 2-hexyldecyl- β /(α)-D-maltoside (2-HDM) was produced from glycosidation between Guerbet alcohol and protected sugars. The acetyl groups were cleared away by deacetylation under basic condition.

2.3.1 Peracetylation: Synthesis of β (/ α)-D-maltose octaacetate (3)

Activated acetyl was prepared by adding 10.0 g (120 mmol) sodium acetate into 100 mL acetic anhydride. The solution was stirred and heated until reflux at 120 °C. 21.0 g (60 mmol) D-maltose monohydrate was slowly added in small fraction into the hot suspension while stirring until the mixture turned into a clear solution. The mixture was further heated at 120 °C up to 2 h while stirring.

After the reaction completed, the crude mixture was poured into a mixture of ice-water and stirred continuously to form sticky white solid. The solid was then filtered and recrystallized from ethanol to give around 80% yield.

2.3.2 Glycosidation: Synthesis of 2-hexyldecyl- β (/ α)-D-glucose tetraacetate (1)

3.9 g (10 mmol) β -D-glucose pentaacetate and 2.9 g (12 mmol) 2-hexyl-1-decanol were dissolved in 100 mL of dichloromethane while stirring in closed vessel at room temperature. 1.7 g (12 mmol) boron trifluoride diethyl etherate was injected into the solution while stirring. The mixture was stirred up to 4 h. The reaction mixture was then quenched with saturated sodium hydrogen carbonate solution. The aqueous phase was extracted 3 times with 20 mL dichloromethane. The organic phase was washed twice with 20 mL de-ionized water. The organic layer was dried over magnesium sulphate anhydrous, filtered and evaporated under vacuum. The crude product was further purified using acetonitrile-hexane separation for 8 times. Acetonitrile layer was collected and the excess solvent was evaporated off to obtain the desired product. The unreacted alcohol was collected from the hexane layer.

The reactions and the purity of the compound were monitored using thin layer chromatography (TLC) with a mixture of 2:1 hexane and ethyl acetate for eluent. The product was further dried in vacuum oven at 50 °C for 24 h. The product was analyzed by ¹H-NMR for purity and anomeric composition determination.

2.3.3 Glycosidation: Synthesis of 2-hexyldecyl- β (/ α)-D-maltose heptaacetate (4)

Synthesis of 2-hexyldecyl- β (/ α)-D-maltose heptaacetate follows the similar procedure as synthesis of compound **1** including the weight of the reagents except β -D-maltose heptaacetate (6.8 g, 10 mmol).

2.3.4 Deacetylation: Synthesis of 2-hexyldecyl- β (/ α)-D-glucoside (2)

The product from the glycosidation stage (2-hexyldecyl- β (/ α)-D-glucose tetraacetate) was dissolved in methanol, in which 1g of product requires 30 mL methanol. A catalytic amount of sodium methoxide was added to maintain a basic medium. The mixture was stirred up to 4 h. The reaction was monitored using TLC with 1:10 mixture ratio of methanol and dichloromethane for eluent. Excess solvent was evaporated under vacuum.

The crude product was purified by solvent extraction using 1-butanol : water. A small amount of diluted hydrochloric acid was added drop by drop to neutralize the excess sodium methoxide. The pH of solution was checked using litmus paper. The organic layer was separated and evaporated off under vacuum to obtain a gold yellowish syrup product. The product was dried in vacuum oven at 50 °C for 24 h. The purity and the structure were determined by ¹H-NMR and FTIR.

2.3.5 Deacetylation: Synthesis of 2-hexyldecyl- β (/ α)-D-maltoside (5)

Synthesis of 2-hexyldecyl- β (/ α)-D-maltoside follows the similar procedure as synthesis of compound **2**. The organic layer was separated and evaporated off under vacuum to obtain a white solid product.

2.4 INSTRUMENTATIONS

2.4.1 Nuclear Magnetic Resonance Spectrophotometer

Purity and anomeric composition of the products were further determined by Proton Nuclear Magnetic Resonance ($^1\text{H-NMR}$) Spectroscopy on a JEOL LAMBDA 400 MHz spectrophotometer. In the sample preparation, 20-25 mg of the compound was dissolved in 1 mL of deuterated solvent. Chloroform-d (CDCl_3) was used for dissolving peracetylated compound, whereas methanol-d4 (CH_3OD) was used for dissolving the final compound. The $^1\text{H-NMR}$ scanning was conducted in 32 times.

2.4.2 Fourier Transform Infrared Spectrophotometer

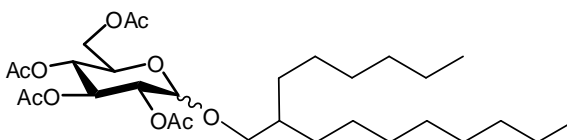
Fourier Transform Infrared (FTIR) spectra were determined from Perkin-Elmer FTIR Spectrophotometer (spectrum 2000). In the sample preparation, the solid product was grained in potassium bromide with ratio 1:10 (wt%) and molded as a thin pallet. The sticky product was directly measured, in which the sample was placed between two sodium chloride glasses.

2.5 RESULTS AND DISCUSSIONS

2.5.1 ¹H-NMR Data of 2-hexyldecyl-β(/α)-D-glucose tetraacetate and 2-hexyldecyl-β(/α)-D-maltose heptaacetate

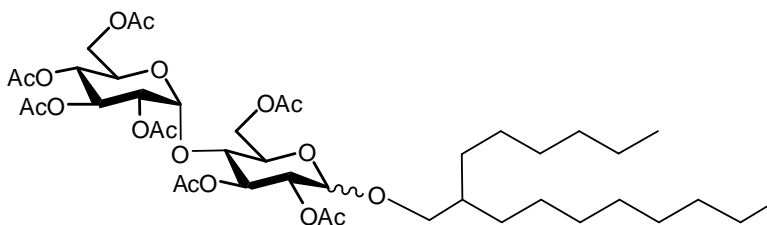
The ¹H-NMR results show purities and anomeric compositions of 2-hexyldecyl-β(/α)-D-glucose tetraacetate and 2-hexyldecyl-β(/α)-D-maltose heptaacetate.

(a) 2-hexyldecyl-β(/α)-D-glucose tetraacetate



$R_f = 0.60$ (2:1 of hexane:ethyl acetate); ¹H-NMR (400 MHz, CDCl₃) δ (ppm): 5.17 (dd, 1H, H-3), 5.06 (dd, 1H, H-4), 4.96 (dd, 1H, H-2), 4.41 (d, 1H, H-1), 4.23 (dd, 1H, H-6a), 4.11 (dd, 1H, H-6b), 3.77 (mc, 1H-H-αa), 3.64 (ddd, 1H, H-5), 3.26 (dd, 1H, H-αb), 2.09, 2.00, 1.99, 1.97 (each: s, 3H, H-4AcO), 1.64 (mc, 1H, H-βCH) 1.23-1.21 (m, 24H, H-12CH₂), 0.86-0.83 (m, 6H, H-2CH₃).

(b) 2-hexyldecyl-β(/α)-D-maltose heptaacetate



$R_f = 0.66$ (2:1 of hexane:ethyl acetate); ¹H-NMR (400 MHz, CDCl₃) δ (ppm): 5.38 (d, 1H, H-1'), 5.33 (dd, 1H, H-3'), 5.22 (dd, 1H, H-3), 5.02 (dd, 1H, H-4'), 4.83 (dd, 1H, H-2'), 4.81 (dd, 1H, H-2), 4.45 (d, 1H, H-1), 4.43 (dd, 1H, H-6a),

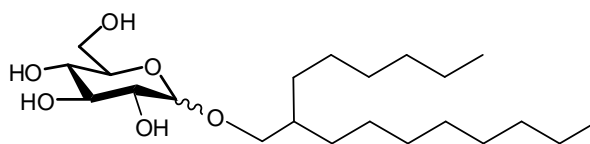
4.21 (dd, 1H, H-6a'), 4.20 (dd, 1H, H-6b), 3.99 (dd, 1H, H-6b'), 3.97 (dd, 1H, H-4), 3.94 (ddd, 1H, H-5'), 3.74 (mc, 1H, H- α a), 3.63 (ddd, 1H, H-5), 3.26 (mc, 1H, H- α b), 2.12, 2.10, 1.99, 1.97 (each s, 3H, H-4AcO), 1.96 (s, 9H, H-3AcO), 1.65 (mc, 1H, H- β -CH), 1.25-1.20 (m, 24H, -CH₂), 0.84 (t, 6H, H-CH₃).

2.5.2 ¹H-NMR and FTIR Data of 2-hexyldecyl- β (/ α)-D-glucoside and 2-hexyldecyl- β (/ α)-D-maltoside

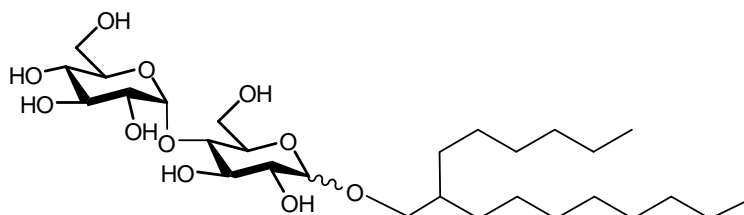
The ¹H-NMR results of 2-hexyldecyl- β (/ α)-D-glucoside (2-HDG) and 2-hexyldecyl- β (/ α)-D-maltoside (2-HDM) show both products are β -dominant.

The FTIR results of 2-HDG and 2-HDM show the disappearance of signal at 1735 - 1750 cm⁻¹ indicate the absence of acetate group (C=O). Thus, the final products are completely deprotected into hydroxyl groups.

(a) 2-hexyldecyl- β (/ α)-D-glucoside (2-HDG)



$R_f = 0.56$ (1:10 of methanol:dichloromethane); ¹H-NMR (400 MHz, CD₃OD)
 δ (ppm): 4.20 (d, 1H, H-1), 3.81 (dd, 1H, H- α a), 3.68 (dd, 1H, H-6a), 3.54 (dd, 1H, H-6b), 3.44-3.25 (m, 4H, H-3, H-4, H-5, H- α a), 3.17 (dd, 1H, H-2), 1.60 (mc, 1H, H- β), 1.40-1.20 (m, 24H, H-12CH₂), 0.91-0.88 (m, 6H, H-2CH₃);
 FTIR $\bar{\nu}$ (cm⁻¹): 3390.5 (O-H stretch), 2922.3, 2855.6 (C-H stretch), 1078.0 (O-C-O stretch).

(b) **2-hexyldecyl- β (/ α)-D-maltoside (2-HDM)**

$R_f = 0.60$ (1:10 of methanol:dichloromethane); $^1\text{H-NMR}$ (400 MHz, CD_3OD)
 δ (ppm): 5.15 (d, 1H, H-1'), 4.22 (d, 1H, H-1), 3.89-3.20 (m, 12H, H-3, H-3', H-4, H-4', H-5, H-5', H-6a, H-6a', H-6b, H-6b', H- α a, H- α b), 3.55 (dd, 1H, H-2'), 3.44 (dd, 1H, H-2), 1.40 (mc, 1H- β -CH), 1.38-1.29 (m, 8H, H-4 CH_2), 0.91-0.88 (t, 6H, H-2 CH_3); FTIR $\bar{\nu}$ (cm^{-1}): 3449.2 (O-H stretch), 2927.7, 2861.0 (C-H stretch), 1035.4 (O-C-O stretch).

Analyses of NMR spectra show the product quality and also indicate the anomeric ratio of the mixture. This can be obtained by comparing the integration of the α -anomer and β -anomer peaks in the technical grade sample (see **Appendix 1**).

In the synthesis, excess alcohol was used and then removed by extraction method. However, improper extraction will not completely remove the alcohol thus leading to remain in the product. Unreacted alcohol is not easily detected in NMR spectrum since the signals of alcohol overlap with sugar signals. Therefore, the ratio between sugar and lipid chain will be used to estimate the presence of the alcohol and the quality of the products.

2.5.3 Percentage of Yield of 2-HDG and 2-HDM

Percentage of yield of the final glucosides and maltosides were calculated for each synthesis batch. **Tables 2.1** and **2.2** show the percentage of yield of products in the final step of the 2-hexyldecyl- β (/ α)-D-glucosides (2-HDG) and 2-hexyldecyl- β (/ α)-D-maltosides (2-HDM) respectively.

Table 2.1: Percentage of yield of 2-hexyldecyl- β (/ α)-D-glucosides (2-HDG).

Batch No.	Symbol	Molecular Formula	Percentage of Yield, %	Molecular Weight, g mol ⁻¹
1	2-HDG	C ₂₂ H ₄₄ O ₆	54	404.58
2	2-HDG	C ₂₂ H ₄₄ O ₆	63	404.58
3	2-HDG	C ₂₂ H ₄₄ O ₆	76	404.58
4	2-HDG	C ₂₂ H ₄₄ O ₆	75	404.58
5	2-HDG	C ₂₂ H ₄₄ O ₆	65	404.58
6	2-HDG	C ₂₂ H ₄₄ O ₆	65	404.58

Table 2.2: Percentage of yield of 2-hexyldecyl- β (/ α)-D-maltosides (2-HDM).

Batch No.	Symbol	Molecular Formula	Percentage of Yield, %	Molecular Weight, g mol ⁻¹
1	2-HDM	C ₂₈ H ₅₄ O ₁₁	74	566.73
2	2-HDM	C ₂₈ H ₅₄ O ₁₁	74	566.73

2.6 CONCLUSIONS

Two nature-like branched-chain glycolipids namely 2-hexyldecyl- β (/ α)-D-glucoside (2-HDG) and 2-hexyldecyl- β (/ α)-D-maltoside (2-HDM) have been successfully synthesized. Both compounds are β -dominant (~90%) anomeric mixtures, which are technical grade that acceptable quality for our study and commercial purposes.

CHAPTER 3:
PHYSICO-CHEMICAL CHARACTERIZATION OF
BRANCHED-CHAIN GLYCOLIPIDS

3.1 INTRODUCTION

This chapter will describe the physico-chemical characterizations of branched-chain glycolipids in dried and hydrated forms. In the last decades, glycolipids have attracted much attention due to their self-assembly properties and potential as bio-surfactants [47,151-152]. Glycolipids are classified as *amphiphilic* molecules composed of both of hydrophilic group from the sugar moiety and hydrophobic group from the alkyl chains, which can self-assemble into various types of self-organized structures. They are also known as *amphitropic* because the compounds can form both thermotropic and lyotropic mesophases (liquid crystalline phases). They can form interesting phase behaviours such as the formation of different thermotropic liquid crystalline phases in dry/pure form and undergo phase transitions in lyotropic phases when contact with solvents such as water [21,23,29,48-49,153].

1,2-dialkyl/diacyl-glycerol-based glycolipids [70,154] and 1,3-glycosyl-glycerol-based glycolipids [155-156] were prepared by Mannock *et al* and Minamikawa *et al.* respectively, and these have been investigated for their phase behaviour properties. In addition, branched-chain glycolipids from glycosylation reaction between Guerbet alcohol with chain length from C₈-C₂₄ and a series of sugar unit ranging from glucose, galactose, maltose and lactose have been prepared and reported by Hashim *et al.* [48-49]. These glycolipids were studied for their thermotropic and lyotropic phases behaviour aiming to correlate the molecular structures and liquid crystal properties. Similar to other amphiphilic/amphitropic molecules, these glycolipids also tend to form self-aggregation structures by forming at least one of the lyotropic liquid crystalline phases such as simple lamellar (L_a), hexagonal (H) and cubic phases (V) [29,48-49,59,153].

In this chapter, physico-chemical characterization of Guerbet branched-chain glycolipids (2-hexyldecyl- β (/ α)-D-glucoside and 2-hexyldecyl- β (/ α)-D-maltoside) will be further discussed. Both dried and hydrated forms of the glycolipids have been investigated. The effect of different head groups polarities on their thermal properties, thermotropic and lyotropic properties have been investigated using thermogravimetric analyzer (TGA), differential scanning calorimeter (DSC), optical polarizing microscopy (OPM) and small-angle X-ray scattering (SAXS).

3.2 MATERIALS

The prepared 2-hexyldecyl- β (/ α)-D-glucoside (2-HDG) and 2-hexyldecyl- β (/ α)-D-maltoside (2-HDM) were further used for characterization. De-ionized filtered water (Milli-Q[®], Millipore) with the strength of an ionic conductivity of 18.2 μ S/cm was used for all sample preparations.

3.3 METHODOLOGY

3.3.1 Samples Preparation for TGA

The glycolipids samples were dried over phosphorus pentoxide under vacuum for at least 24 h to minimize moisture content. 5-10 mg of 2-HDG and 2-HDM were utilized in the measurement. The TGA measurement was conducted by increasing temperature gradually by a factor of 10.0 °C and this was repeated a second time for confirmation.

3.3.2 Samples Preparation for DSC

The glycolipids samples were dried as above procedure mentioned in 3.3.1. 5-10 mg of each sample was measured in medium pressure crucible made of stainless steel, tighten with a Viton o-ring. The DSC measurement for 2-HDG was conducted from -10.0°C to 150.0 °C, while that for 2-HDM was from -10.0°C to 200.0 °C based on TGA results. The heating rate in this measurement was fixed to 5.0 °C/min.

3.3.3 Thermotropic and Lyotropic Determination by Optical Polarizing Microscope (OPM)

The OPM analysis was divided into two conditions: thermotropic and lyotropic. The sample preparations are described as follows.

In the *thermotropic* determination, the sample was placed on a glass slide and gently covered with a cover slip as shown in **Figure 3.1**. The sample was heated up to 70.0 °C and 180.0 °C for 2-HDG and 2-HDM respectively. The first stage of heating is to eliminate any moisture trapped in the sample and to form a thin film of the glycolipids on the slide. The cover slip was gently pressed during heating to produce more uniform sample, in order to obtain better textures. The sample was then cool down to 25.0 °C before heated up again for the second time by slow heating and cooling repeatedly. The texture of the sample was observed under polarized light and the phase was identified from the observed texture.

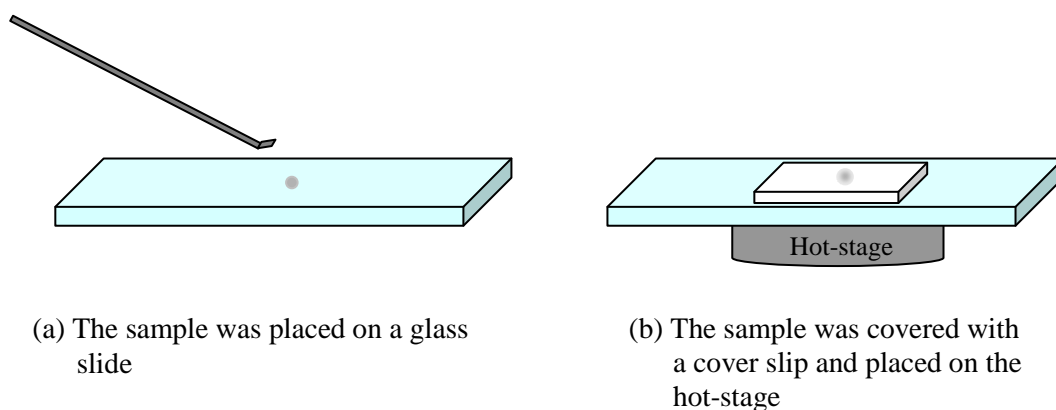


Figure 3.1: Sample preparation for thermotropic study.

Similar sample treatment was adopted for the *lyotropic* phase determination. In addition, the sample was introduced to a solvent such as water at the edge of the cover slip. The water penetrates by capillary forces into the sample as shown **Figure 3.2**. The method also known as contact penetration or Lawrence experiment. The solvated sample was studied under polarized light and the phases were identified from the observed textures. Different phases at different concentrations were observed by the appearance of different textures under polarizing microscope.

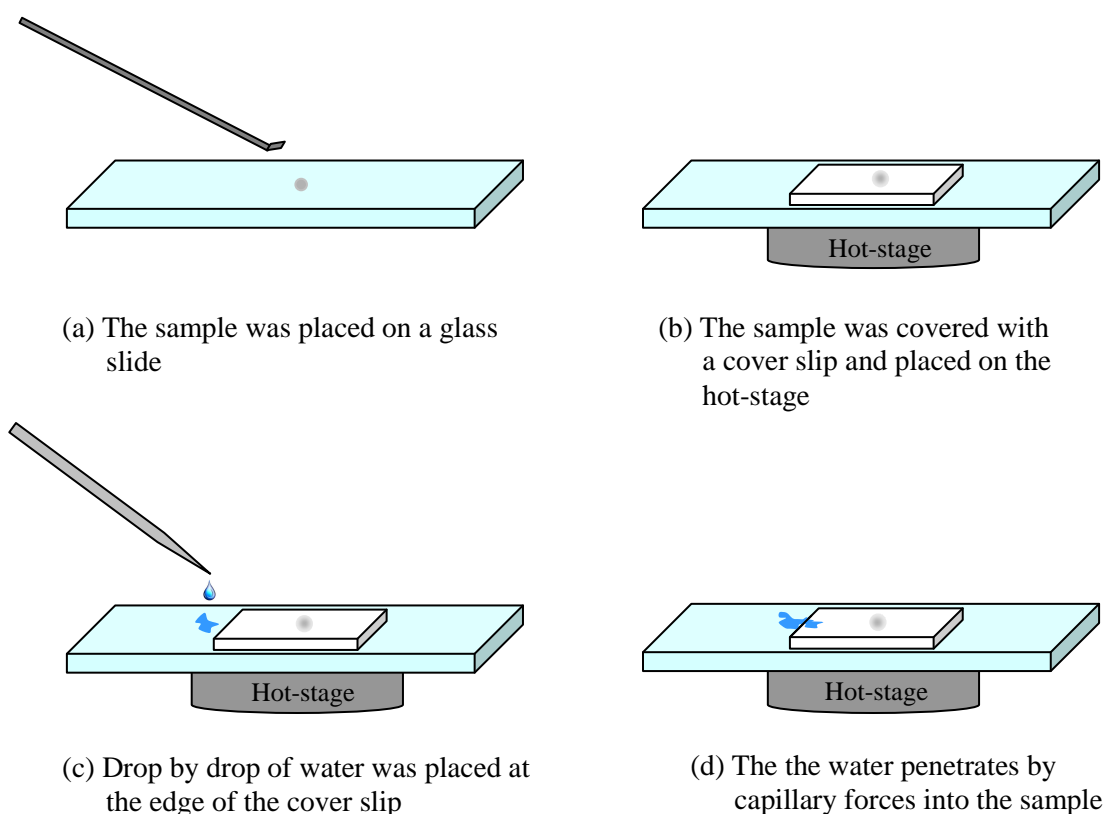


Figure 3.2: Contact penetration technique for lyotropic study.

3.3.4 Liquid Crystalline Pattern by Small- and Wide-Angle X-Rays Scattering (SWAXS)

Each of the dried and hydrated 5.0 wt% glycolipids was placed in a Hilgenberg glass capillary of 80 mm length, 1 mm diameter and 0.01 mm wall thickness. The sample was centrifuged using a 5804 R Eppendorf Centrifuge at 3500 rpm for 5 min to ensure the sample was properly settled at the bottom of the capillary for about 4 cm height. Each sample was sealed by closing the top of the capillary under a sheet of flame. The sample was measured by SWAXS at 25.0 °C for 30 min.

3.4 INSTRUMENTATIONS

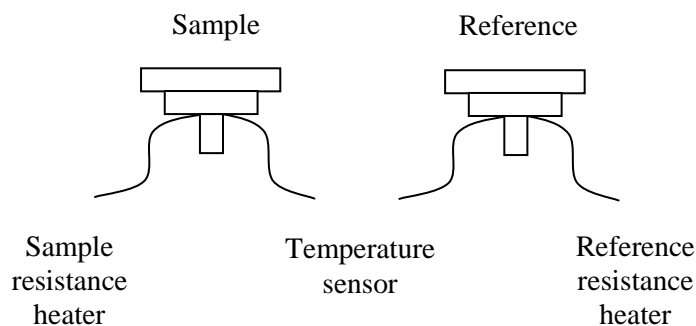
3.4.1 Thermogravimetric Analyzer (TGA)

Thermogravimetric Analysis (TGA) is a technique to determine different sample weight by changing the temperature of the samples. It is commonly employed to determine the characteristics of materials such as the absorbed moisture or impurities content in the material and also the decomposition temperatures. A Mettler Toledo TGA/SDTA 851°/SF Thermogravimetric Analyzer has been used for this purpose. It was conducted by increasing temperature by the factor of 10.0 °C/min. Data treatment was performed with STAR° SW 9.20 software.

3.4.2 Differential Scanning Calorimeter (DSC)

Differential Scanning Calorimetry (DSC) is a technique in which the difference in the amount of heat required to increase the temperature of a sample and that of the reference is measured as a function of temperature. Both the sample and reference are maintained at nearly the same temperature throughout the experiment. Generally, the temperature program for a DSC analysis is designed such that the temperature of the sample holder increases linearly as a function of time. The reference sample should have a well-defined heat capacity over the range of temperatures to be scanned. The basic principle underlying this technique is that, when the sample undergoes a physical transformation such as a phase transition, more or less heat will need to flow to it than to the reference to maintain both at the same temperature (**Figure 3.3**). Whether less or more heat must flow to the sample depends on whether the process is exothermic or endothermic. On heating, the phase transition observed is endothermic such as from

smectic A phase to isotropic phase. Heat is absorbed and therefore heat flow into the sample is higher than that to the reference (empty crucible). Thus, $\Delta dH/dt$ is positive. In an exothermic process such as crystallization, the opposite condition is applies. Thus, $\Delta dH/dt$ is negative.



$$\Delta \frac{dH}{dt} = \left(\frac{dH}{dt} \right)_{sample} - \left(\frac{dH}{dt} \right)_{reference} \quad (3.1)$$

Figure 3.3: A schematic diagram of a heat flux differential scanning calorimeter.

DSC reveals the presence of mesophases by detecting the enthalpy change that is associated with a phase transition. The technique partially identifies the type of liquid crystal phase, since it gives the level of enthalpy change which is related to the degree of molecular ordering when the phase transformation occurs.

A Mettler Toledo DSC 821^e Differential Scanning Calorimeter with nitrogen atmosphere, calibrated with Indio and Zinc standards was utilized. The range for DSC measurement is from -150.0 °C to 500.0 °C, whereas the heating/cooling rate is from 0.1 to 20.0 °C/min. The “peak temperature” was indicated the phase transition during heating. Data treatment was performed with STAR^e SW 9.20 software.

3.4.3 Optical Polarizing Microscope (OPM)

Identification of liquid crystal phases can be achieved by optical polarizing microscope (OPM). For texture studies, the analyzer is oriented at the right angle to the polarizer, i.e. when no birefringent, the field of view is black. In liquid crystal phases (mesophases), the birefringence can be detected with some areas appear light and some other areas appear dark. Each different liquid crystal shows different optical texture such as schlieren, fan-shaped, focal conic, etc [27]. This optical polarizing microscopy is the most extensively used tool of measurement employed in this study in order to investigate the thermotropic and lyotropic properties of glycolipids.

The thermotropic and lyotropic studies were conducted using a Leica Reichert Polyvar 2 optical polarizing microscope with digital Sony CCD-Iris camera. Non-polarized and polarized light were applied to study thermotropic and lyotropic behaviours of the novel glycolipids; 2-HDG and 2-HDM. A hot-stage of the type T95-PE from Linkam was used to control the temperature during heating and cooling process. Images of the textures were captured and stored using analysis[®] Imager software Leica IM500. An optical polarizing microscope is an essential piece of equipment for the determination of liquid crystal texture, particles and droplets size distribution.

The preparation of sample for this technique has been mentioned previously in 3.3.3. The glass slide with the sample was put on the microscope stage just underneath the objective lens (**Figure 3.4**). The image of sample was observed and captured using either 4x, 10x, 20x, 50x or 100x magnification objective lenses depending on the quality of observed images.

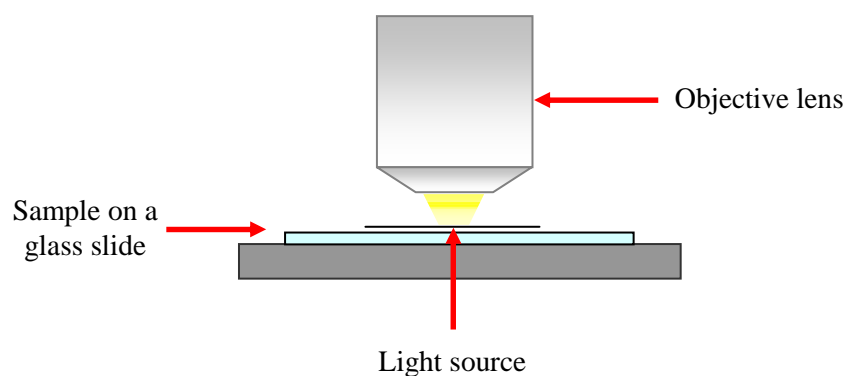


Figure 3.4: Sample observation under optical polarizing microscope.

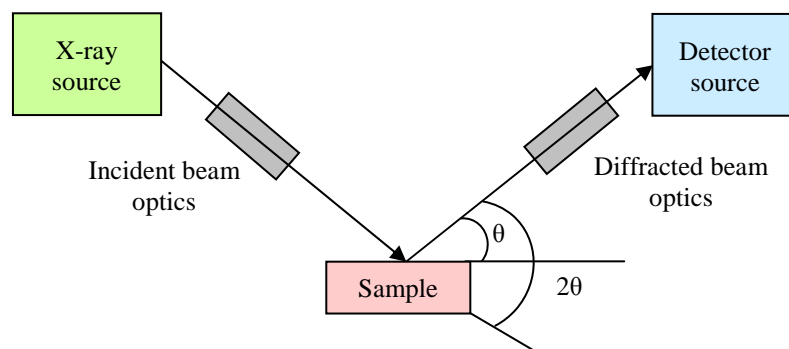
3.4.4 Small- and Wide-Angle X-Ray Scattering (SWAXS)

The X-ray scattering technique is usually considered as the definitive technique for the determination of phase structures, where different liquid crystal phases give different X-ray scattering patterns. X-ray measurements at small- and wide-angle were performed in a S3 MICRO instrument (Hecus X-ray Systems, Graz, Austria) with point focalization, equipped with a GENIX microfocus X-ray source and a FOX 2D point-focusing element (both from Xenocs, Grenoble, France). The scattered intensity (in Arbitrary Units, A.U.) was recorded using two position-sensitive detectors (PSDs, Hecus) as a function of the scattering angle defined as θ . The wavelength, λ was 0.154 nm and the measurements were performed at 50 kV and 1 mA. The SAXS detector covers a range between 0.2° and 8.0° , while the WAXS detector covers from 18° to 26° . The temperature controller was an AP Paar K-PR Peltier device.

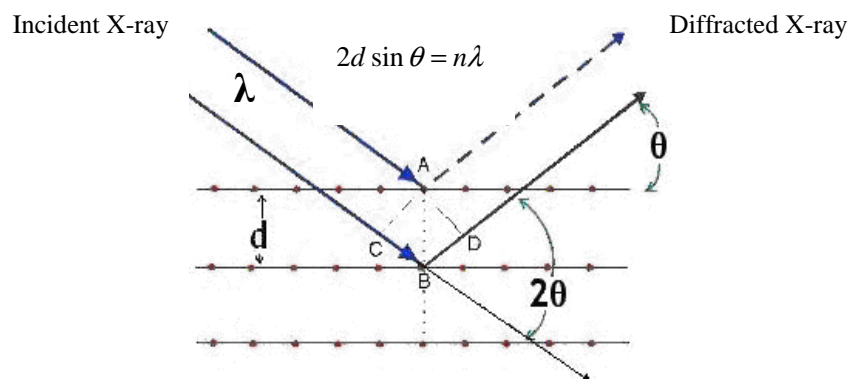
The liquid crystalline phases were characterized by the SAXS peak ratios when plotting intensity (%) as a function of the scattering vector ($q = 4\pi/\lambda \sin(\theta/2)$), which is the difference between the incident beam optics (wave vector) and the scattered one to an angle θ (**Figure 3.5**). The interlayer d-spacing of liquid crystalline phases was determined from the Bragg equation,

$$2d \sin \theta = n\lambda \quad (3.2)$$

where θ is the angle of incidence, n is an integer, λ is the wavelength and the diffraction angle is 2θ .



(a)



(b)

Figure 3.5: A schematic diagram of the (a) X-ray scattering measurement and (b) Bragg's Law.

3.5 RESULTS AND DISCUSSIONS

3.5.1 Thermogravimetric Analysis

Thermogravimetric plots of 2-HDG and 2-HDM have shown distinctive decomposition temperatures as shown in **Figure 3.6**. Both of 2-HDG and 2-HDM have reduced ~1% mass at 100 °C indicate the lost of moisture in the samples. The plot started to deviate at 175 °C and 225 °C indicating the decomposition of 2-HDG and 2-HDM respectively. These probably because of higher number of sugar head group in 2-HDM possessed the higher molecular interaction (hydrogen bonding) than in 2-HDG.

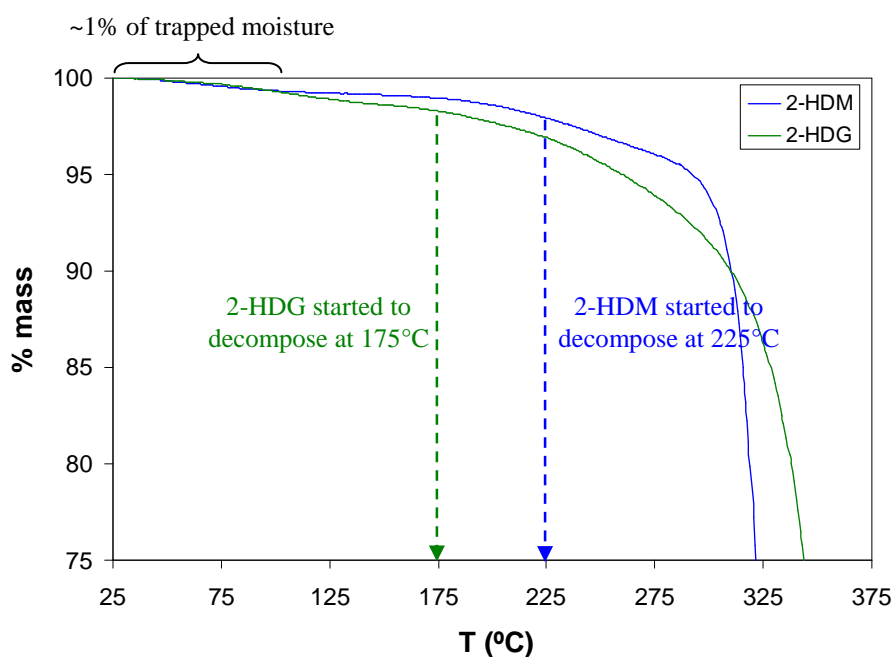
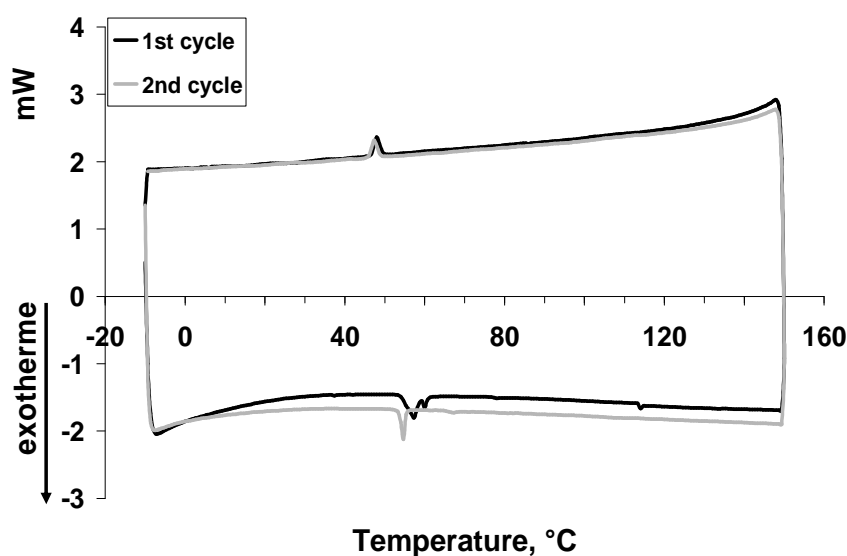


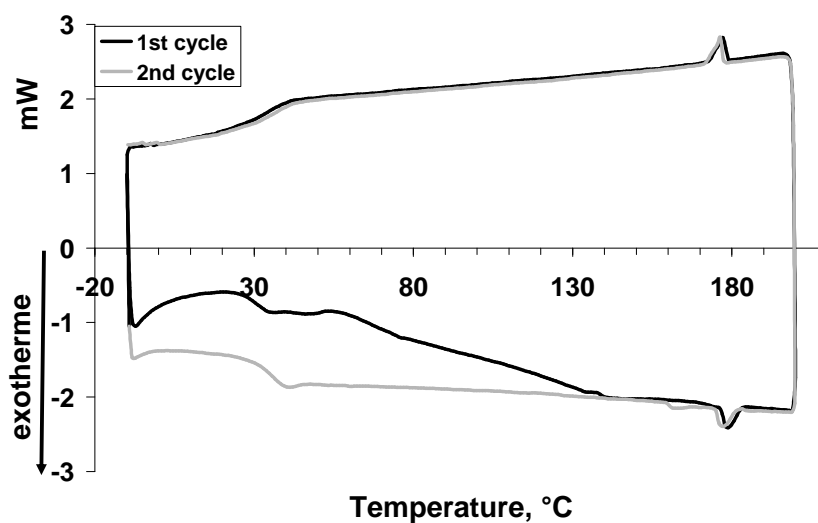
Figure 3.6: TGA thermogram of 2-hexyldecyl- β (/ α)-D-glucoside (2-HDG) and 2-hexyldecyl- β (/ α)-D-maltoside (2-HDM).

3.5.2 Differential Scanning Calorimetry

The glycolipids compounds studied melted from the crystal phase through a liquid crystal phase into the isotropic liquid. DSC measurements have shown that the phase transition of 2-HDG occurred around 57 °C (**Figure 3.7a**) and the enthalpy change of first order was calculated as $-0.7 \pm 0.1 \text{ J.g}^{-1}$ (mean value obtained from three measurements based on the second cycle). On the other hand, 2-HDM exhibited a phase transition around 180 °C and the enthalpy change was calculated as $-1.3 \pm 0.1 \text{ J.g}^{-1}$ (**Figure 3.7b**). The clearing temperature of 2-HDM was higher than 2-HDG due to an additional glucose unit in the head group of maltoside since the head group of the former is formed of two glucose units via an $\alpha 1 \rightarrow 4$ glycosidic linkage. Increasing the number of sugar units in the head group results not only in an increase in its size and molecular weight but also its hydrogen bonding between the head groups.



(a)



(b)

Figure 3.7: DSC thermograms of (a) 2-HDG and (b) 2-HDM upon heating and cooling (two cycles).

The cooling cycle of both compounds showed a slight reduced in the transition temperature compared to that observed during heating. Moreover, the transition temperature for the second heating and cooling cycle also showed a slight smaller value compared to that for the first heating and cooling cycle as shown in **Table 3.1**. This can be explained by some minor degradation occurred when the compounds were heated at a higher temperature than the clearing point. However, the differences are negligible and the reproducibility of DSC peaks upon second heating and cooling indicates the compounds are stable towards thermal degradation.

Table 3.1: The overall DSC results for 2-HDG and 2-HDM.

Sample	Molecular Formula	Molecular Weight / g mol^{-1}	Clearing Temperature / $^{\circ}\text{C}$ (First Cycle)		Clearing Temperature / $^{\circ}\text{C}$ (Second cycle)	
			Heating	Cooling	Heating	Cooling
2-HDG	$\text{C}_{22}\text{H}_{44}\text{O}_6$	404.58	57.8	48.1	55.4	47.2
2-HDM	$\text{C}_{28}\text{H}_{54}\text{O}_{11}$	566.73	179.8	177.3	176.9	176.1

3.5.3 Thermotropic Behaviour of Branched-chain Glycolipids

In the thermotropic study, the behaviour of dry surfactant at different temperatures can be observed under optical polarizing microscopy (OPM). Anisotropic phases such as the columnar (hexagonal) and the smectic A (lamellar) phases are visible under polarized light with birefringence characteristic. Smectic A phase shows lower birefringence characteristic compared to columnar phase. These phases can be identified from its typical textures [49].

In the case of 2-HDG, a focal conic texture of the columnar phase was clearly observed as shown in **Figure 3.8** for heating and **Figure 3.9** for cooling. The texture upon cooling is more defined than the heating condition. It has been observed that a clearer focal conic texture appears when the rate of cooling is slower because the molecules have more time to rearrange themselves. From the observation, the clearing temperature of 2-HDG compound was found to be between 55 and 60 $^{\circ}\text{C}$. This can be determined from the changed of columnar phase (birefringence characteristic) to dark isotropic phase.

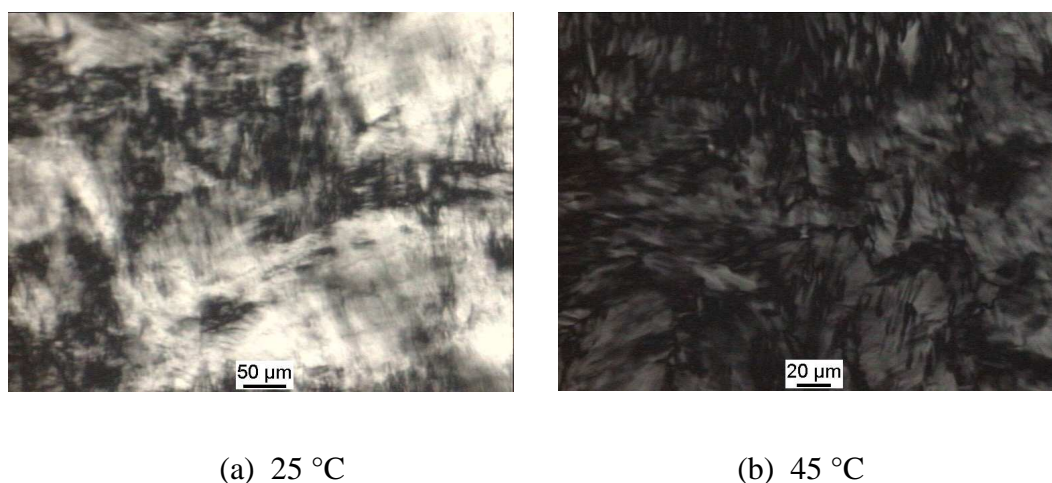


Figure 3.8: Optical polarizing micrographs of phase transitions of the 2-HDG upon heating. The texture corresponds to those of a columnar phase.

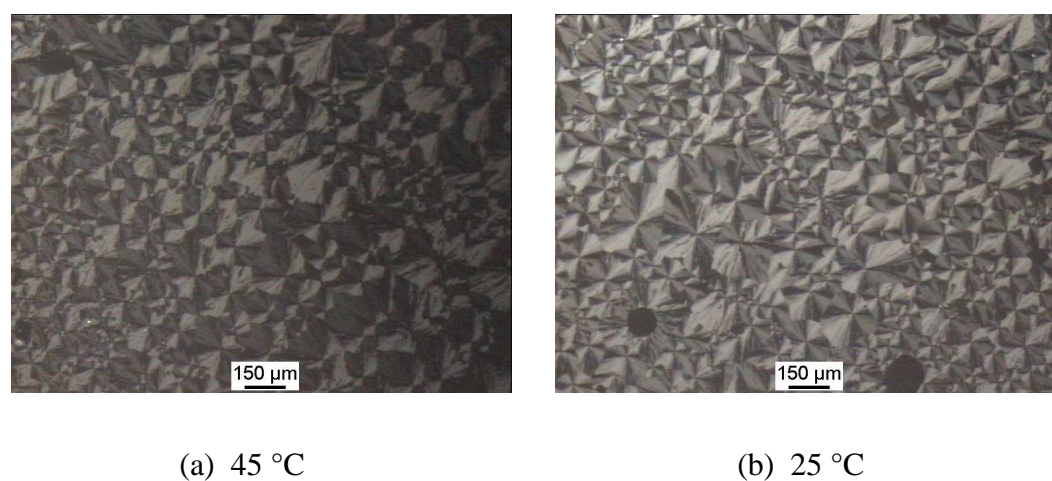


Figure 3.9: Optical polarizing micrographs of phase transitions of the 2-HDG upon cooling. The focal conic texture corresponds to the columnar phase.

2-HDM shows a typical fan-shaped texture of smectic A phase as shown in **Figure 3.10** for heating and **Figure 3.11** for cooling. From the observation, the clearing temperature of 2-HDM compound was found to be between 180 and 185 °C. This can be determined from the changed of smectic A phase (birefringence characteristic) to dark isotropic phase.

The clearing point of 2-HDG and 2-HDM obtained by OPM confirmed the clearing point determined by DSC. Both results are comparable to those measured previously and within the error, as well as described for pure β -glycosides [49,59].

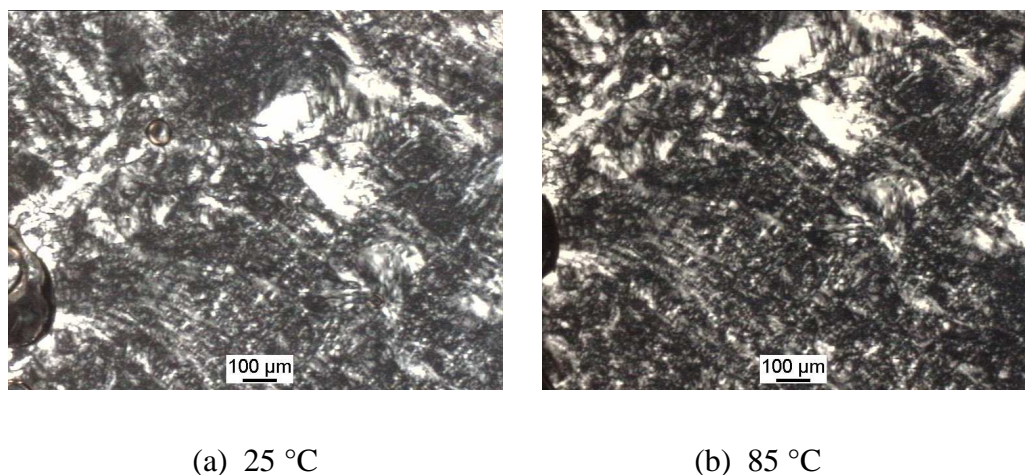


Figure 3.10: Optical polarizing micrographs of phase transitions of the 2-HDM upon heating. The texture corresponds to those of a smectic A phase.

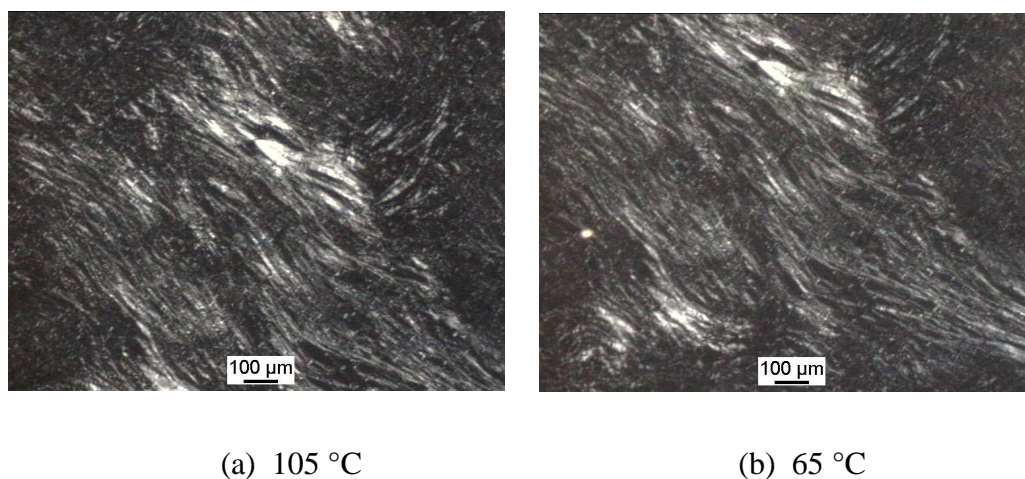


Figure 3.11: Optical polarizing micrographs of phase transitions of the 2-HDM upon cooling. The fan-shaped texture corresponds to those of a smectic A phase.

3.5.4 Lyotropic Behaviour of Branched-chain Glycolipids

The investigation of lyotropic liquid crystal phases of the branched-chain glycolipids was carried out using contact penetration experiment. Water has been chosen because it is compatible to the biological systems. It is also a typical solvent to make up a solution of polar amphiphiles. It is a protic solvent, capable to form H-bonding with the sugar groups and providing high cohesive-energy density in these regions, which stabilized the mesophases.

In the case of 2-HDG, an isotropic phase (L) could be observed, followed by an anisotropic phase. The optical polarized micrograph of 2-HDG (**Figure 3.12**) shows two phase transitions from high to low water gradient, namely isotropic phase (L) \rightarrow inverted hexagonal phase (H_{II}) at 25.0 °C.

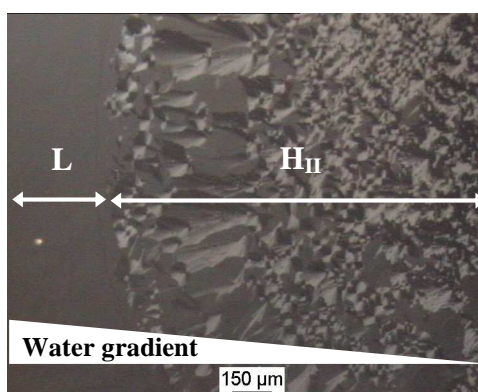


Figure 3.12: Optical polarized micrographs of the contact penetration experiment for 2-HDG. (L = isotropic phase and H_{II} = inverted hexagonal phase).

The optical polarized micrograph of 2-HDM (**Figure 3.13**) shows three phase transitions from high to low water gradient, namely isotropic phase (L) \rightarrow lamellar phase (L_{α}) \rightarrow smectic A phase (SmA) at 25.0 °C. As can be clearly seen, when water diffused into the solid, the formation of Maltese-cross structures could be observed immediately (highlighted by a white circle). The Maltese-cross structures indicates the

presence of a lamellar liquid crystalline phase and moreover vesicle formation is probable. In fact, vesicle contained more than one layer and can be demonstrated by the mass contrast difference in the micrograph where the inner volume is surrounded by at least one bilayer and therefore appears like a Maltese-cross structure. The third phase is the solid sample of anomeric mixture of α/β -maltoside before contact with water and can be assigned as a smectic A phase, as previously observed in the pure anomer β -maltoside compound [49].

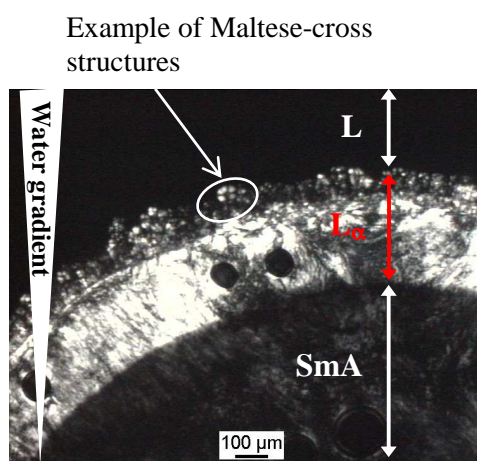


Figure 3.13: Optical polarized micrographs of the contact penetration experiment for 2-HDM. (L = isotropic phase, L_α = lamellar phase and SmA = smectic A phase).

3.5.5 SAXS Results of Dried Branched-chain Glycolipids

The X-ray scattering technique is considered an appropriate technique to determine the phase structure, since different liquid crystal phases have different X-ray patterns. Therefore, X-ray scattering confirmed the formation of columnar phase of 2-HDG initially observed under optical polarizing microscope. The three peaks indicated by arrows in **Figure 3.14** possess the typical reflections for a columnar phase which is $1:\sqrt{3}:\sqrt{4}$ [15]. Using $2d/\sqrt{3}$ (for columnar/hexagonal), a lattice spacing

of 3.0 nm was calculated from the first order peak positions. Theoretical calculation of the surfactant length of a pure 2-hexyldecyl- β -D-glucoside gave an overall molecule length of 3.5 nm [157].

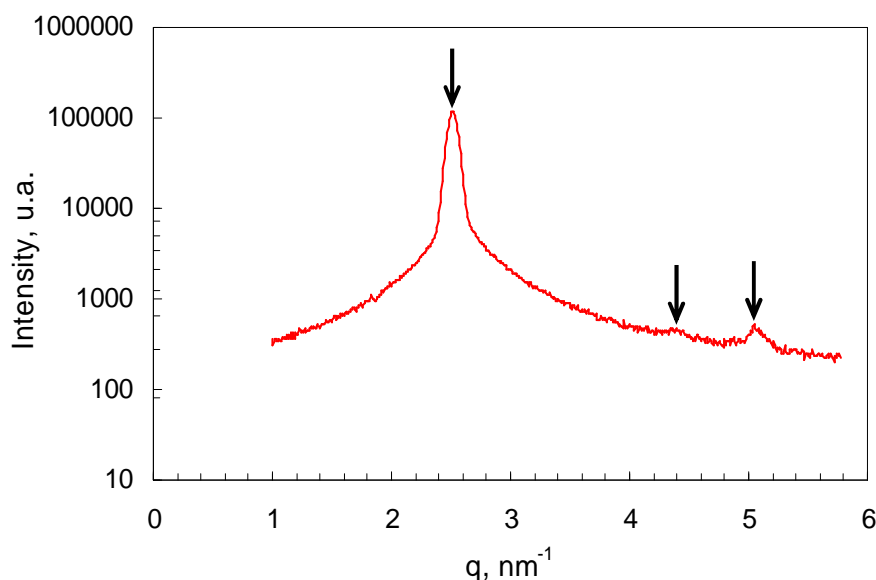


Figure 3.14: SAXS spectrum of dried 2-HDG at 25.0 °C.

2-HDM shows only a single sharp peak in the SAXS spectrum (**Figure 3.15**). The sharp peak indicates a degree of ordering of 2-HDM and therefore cannot be characterized as amorphous structure. However, the absence of high order peaks in the SAXS spectra can be attributed to disordered alkyl chains, which produce a relatively less crystalline state, giving rise to the presence of a liquid crystalline phase. It has been reported that a smectic A phase formed from a pure 2-hexyldecyl- β -D-maltoside examined by synchrotron X-ray diffraction facilities [157]. A smectic A phase was also formed by the similar maltosides possessing branched-chains [155,158]. In this case, the formation of a smectic A phase also can be assumed for the β -dominant anomeric maltoside. **Table 3.2** summarizes the results from SAXS experiments for dried glycosides at 25.0 °C.

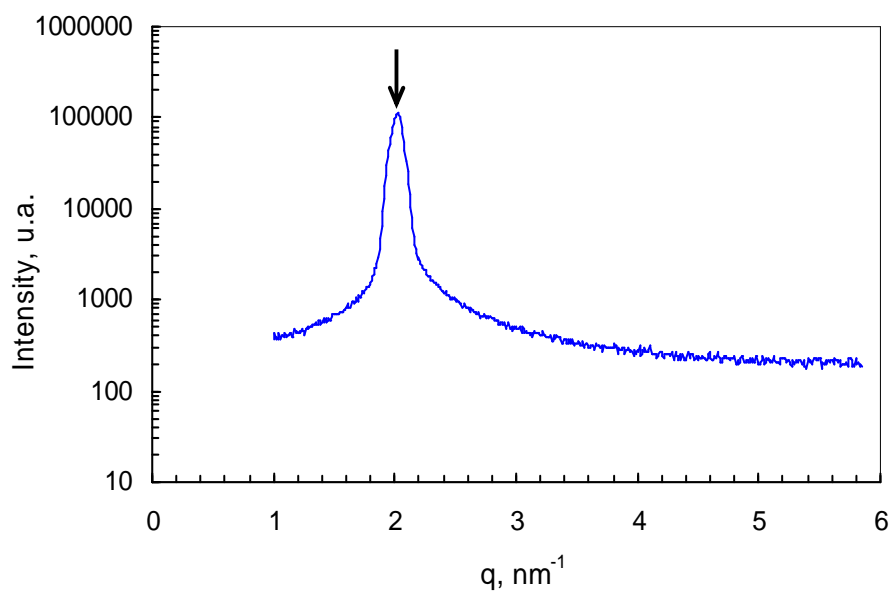


Figure 3.15: SAXS spectrum of dried 2-HDM at 25.0 °C.

Table 3.2: d-spacing and lattice spacing (nm) of dried 2-HDG and 2-HDM obtained by SAXS experiments at 25.0 °C.

Sample	d-spacing (nm) ($d = 2\pi/q$)	Lattice spacing / repeat distance, a (nm)
2- HDG	2.5	3.0
2-HDM	3.1	-

3.5.6 SAXS Results of Hydrated Branched-chain Glycolipids

The X-ray scattering was further conducted to confirm the lyotropic results of branched-chain glycolipids. **Figure 3.16** shows the SAXS spectrum of the settled hydrated 5.0 wt% 2-HDG at 25.0 °C. The three equidistant peaks show a typical pattern of hexagonal phase. The lattice spacing is bigger and the patterns are more intense compared to the dried sample indicating that the hydrated molecules swell further and better organized in water. This can be due to the water molecule strongly bonded to the hydroxyl group in glucoside polar head through H-bonding. Therefore, 2-HDG formed a more ordered hexagonal phase with lattice spacing of 4.4 nm.

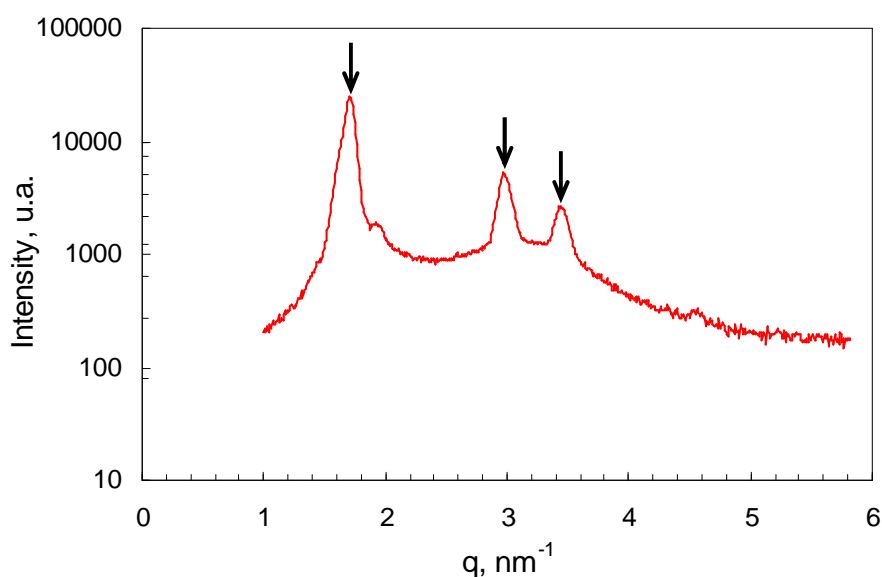


Figure 3.16: SAXS spectrum of hydrated 5.0 wt% 2-HDG at 25.0 °C.

Figure 3.17 shows the SAXS spectrum of the settled hydrated 5.0 wt% 2-HDM at 25.0 °C. The three equidistant peaks can be observed, which indicates the typical pattern of a lamellar phase. The settled hydrated 2-HDM formed a lamellar liquid crystalline phase with lattice spacing of 4.3 nm. This hydrated molecules swell further and better organized in water due to the water molecule strongly bonded to the hydroxyl group in maltoside polar head through H-bonding. Accordingly, X-ray scattering of the hydrated 5.0 wt% 2-HDM at 25.0 °C confirmed the existence of the lyotropic lamellar phase in OPM measurement. **Table 3.3** summarizes the results from SAXS experiments for the hydrated glycosides at 25.0 °C.

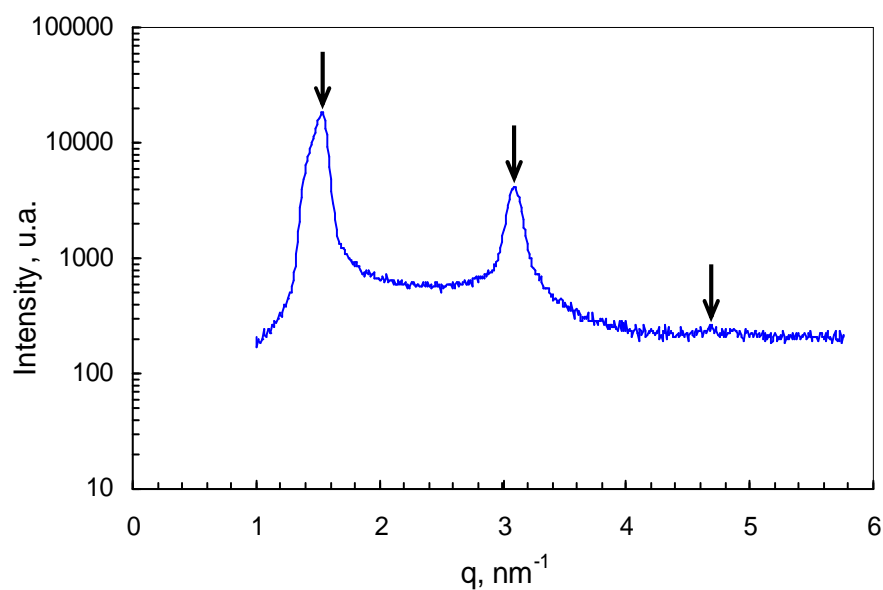


Figure 3.17: SAXS spectrum of hydrated 5.0 wt% 2-HDM at 25.0 °C.

Table 3.3: d-spacing and lattice spacing (nm) of hydrated 5.0 wt% 2-HDG and 2-HDM obtained by SAXS experiments.

Sample	d-spacing (nm) ($d = 2\pi/q$)	Lattice spacing / repeat distance, a (nm)
2- HDG	3.8	4.4
2-HDM	4.3	4.3

3.6 CONCLUSIONS

2-hexyldecyl- β (/ α)-D-glucoside (2-HDG) and 2-hexyldecyl- β (/ α)-D-maltoside (2-HDM) are two new nature-like branched-chain glycolipids with interesting phase behaviours. In a thermotropic study, the more hydrophobic surfactant 2-HDG was characterized by a columnar phase, whereas the more hydrophilic surfactant 2-HDM exhibited a smectic A phase. In a lyotropic study (from high to low water gradient), 2-HDG showed two phase transitions, namely isotropic phase (L) \rightarrow inverted hexagonal phase (H_{II}), whereas 2-HDM showed three phase transitions, namely isotropic phase (L) \rightarrow lamellar phase (L_{α}) \rightarrow smectic A phase (SmA). X-ray scattering confirmed the OPM results in which 2-HDG was characterized by hexagonal phase in the dried and hydrated form, whereas 2-HDM exhibited a lamellar phase in the hydrated form.

CHAPTER 4:

BINARY PHASE BEHAVIOUR OF BRANCHED-CHAIN GLYCOLIPIDS/WATER SYSTEM TOWARDS FORMATION OF HEXOSOMES AND VESICLES

4.1 INTRODUCTION

This chapter will describe the formation of hexosomes and vesicles from the binary phase of 2-hexyldecyl- β (/ α)-D-glucoside (2-HDG) and 2-hexyldecyl- β (/ α)-D-maltoside (2-HDM) in aqueous medium. The colloidal properties and phase behaviours of both glycolipids probably deviate from the pure compounds because they were prepared as a technical grade compounds with β -dominant (~90%) anomeric mixtures. Even though they are mixture of α - and β - anomers, both show as surfactant functions [48]. It is important to understand the physico-chemical properties of the branched-chain glycolipids in aqueous medium which determine the formation of self-assembly structures such as hexosomes (inverted hexagonal liquid crystal dispersion) [87-88] and vesicles [159-160].

From the previous physico-chemical characterization (Chapter 3), the more hydrophobic surfactant 2-HDG forms an inverted hexagonal liquid crystalline phase, and is expected to form hexagonal or spherical-shaped particles (hexosomes) in aqueous medium. On the other hand, the more hydrophilic surfactant 2-HDM forms a lamellar liquid crystalline phase, and is expected to form vesicles in aqueous medium. Thus, 2-HDG and 2-HDM dispersions may be used as innovative drug carrier systems, where hydrophilic or hydrophobic active compounds can be incorporated due to high amounts of amphiphilic surfactants [87-88,159-161] in the system.

In this work, the solution of glycolipids and their mixture with dioctyl sodium sulfosuccinate (AOT) and sodium dodecyl sulfate (SDS) were prepared in aqueous media in order to determine their critical aggregation concentrations (CAC). The CAC results show the presence of aggregate molecules from the appearance of the surfactant solutions from clear (one-phase) to turbid (two-phase) solution at very low concentrations and therefore further investigations on binary phase behaviour of

glycolipids/water systems were conducted. The purpose of this investigation is to determine the one-phase and two-phase regions of glycolipids/water system as a function of different concentrations and temperatures. Once these regions are known, samples with two-phase region have been further studied using X-ray scattering technique to determine their phases. The 2-HDG and 2-HDM dispersions were further characterized using 3D-photon correlation spectrometer (3D-PCS) and cryogenic transmission electron microscopy (Cryo-TEM) in order to determine their particles size, stability and images. The effect of anionic surfactants such as SDS and AOT towards the glycolipids aggregation also has been explored.

4.2 MATERIALS

The prepared 2-hexyldecyl- β (/ α)-D-glucoside (2-HDG) and 2-hexyldecyl- β (/ α)-D-maltoside (2-HDM) were further used for characterization. Anionic surfactants such as dioctyl sodium sulfosuccinate/Aerosol OT (AOT) (98%) and sodium dodecyl sulfate (SDS) (98%) were purchased from Aldrich. De-ionized filtered water (Milli-Q[®], Millipore) with the strength of an ionic conductivity of 18.2 μ S/cm was used for all sample preparations.

4.3 METHODOLOGY

4.3.1 Samples Preparation for Critical Aggregation Concentration (CAC) Determination

The critical aggregation concentrations (CAC) of two branched-chain glycolipids (2-HDG and 2-HDM) were determined with surface tension measurements. A stock solution of 2-HDG and 2-HDM were prepared with final concentrations of 0.10 mM and 0.20 mM respectively. A series of 2-HDG and 2-HDM solutions with different concentrations were prepared by subsequent dilutions from the stock solution. Homogeneity of the samples was attained using a Heidolph REAX top model vortex mixer. In this work, the effect of added component was studied to which the profile showed a very large reduction in surface tension at the low concentration and it remained constant at the critical concentration. The influence of anionic surfactants such as SDS and AOT towards the glycolipids aggregation was also investigated. The mixing ratio was fixed to 10:1 of glycolipid (nonionic surfactant) to anionic surfactant. The selection of this mixing ratio is due to the stability of the system against precipitation.

4.3.2 Preparation of Glycolipids/Water System

A series of 2-HDG and 2-HDM samples with different concentrations from 0.002 wt% to 0.050 wt% were prepared in water with a total mass of 2.0 g. After weighing each sample, it was then closed with parafilm to avoid from evaporation or contamination. All samples were then centrifuged using 5804 R Eppendorf Centrifuge for about 5 min with the speed of 3000 rpm to ensure that all components were located at the bottom of the tubes. Finally, the glass tubes were sealed hermetically with flame to avoid the samples being evaporated or contaminated during the heating or cooling

process. Subsequently, all samples were homogenized by stirring with a Heidolph REAX top model vortex mixer for a few minutes to form homogeneous solution and placed in the freezer for 24 h.

The binary phase behaviour determination was conducted in a ThermoScientific water bath (DC 10) equipped with thermostat (EK 20) starting from 5.0 °C to 95.0 °C, by monitoring the physical changes as a function of temperature for every 5.0 °C. Any physical changes such as the formation of one-phase (clear) or two-phase (turbid/phase separation) was monitored and recorded. The selected turbid samples were further observed under cross polarizer filters to determine the liquid crystalline region.

4.3.3 Preparation of Hexosomes

A 0.50 wt % solution of 2-HDG in water was heated at 70.0 °C for 2 h. Each sample was sonicated for 30 min in a P-Selecta ultrasound water bath and 15 min with MS 72 probe of a Bandelin Sonoplus ultrasonic homogenizer (30%, 15 kJ), which resulting a turbid dispersion. The hexosomes were therefore in a large amount of excess water and far from the water separation line. This study was focusing at 0.50 wt% in which a big number of hexosomes particles could be observed under cryo-TEM.

4.3.4 Preparation of Vesicles

A 0.50 wt% solution of 2-HDM in water was heated at 70.0 °C for 2 h. Each sample was sonicated for 30 min in a P-Selecta ultrasound water bath and 15 min with the MS 72 probe of a Bandelin Sonoplus ultrasonic homogenizer (30%, 15 kJ), which resulting a turbid dispersion (vesicles formation). In the case of glycolipid mixed with anionic surfactants (AOT and SDS), 5 min of ultrasonication was sufficient for homogenizing the samples.

4.4 INSTRUMENTATIONS

4.4.1 Tensiometer

A tensiometer balance from KRÜSS (Germany) with K12 tensiometer processor has been used to determine the critical aggregation concentration (CAC) of 2-HDG and 2-HDM (nonionic surfactant) and mixtures of glycolipids and anionic surfactants in aqueous solution. CAC can be determined by either surface tension or interfacial tension measurement. In this work, CAC of all samples were measured by air-water surface tension measurement. The Wilhelmy plate method was used for this purpose (**Figure 4.1**), which does not require correction factor, but necessary calibration with distilled-deionized water is required prior to measurement. The acceptable requirement surface tension value for distilled-deionized water is between 71-72 mN/m at 25.0 °C.

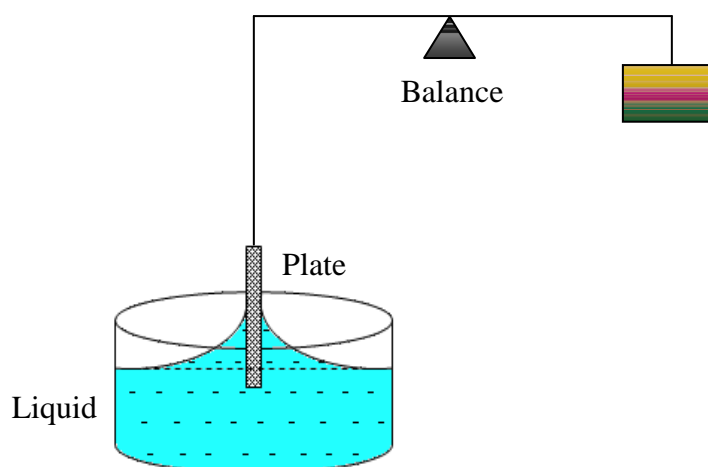


Figure 4.1: A schematic diagram of Wilhelmy plate method used for measuring the surface tension of the solution.

4.4.2 3D-Photon Correlation Spectrometer (3D-PCS)

A 3D-Photon Correlation Spectrometer from LS Instruments (Fribourg, Switzerland) was used for dynamic light scattering (DLS) at an angle of 90° and static light scattering (SLS) for angles between 20° and 140° (**Figure 4.2**). DLS measured the particles radii and their polydispersity index, whereas SLS gave the overall size and shape of the particles. Multiple scattering is suppressed using 3D-cross correlation technology (down to 5% of transmission for sub-micrometer sample thickness). The instrument was equipped with a He-Ne laser (632.8 nm). Triplicate readings of 200 s were recorded for each sample. The particles (hexosomes and vesicles) radii were calculated by a manual exponential fitting of the first cumulant parameter. For a better visualization, the Contin analysis was performed to give the size distribution and ALV software from Dullware was utilized for better visualization. The measurement temperature was maintained at 25.0°C by a decaline bath, which matches the refractive index of glass and therefore does not interfere with the measurement.

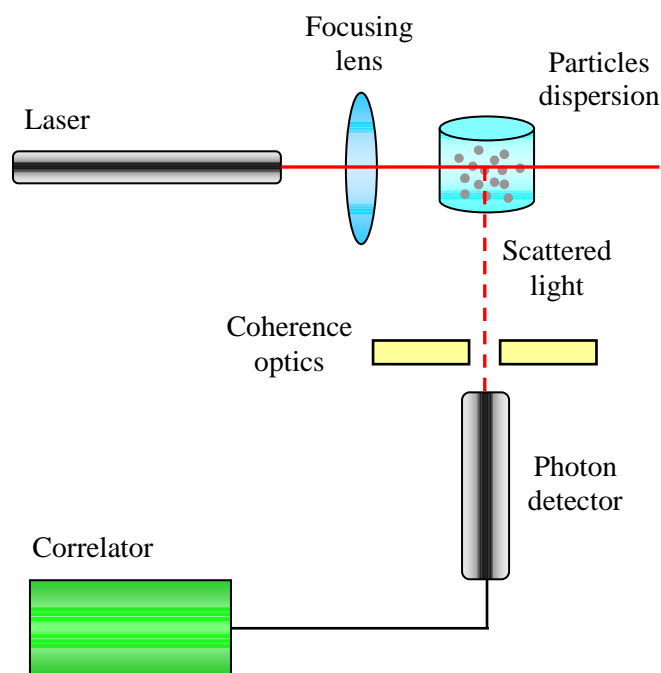


Figure 4.2: A schematic diagram of a conventional photon correlation spectrometer.

4.4.3 Nano-Zetasizer

Nano-Zetasizer from Malvern was used to study the zeta potential of the glycolipids dispersions (hexosomes and vesicles). A schematic diagram of zeta potential measurement is shown in **Figure 4.3**. Three measurements of 20 sub-runs were performed for each sample by using a zeta-potential DTS1060C cell. Reference materials were liposomes with a refractive index of 1.40. The Smoluchowski model (4.1) and auto mode was applied to treat data.

$$\mu = \frac{\zeta \cdot \epsilon \cdot \epsilon_0}{\eta} \quad (4.1)$$

where ϵ_0 is the dielectric constant of a vacuum; ϵ is the dielectric constant of the buffer solution, η is the viscosity of the buffer solution and μ is the electrophoretic mobility.

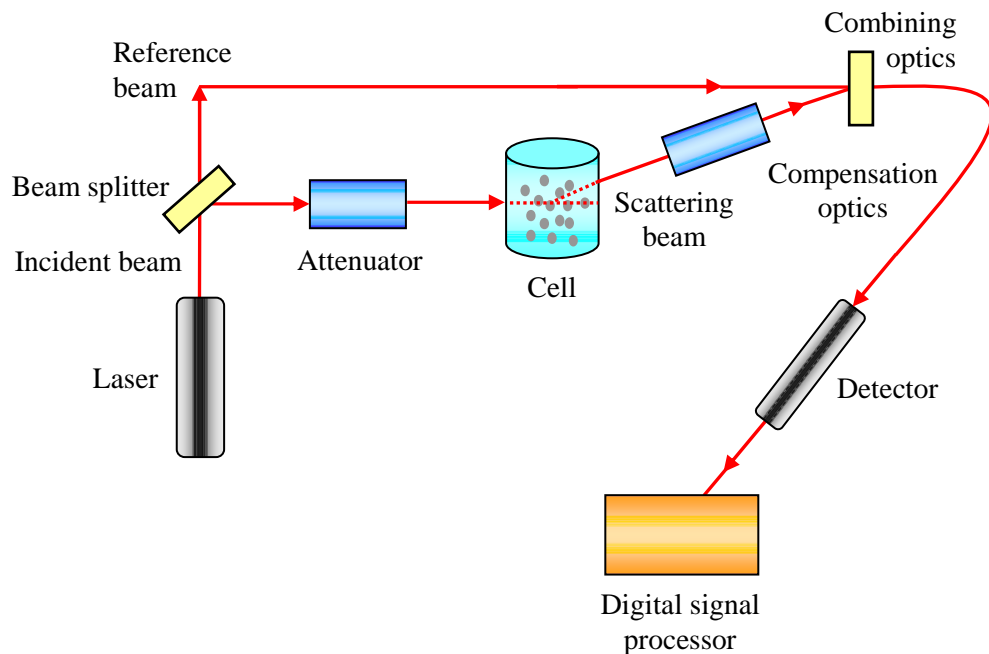


Figure 4.3: A schematic diagram of the Nano-Zetasizer setup for zeta potential measurement.

4.4.4 Cryogenic Transmission Electron Microscopy (Cryo-TEM)

Cryo-TEM measurement was performed at the Microscopy Service, Autonomous University of Barcelona to determine the actual size and to obtain images of hexosomes and vesicles. A JEOL JEM-2011 Transmission Electron Microscope (Jeol LTD. Tokyo, Japan) was operating at voltage acceleration of 200 kV. **Figure 4.4** shows the principle of a transmission electron microscope.

The sample holder used for cryo measurement was tilted at 60°. The images were recorded with a slow scan digital camera of Gatan 794 MSC 600HP or onto negatives for high-resolution analysis. The resolution for this measurement is 0.14 – 0.19 nm while the magnification is 2000 – 3,000,000x. The FASTEM control system with R-X EDS INCA micro-analyzer was utilized for this purpose.

For samples preparation, 5.0 µL of dispersion was deposited onto a QUANTIFOIL[®] R 1.2/1.3 grid and the excess was eliminated with Whatman N°1 paper. The vitrification was done with a Cryo Preparation Chamber (CPC) from Leica by immersing the grid in liquid ethane. Then, the frozen grids were stored in liquid nitrogen and transferred into a Cryo-holder that was kept at -180.0 °C.

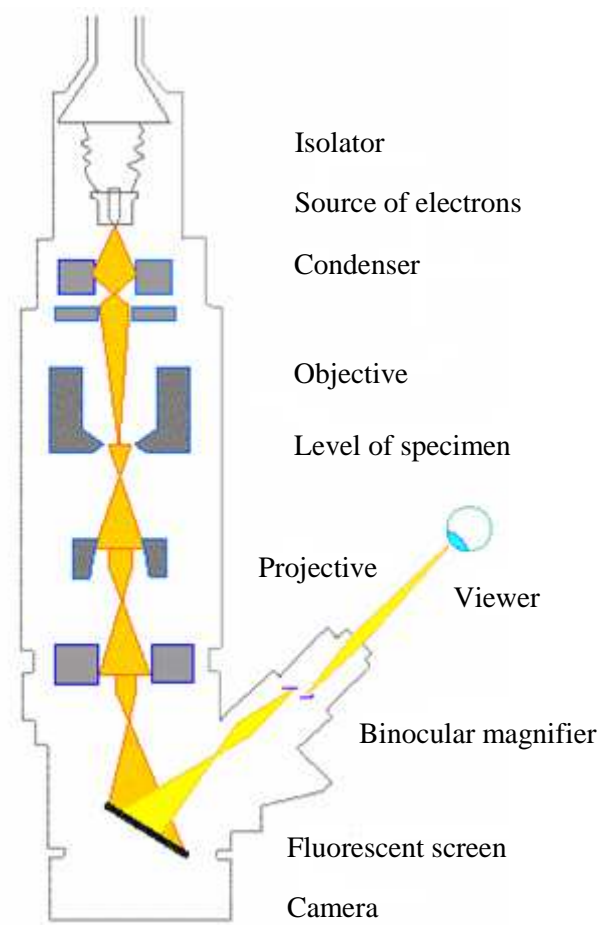


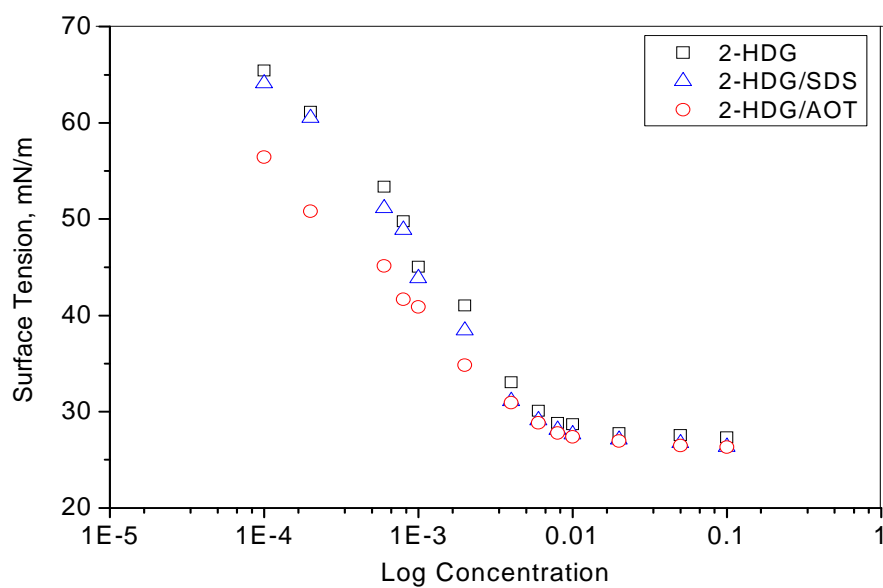
Figure 4.4: A schematic diagram of a transmission electron microscope (TEM). The electron beam is highlighted in yellow while electron-optical lenses are depicted in grey.

4.5 RESULTS AND DISCUSSIONS

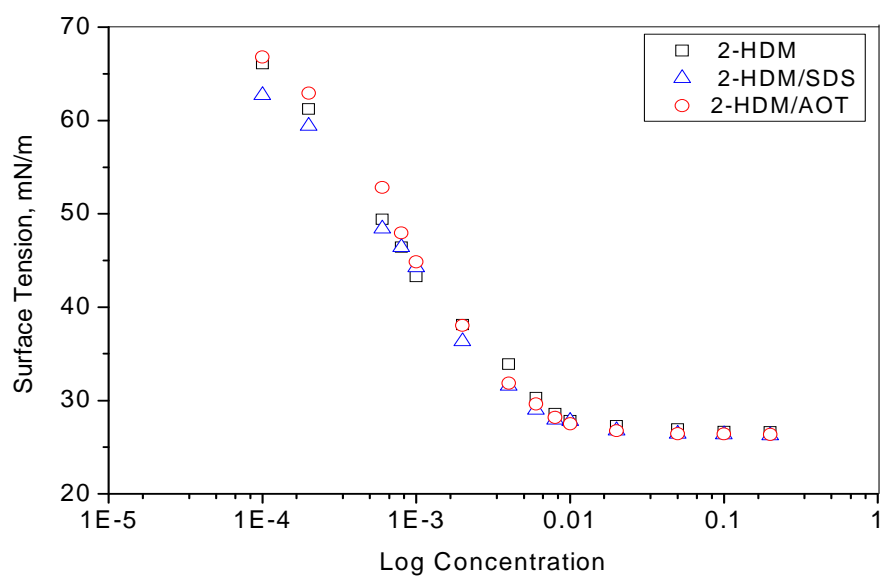
4.5.1 Critical Aggregation Concentration (CAC)

The surface tensions of the surfactant solution with different log concentration have been determined and the profiles are given in **Figures 4.5a** and **4.5b**. From the profiles, the surface tensions of the solutions decrease with increasing concentrations but the slopes of the profiles change drastically at 0.007 mM and 0.0085 mM for 2-HDG and 2-HDM respectively (**Table 4.1**). It is evident that these glycolipids molecules prefer to accumulate at the surface rather than to stay solubilized in the bulk solution. This implies that they are highly surface-active materials. These also suggest that lower hydrophilic surfactant (2-HDG) is easier to aggregate than 2-HDM (higher hydrophilic group). CAC of 2-HDM is higher because of it has more polar head group (bigger head group size) [6].

The effect of SDS and AOT on 2-HDG and 2-HDM has also been investigated using similar method. A ratio of 10:1 in weight percent of glycolipids to SDS or AOT was chosen due to the stability of the system against precipitation. The profiles of the surface tension of 2-HDG and 2-HDM solutions in the presence of SDS or AOT show similar trends (**Figures 4.5a** and **4.5b**). Although the difference is not significant, the addition of anionic surfactant slightly increased the solubility of 2-HDG and 2-HDM in water and thus, the CAC of 2-HDG and 2-HDM increased to higher concentrations. These indicate that the anionic surfactants have better interaction with the polar head group of glycolipids (nonionic surfactants) through ion dipole interactions (hydrogen bonding) [4,7,14], resulting them better solubilized in aqueous media. However, the CAC of 2-HDM/anionic mixtures are still higher than those of 2-HDG/anionic mixtures as shown in **Table 4.1**.



(a)



(b)

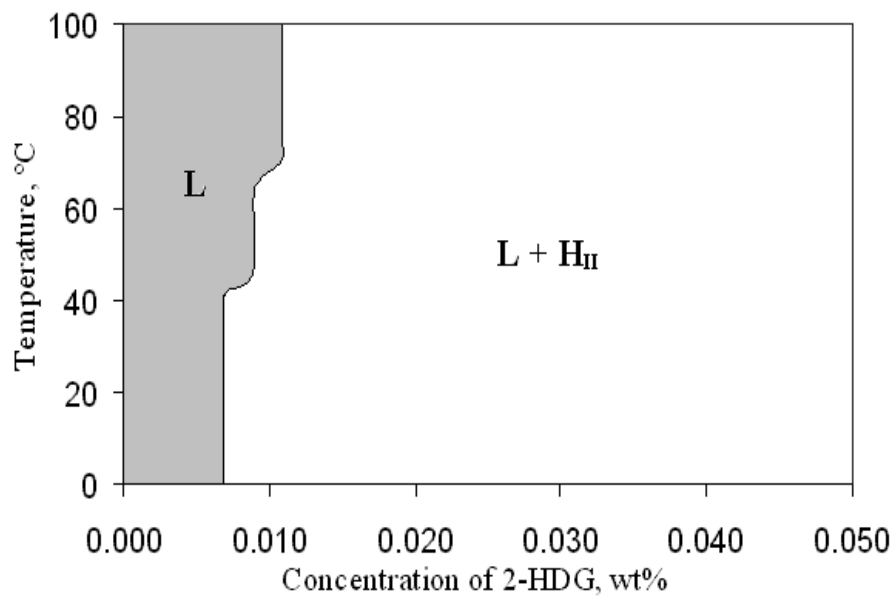
Figure 4.5: Surface tension profiles of (a) 2-HDG and (b) 2-HDM alone and mixed with SDS or AOT as a function of log concentration at 25.0 °C.

Table 4.1: The CAC values of 2-HDG and 2-HDM alone and mixed with SDS or AOT in aqueous solution at 25.0 °C. The 2-HDG or 2-HDM/SDS or AOT ratio was fixed to 10:1.

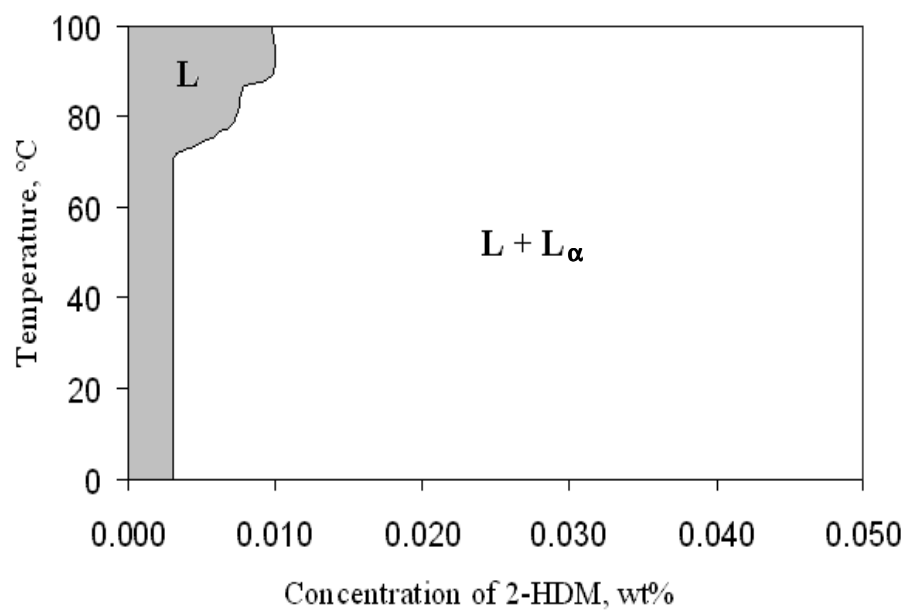
Surfactant solution	CAC, mM
2-HDG	0.007
2-HDG/SDS	0.008
2-HDG/AOT	0.009
2-HDM	0.0085
2-HDM/SDS	0.0095
2-HDM/AOT	0.010

4.5.2 Binary Phase Behaviour of 2-HDG/Water and 2-HDM/Water Systems

The binary phase behaviour of 2-HDG and 2-HDM from 0.002 wt% to 0.050 wt% in water were studied at various temperatures. From the pseudo-binary phase diagram of 2-HDG/water system (**Figure 4.6a**), a one-phase region (isotropic solution, L) was observed from 0.002 wt% up to 0.006 wt%, whereas a one-phase region of 2-HDM/water system (**Figure 4.6b**) is only observed up to 0.002 wt% at 25.0 °C. Two-phase region has been observed at a higher concentration than 0.006 wt% and 0.002 wt% of 2-HDG and 2-HDM respectively. An interesting observation in the 2-HDG and 2-HDM phase diagrams is the solubility of surfactant in water increased with temperature at lower concentration. As can be seen in **Figure 4.6a**, the solubility of 0.008 wt% of 2-HDG increased at 45.0 °C, while 0.010 wt% at 70.0 °C (one-phase region). On the other hand, the solubility of 0.004 wt% of 2-HDM is increased at 75.0 °C, while that for 0.006 wt% is at 80.0 °C and that for 0.008 wt% is at 90.0 °C (one-phase region), as shown in **Figure 4.6b**.



(a)



(b)

Figure 4.6: Pseudo-binary phase diagram of (a) 2-HDG/water and (b) 2-HDM/water systems as a function of temperature. One-phase region of isotropic phase (grey) and two-phase region of (a) an inverted hexagonal liquid crystalline phase and (b) lamellar liquid crystalline phase dispersed in water (white).

The occurrence of phase separation (two-phases in coexistence) is probably because of the attractive Van der Waals force between the aggregates increases with increasing aggregates sizes and the minimum aggregates interaction curve exceeded the thermal motion [4,7,14]. Furthermore, the lamellar phase of 2-HDM is difficult to swell. This fact implies that there is no or little undulations in the lamellar structure (2-HDM) compared to hexagonal (2-HDG), which can give rise to a long-range stabilizing repulsive effect. The solubility of maltoside also differs from the glucoside. This is due to its molecular structure, molecular weight and polarity, which is much higher compared to glucoside.

According to the previous optical polarizing microscopy and small-angle X-ray scattering results (Chapter 3), it can be shown that in the two-phase region, 2-HDG forms colloidal dispersions of inverted hexagonal liquid crystalline phase in the aqueous solution. These dispersions, denominated hexosomes are known to form in region of the phase diagram, where an inverted hexagonal phase (H_{II}) coexists in equilibrium with an aqueous solution, made of excess water [80,88]. It should be noted that the formation of hexosomes has been described in water/glycerol monooleate/tricaprilin systems [65] although the presence of a stabilizer such as Pluronic F127 was found to improve their stability [88]. On the other hand, the two-phase region of 2-HDM can be attributed to the lamellar liquid crystalline (L_{α}) dispersion in water, which led to the formation of vesicles [162-164].

4.5.3 Hexosomes Formation from 2-HDG

Dispersion of 2-HDG in water results to the formation of hexosomes (**Figure 4.7**) from an inverted hexagonal liquid crystalline phase. The presence of an inverted hexagonal phase is due to the surfactant possesses rather hydrophobic characteristic. The large hydrophobic part in the alkyl branched-chain and the single glucose unit in the hydrophilic part tip the hydrophilic-lipophilic balance to favour the formation of an inverted hexagonal phase. Indeed, the surfactant packing parameter ($P = v/a_0l$) [33] of 2-HDG is 1.45. A necessary condition for the formation of inverted structures is when $P > 1$ [4], thus the value of 1.45 obtained for the glucoside derivative confirmed the formation of an inverted hexagonal phase.

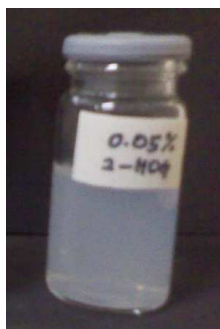


Figure 4.7: An example of 2-HDG hexosomes sample.

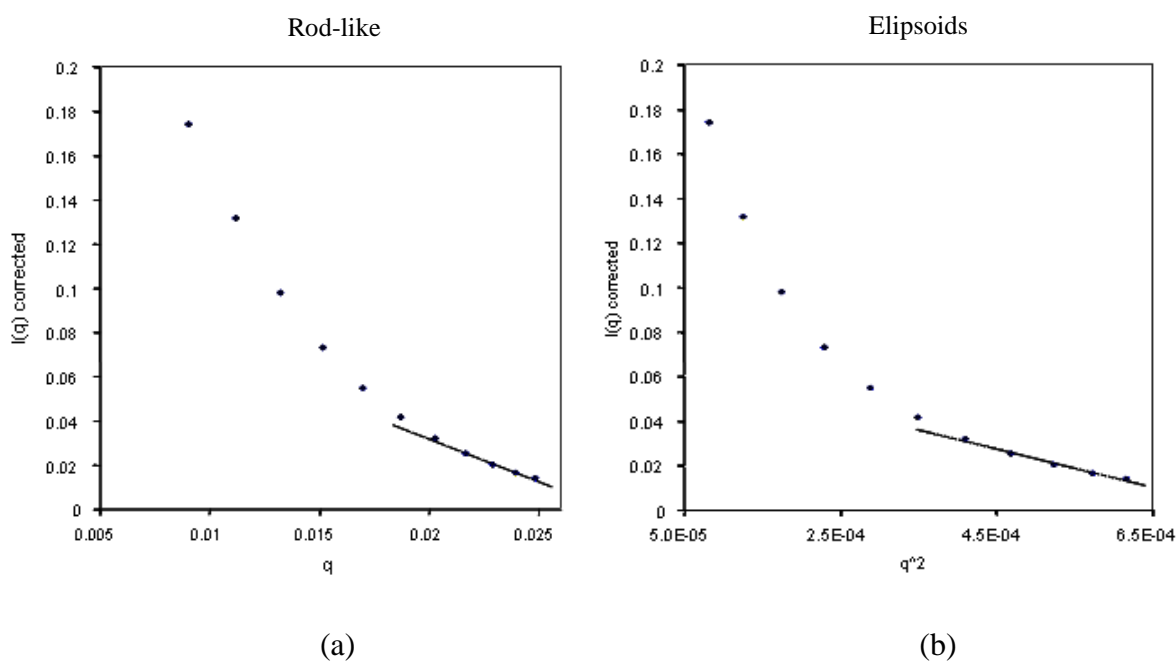
The actual size, inner structure and morphology of the well-organized hexosomes in water have been further characterized by cryo-TEM, whereas the particle shape, size distribution and stability of hexosomes were investigated by SLS and DLS techniques.

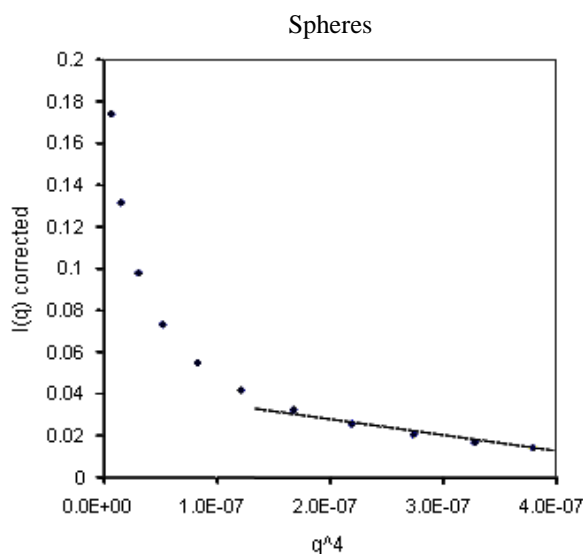
Static Light Scattering (SLS)

The static light scattering was conducted for 2-HDG hexosomes sample. Different angles were measured to determine the overall particles size in the hexosomes system as shown in **Table 4.2**. The purpose of this measurement is to have an overall idea of the expected particle size and shape of hexosomes, before cryo-TEM being conducted as a confirmation of hexosomes formation. Thus, **Figure 4.8** shows the most rationalized hexosomes particle's shape is that of a sphere.

Table 4.2: Static light scattering measurement at different angles.

Angle	R, nm
50°	390
90°	123
130°	70





(c)

Figure 4.8: Static light scattering of 2-HDG hexosomes and MALLS (multi-angle laser light scattering) measurements.

Dynamic Light Scattering (DLS)

Dynamic light scattering measurement has been conducted for 2-HDG hexosomes sample with concentration of 0.50 wt%. The selection of this concentration is due to the high amount of amphiphilic glycolipids in aqueous medium; thus, it could form more hexosomes particles in the sample. DLS measurement of the dispersions gives the hydrodynamic radius of hexosomes to be about 100 nm (**Figure 4.9**). **Figure 4.10** shows the electron micrograph of hexosomes measured by cryo-TEM, which are visualized as hexagonal or spherical-shaped particles of about 50-100 nm in diameter.

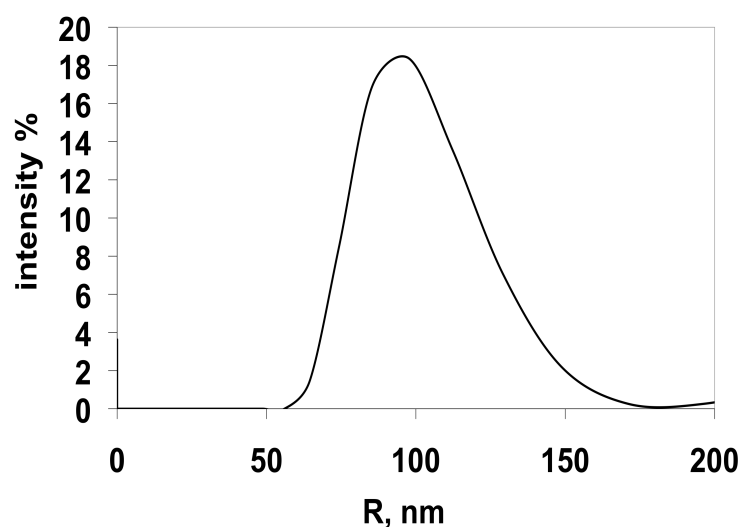


Figure 4.9: Radius distribution of hexosome dispersion with 0.50 wt% of 2-HDG in water obtained by a Contin data analysis of dynamic light scattering results.

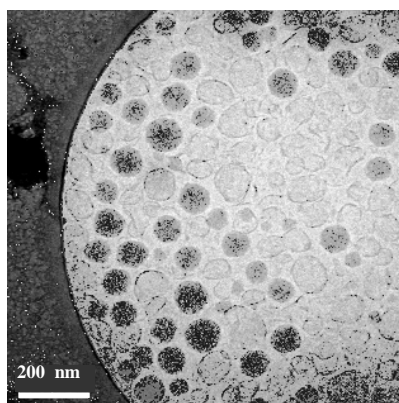


Figure 4.10: Cryo-TEM micrograph of hexosomes dispersion with 0.50 wt% of 2-HDG in water. Hexosomes are visible as dark grey hexagonal or spherical-shaped particles.

As expected, the hexosome particle size measured by Cryo-TEM is smaller compared to the particle size measured by photon correlation spectroscopy. This is reasonable, since particle sizes obtained from light scattering are hydrodynamic radii, i.e. the actual particle radius plus strongly bound water, which moves with the object through the bulk phase. As a consequence, the hydrodynamic radius measured by

light scattering is usually bigger than that observed by electron microscopy, which shows the actual radius. Moreover, it cannot be excluded that the freezing of the sample, even rapidly performed, shrank the particles, which would also lead to smaller particle sizes. In addition, the relatively high polydispersity index obtained by light scattering measurements (0.3) could indicate the existence of bigger particles or aggregates, which will increase the mean radius of the DLS measurements.

The 2-HDG/water dispersions were not stable, and the particle settled down after several days. There are several reasons for the low dispersion stability. Firstly, a weak electrostatic stabilization could be assumed, even though the zeta potential of hexosome dispersion with 0.50 wt% of 2-HDG in water was measured to -33.5 mV, which is usually sufficient for an electrostatic stabilization. Secondly, the relatively high polydispersity (**Figure 4.10**) influenced significantly the dispersion stability. Finally, the inability of the glycolipid (2-HDG) to form lamellar bilayers is also a factor to the low dispersion stability. Usually, hexosomes are particles of an inverted hexagonal liquid crystalline structure, stabilized by a layer of surfactant on the water-hexosome interface. Hexosomes based on the hydrophobic surfactant; 2-HDG might not be sufficiently stabilized, since the hydrophilic-lipophilic balance of the surfactant does not allow the formation of a stable double layer. Similar cases in the literatures described the stabilization of hexosomes with Pluronic F127 [88].

4.5.4 Vesicles Formation from 2-HDM

Lamellar liquid crystalline phases form under high energy input leads to the formation of multilamellar vesicles in water (**Figure 4.11**), where the energy input can be in the form of applied shear [165] or ultrasonication [162]. This work presents lamellar dispersions obtained by ultrasonication technique. Dynamic light scattering measurements at 25.0 °C showed a main population at 179 nm in the hydrodynamic radius and a wide size distribution for 2-HDM vesicles sample with concentration of 0.50 wt%. The preliminary result shows that the supplied energy input significantly influenced the size of vesicles. Higher energy input led to the formation of smaller vesicles, which might be of the unilamellar type. Thus, changing the multilamellar structure to unilamellar.



Figure 4.11: An example of 2-HDM vesicles sample.

In order to visualize the vesicles, lamellar dispersion with 0.50 wt% of 2-HDM in water was investigated by Cryo-TEM. **Figure 4.12** shows the electron micrograph of multilamellar vesicles (MLVs) in the range of 50-100 nm in radius, which was smaller than the hydrodynamic radius measured by dynamic light scattering. However, the micrograph shows high polydispersity. The vesicles are composed of multilayers, which are common for the concentrated solutions, such as phospholipids [162,166].

The number of layers can be estimated as 3-10, as observed by Cryo-TEM, and the interlayer distance can be estimated around 3.5-4.0 nm, which corresponds to the d-spacing measured by SAXS on the hydrated solid surfactant.

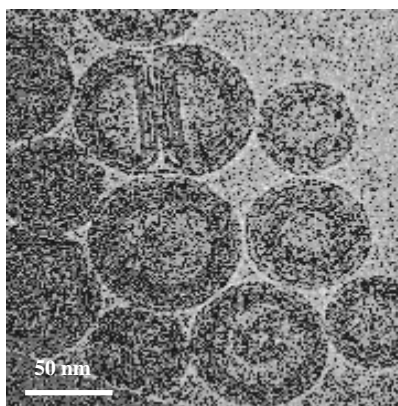


Figure 4.12: Cryo-TEM micrograph of 0.50 wt% of 2-HDM dispersion. Multilamellar vesicles (MLVs) with polydisperse nature can be observed.

The stability of the vesicles was very low and a white precipitate was observed after several days. This can be explained by the high polydispersity, which promotes vesicles fusion, the multilamellar structure or the temperature dependence of the spontaneous curvature H_0 of the surfactant [167]. Multilamellar vesicles are obtained by high energy input and they are therefore not in thermodynamic equilibrium [162]. In addition, low electrostatic repulsion was observed by electrophoretic mobility measurements. The zeta-potential of -19.3 mV is too low to stabilize the vesicle formation.

4.5.5 Effect of Adding Anionic Surfactant to 2-HDM Vesicles

In order to enhance the stability of 2-HDM vesicles, preliminary studies on 2-HDM/anionic surfactant mixtures were performed. Two standard anionic surfactants (ASs) have been chosen for this purpose, namely Aerosol OT (AOT) and sodium dodecyl sulfate (SDS).

For the preliminary test on the influence of anionic surfactants on the aggregation behaviour of 2-HDM in water, a ratio of 10:1 (wt%) of 2-HDM to anionic surfactant was chosen. 1.0 wt% dispersions of 2-HDM/AOT has been prepared and appeared as more translucent compared to the corresponding 2-HDM dispersion. However, dynamic light scattering measurements (**Figure 4.13**) of the 2-HDM/AOT mixture shows a broad polydispersity, with at least two populations. Indeed, the Cryo-TEM micrograph (**Figure 4.14**) shows two types of unilamellar vesicles with different range of sizes which are small unilamellar vesicles (SUVs) with size between 20-100 nm and large unilamellar vesicles (LUVs) with size between 100-200 nm.

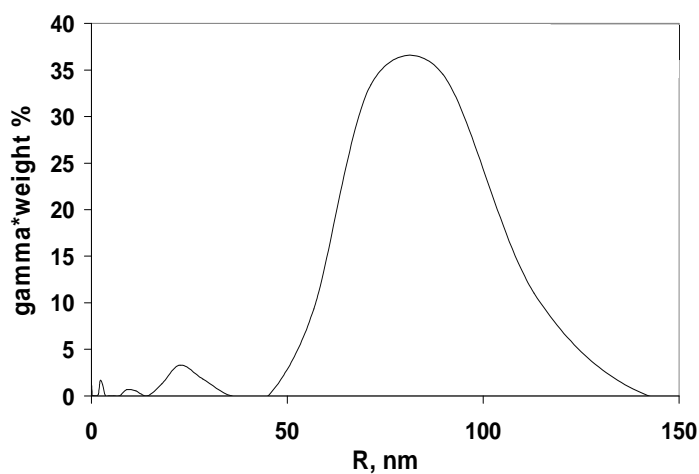


Figure 4.13: Radius distribution of 1.0 wt% of 2-HDM/AOT dispersion in water. Two main populations were observed at 80 and 25 nm.

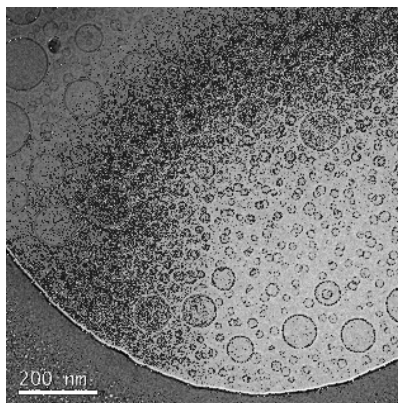


Figure 4.14: Cryo-TEM micrographs of 1.0 wt% of 2-HDM/AOT dispersions. Spherical unilamellar vesicles were observed, indicating that AOT induced the formation of small and large unilamellar vesicles.

On the other hand, addition of SDS to the 2-HDM dispersion led also to a translucent dispersion with a main hydrodynamic radius of 40 nm, which was measured by dynamic light scattering (**Figure 4.15**). The radius distribution was still broad, but no other population significantly detected by DLS. Cryo-TEM micrographs indicated that only small unilamellar vesicles (SUVs) were formed (**Figure 4.16**), with size between 30-80 nm which corresponds to the hydrodynamic radius measured by dynamic light scattering. Thus, the stability of 2-HDM/SDS dispersions was increased for more than one week.

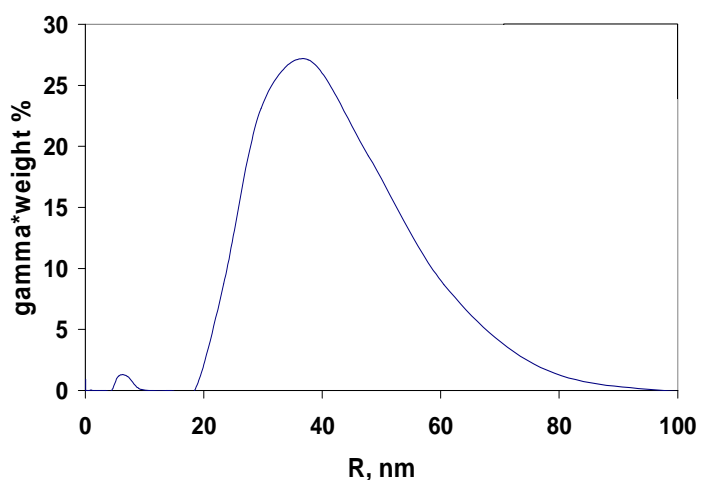


Figure 4.15: Radius distribution of 1.0 wt% of 2-HDM/SDS dispersion in water. Main population was observed at 40 nm.

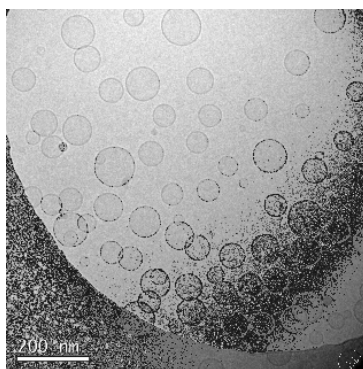


Figure 4.16: Cryo-TEM micrographs of 1.0 wt% of 2-HDM/SDS dispersions. SDS induced the formation of small unilamellar vesicles.

The difference between the addition of AOT and SDS might be explained by the different numbers of alkyl chains of the surfactants. SDS is a monoalkylated surfactant, while AOT possesses two alkyl chains in the hydrophobic part. In the aggregation process, the presence of two alkyl chains may disturb more significantly the organization of the 2-HDM surfactant, which led to the formation of two populations with different radii. On the other hand, the monoalkylated SDS might be more adapted for the issue, allowing the formation of small unilamellar vesicles of a single size distribution [112,116]. However, further investigation on 2-HDM/AS mixtures will be conducted in the future in order to optimize the systems' stabilities in view of their application for drug delivery.

4.6 CONCLUSIONS

In glycolipids/water dispersion, the more hydrophobic surfactant 2-HDG formed an inverted hexagonal liquid crystalline dispersion called hexosomes, whereas the more hydrophilic surfactant 2-HDM with more balanced hydrophilic-lipophilic properties formed lamellar liquid crystalline dispersion, which led to the formation of multilamellar vesicles (MLVs). Additions of AOT and SDS to the 2-HDM dispersion induced the formation of unilamellar vesicle with higher stability. This justifies further research on the possible incorporation and release of drug could be conducted in the future.

CHAPTER 5:
INFLUENCE OF BRANCHED-CHAIN GLYCOLIPIDS ON
TERNARY NANO-EMULSION AS DRUG DELIVERY
SYSTEMS

5.1 INTRODUCTION

This chapter will describe the influence of branched-chain glycolipids on ternary nano-emulsion for drug delivery system. From the literature survey, the application of glycolipids as biosurfactants has received tremendous attention in the recent years for examples [168-181], due to their unique properties such as nonionic, mild production conditions, lower toxicity, higher biodegradability, environmental compatibility and self-assembly properties. Furthermore, nano-emulsions prepared using glycolipids have also been reported extensively, for examples [117-118,182-185]. Thus, studies on any novel synthetic glycolipids especially those which are closely related structurally to the natural ones are justified.

Among the synthetic glycolipids, branched-chain glycolipids provide a versatile alternative for natural ones, since apart from higher chain hydrophobicity factor, their double chain structure provide a suitable model that mimic the natural glycolipids. In this study, the influence of branched-chain glycolipids (2-hexyldecyl- β / α -D-glucoside and 2-hexyldecyl- β / α -D-maltoside) on the reference O/W nano-emulsion system of water/Cremophor[®] EL/medium chain triglyceride oil [150] was investigated with the inclusion of an active ingredient (a drug). Incorporation of small concentrations of the novel glycolipids in nano-emulsions of the reference system is expected to have an influence in their properties. Therefore, this study will contribute to the basic knowledge on nano-emulsions and may allow for expansion on the application field of these novel surfactants.

Accordingly, all nano-emulsions are further characterized using 3D-photon correlation spectrometer (3D-PCS), stability analyzer and cryogenic transmission electron microscopy (Cryo-TEM) in order to determine their droplets size, stability and images. Finally, the released drug concentrations from nano-emulsions and oil solution are analyzed by high-pressure liquid chromatography (HPLC).

5.2 MATERIALS

De-ionized filtered water (Milli-Q[®], Millipore) with the strength of an ionic conductivity of 18.2 $\mu\text{S}/\text{cm}$ was used for all sample preparations. Cremophor[®] EL (Crem EL) was obtained from BASF, Germany. Medium chain triglyceride (MCT) oil with density of 0.946 g/mL was purchased from Fagron Iberica, S.A.U. (RS)-2-(3-benzoylphenyl)propanoic acid (Ketoprofen) (99.9 %) was purchased from Sigma. Potassium dihydrogen phosphate ($\geq 99.5\%$), ortho-phosphoric acid (85.0 %) and methanol with density of 0.79 kg/L were purchased from Merck, while sodium phosphate dibasic anhydrous ($\geq 99.0\%$) was obtained from Fluka. Dialysis bags used in the release experiments were made of regenerated cellulose tubular membrane – Cellu-Sep with molecular weight cut-off of 12,000-14,000 Da. All purchased chemicals were of chemical grade and used as received. The prepared 2-hexyldecyl- β (/ α)-D-glucoside (2-HDG) and 2-hexyldecyl- β (/ α)-D-maltoside (2-HDM) were further used in the nano-emulsion formulation as prepared by [150].

5.3 METHODOLOGY

5.3.1 Preparation of Nano-emulsions

All nano-emulsion samples were prepared by low energy emulsification method (phase inversion composition) consisting of stepwise addition of water to mixtures of the other two components (oil and surfactant) while stirred by means of a Heidolph REAX top model vortex mixer [122,125] (**Figure 5.1**). The standard nano-emulsions with 90 wt% of water and different oil-surfactant (oil-Cremophor[®] EL) ratios were prepared ranging from 60/40, 50/50 to 40/60, whereas the surfactants mixtures were Cremophor[®] EL/2-HDG and Cremophor[®] EL/2-HDM with ratios of 95/5, 90/10, 85/15, 80/20, 70/30, 60/40 and 50/50. Preparation of samples were performed at 25.0 °C and 70.0 °C and the resulting nano-emulsions were kept at 25.0 °C and 37.0 °C for 1 month for stability study.

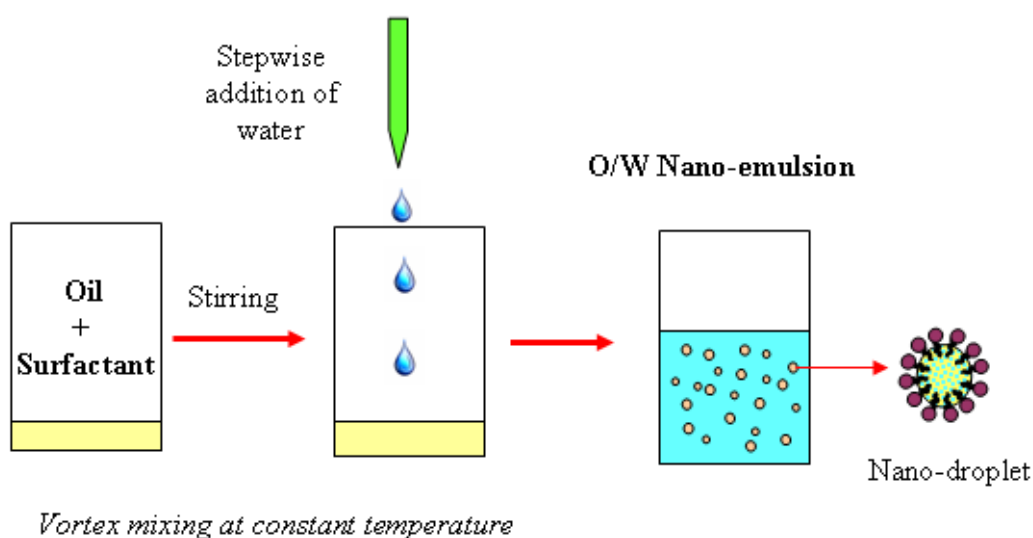


Figure 5.1: Low-energy emulsification method: Phase Inversion Composition (PIC).

5.3.2 Incorporation of Drug into Nano-emulsions

Ketoprofen (2-(3-benzoylphenyl)-propionic acid) with molecular weight of 254.281 g mol⁻¹ (**Figure 5.2**) is a non-steroidal anti-inflammatory drug (NSAID) with analgesic and antipyretic effects, was chosen for drug delivery study. It has a pKa of 5.94 in methanol:water (3:1) and in n-octanol:water partition coefficient of 0.97 (buffer pH 7.4). Ketoprofen is a white, odorless, non-hygroscopic, fine to granular powder and melts at about 95 °C. It is freely soluble in ethanol, chloroform, acetone, ether and soluble in benzene and strong alkali, but practically insoluble in water at 20.0 °C.

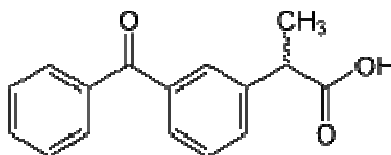


Figure 5.2: Chemical structure of ketoprofen.

Ketoprofen (hydrophobic drug) was incorporated into oil/surfactant mixtures prior to the addition of water to form the nano-emulsion. Then the samples were homogenized with a vortex mixer and then finally kept in water bath at 25.0 °C. The stability was examined by visual observation for at least 24 h after preparation. The optimized percentage of drug, which can be encapsulated was determined by the stability of the drug in nano-emulsion against precipitation. The stable encapsulated system was then carried out for drug release experiment.

5.3.3 *In-Vitro* Drug Release Experiment

3.0 g of nano-emulsion containing ketoprofen was filled in a dialysis bag and immersed for 24 h in a receptor solution (130 mL) consisting of a phosphate buffer solution at pH 7.4 which is considered to be the pH of blood. A Mettler Toledo Seven Easy model pH meter was used to determine the pH of the buffer solution. The diffusion cells consisted of three cylindrical thermo-jacketed glass vessels connected to a water bath set at 25.0 °C and closed to avoid loss of receptor solution by evaporation. The receptor solution was stirred by means of OVAN MultiMix Heat D (MMH90E) multi-places magnetic stirrer as shown in **Figure 5.3**.

The aliquot withdrawn was replaced with the same volume of receptor solution in order to maintain its volume constant. The volume of the receptor solution used, ensured sink conditions throughout the diffusion experiments, i.e. the concentration of the drug in the receptor solution was not higher than 10% of its solubility in this medium. Aliquots of receptor solution were withdrawn at time intervals for the determination of released drug and analyzed by Waters 1500 Series HPLC.

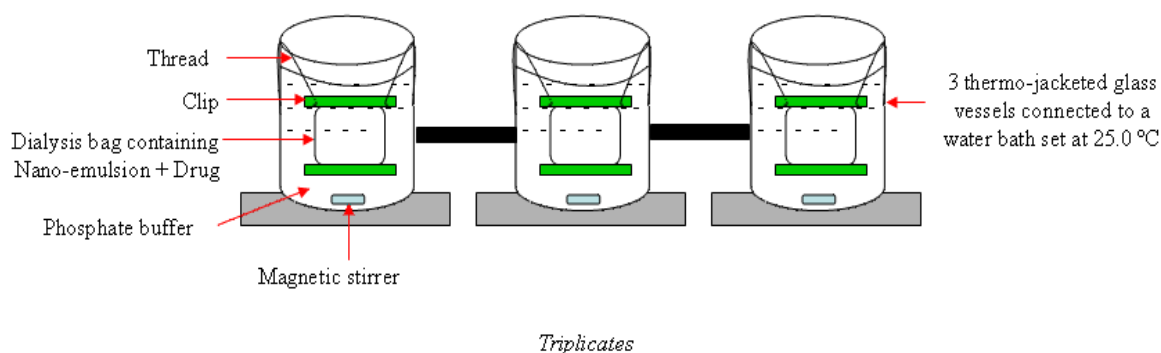


Figure 5.3: *In-vitro* drug release experiment (dialysis bag method).

5.4 INSTRUMENTATIONS

5.4.1 3D-Photon Correlation Spectrometer (3D-PCS)

The oil droplet radius of nano-emulsion was determined by dynamic light scattering (DLS) using a 3D-Photon Correlation Spectrometer from LS Instruments (Fribourg, Switzerland). The 3D-cross correlation technology allows the suppression of multiple scattering of turbid solutions. This instrument is equipped with a He-Ne laser (632.8 nm). Triplicate readings of 200 s were recorded at an angle of 90°. The radius was obtained by a manual exponential fitting of the first cumulant parameter. The measurement temperatures (25.0 °C and 37.0 °C) were maintained by a decaline bath, which match the refractive index of glass and therefore do not interfere with the measurement.

5.4.2 Cryogenic Transmission Electron Microscopy (Cryo-TEM)

A JEOL JEM-1400 Cryogenic Transmission Electron Microscope (Jeol LTD. Tokyo, Japan) with voltage acceleration of 80-200 kV was used for nano-emulsions imaging and droplet size determination. The images were recorded with a slow scan digital camera of Gatan 794 MSC 600HP or onto negatives for high-resolution analysis. The resolution for this measurement is 0.14 – 0.19 nm, while the magnification is 2000-3,000,000x. The FASTEM control system with R-X EDS INCA micro-analyzer was utilized for this purpose.

For samples preparation, 5.0 µL of the sample was deposited on a QUANTIFOIL® R 1.2/1.3 grid and the excess was eliminated with Whatman N°1 paper. The vitrification was done with a Cryo Preparation Chamber (CPC) from Leica by immersing the grid as fast as possible in liquid ethane. Then the frozen grids were stored in liquid nitrogen and transferred into a Cryo-holder that was kept at -180 °C.

5.4.3 Stability Analyzer

The stability of the nano-emulsion was studied using light backscattering technique. The light backscattering was performed with a TURBISCAN MA 2000 (France) equipped with a 850 nm laser and two detectors for recording backscattered light (135°), as well as transmission (0°) as shown in **Figure 5.4**. Backscattering was recorded as a function of sample height for 24 h. The detection head scanned the entire length of samples of about 65 mm.

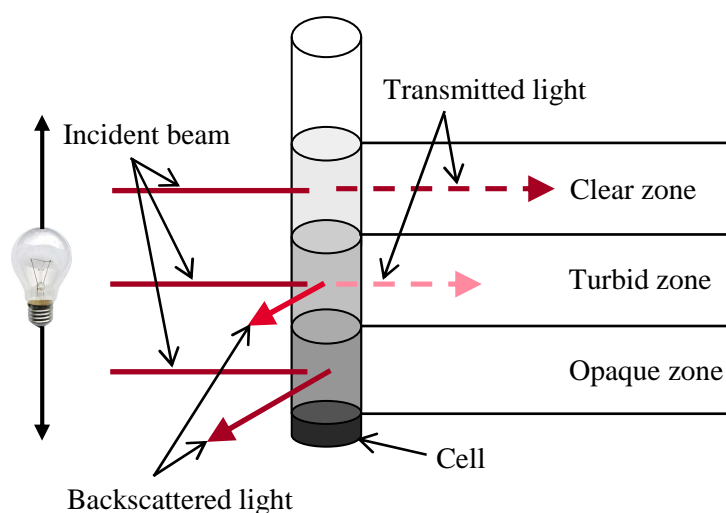


Figure 5.4: Turbiscan operating principle.

5.4.4 High-Pressure Liquid Chromatography (HPLC)

The concentration of released ketoprofen was determined using HPLC. The chromatographic system consisted of a UV detector set at 260 nm wavelength and connected to a Waters 1500 Series HPLC pump equipped with a 5 mm x 15 cm x 0.46 cm Spherisorb ODS column (**Figure 5.5**). Ketoprofen analysis was carried out at room temperature with a 6:4 of methanol:water (v/v) mobile phase that was adjusted to a pH of 1.5 with *ortho*-phosphoric acid. 20.0 μL of sample was injected at a flux flow rate of 1 mL/min. The retention time was 8 min.

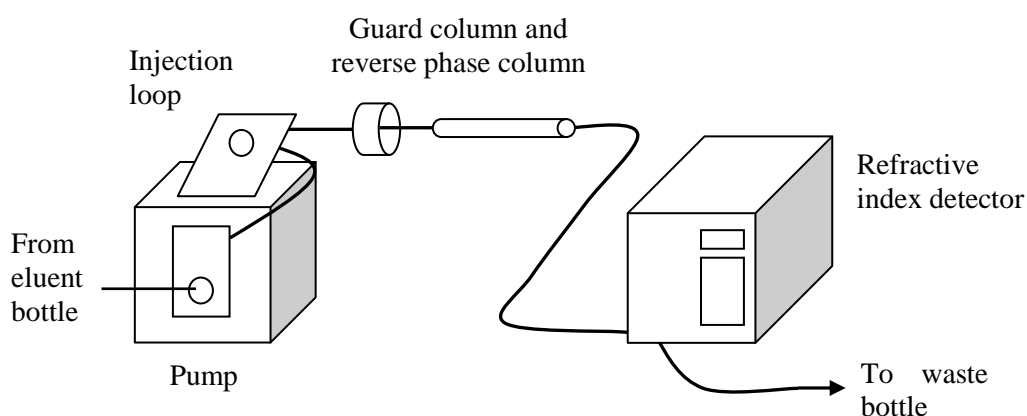


Figure 5.5: A schematic diagram of HPLC setup for drug release experiment.

5.5 RESULTS AND DISCUSSIONS

5.5.1 Formation of Nano-emulsion

Three samples of nano-emulsion were prepared at different ratios of water/non-ionic surfactants/oil mixtures by phase inversion composition (PIC) method and one of these is the reference system of water/Cremophor[®] EL/MCT oil. The other two mixtures contain this base reference system but with added 2-HDG and 2-HDM.

Nano-emulsion suitable for pharmaceutical application for oil soluble drug (lidocaine) was previously studied by Sadurní et al. [150]. Sadurni et al. reported nano-emulsion formation in the water/Cremophor[®] EL/MCT oil system at water contents above 50% with an oil-surfactant (O/S) ratios between 10/90 and 60/40. Although they have studied extensively this ternary system and produced its phase diagram, the present work confined the study to the region of phase diagram, which contain the nano-emulsion phase at a fixed high water content of 90 wt%. In order to arrive at the optimum formulation, the oil/surfactant ratio was varied and three formulations were prepared using O/S ratios of 60/40, 50/50 and 40/60. The nonionic surfactant used for these three compositions was Cremophor[®] EL. The nano-emulsion was prepared by stepwise addition of water and continuously stirring by means of a vortex mixer to previously homogenized oil/surfactant mixtures. By approximately 50 wt% of water added to all the three oil/surfactant mixtures (60/40, 50/50 and 40/60), transparent-bluish liquid dispersions appeared, indicating the presence of nano-emulsions at high water content region as shown in the phase diagram (**Figure 5.6**). However, upon further addition of water, the nano-emulsions with 60/40 and 50/50 of oil/surfactant ratio appeared more opaque/milky, while that of 40/60 appeared as translucent-bluish,

indicating the presence of nano-emulsion with smaller droplets size. A more opaque aspect usually indicates bigger oil droplet size and a resulting lower stability. Light scattering measurements with 60/40 and 50/50 of oil/surfactant ratio could not be performed due to the high opacity of the samples. Thus, oil/surfactant ratio of 40/60 was selected for further studies.

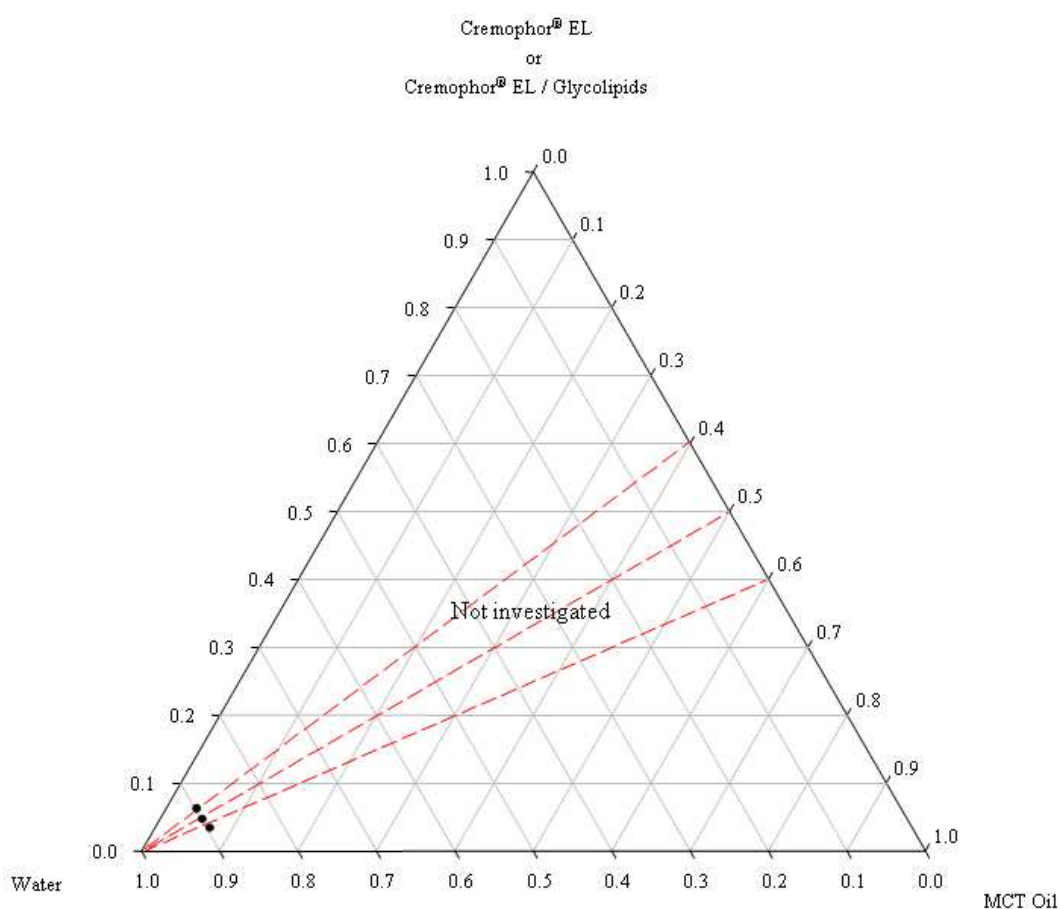


Figure 5.6: Pseudo-ternary phase diagram of water/Crem EL/MCT oil at 25.0 °C.

The effect of Crem EL/glycolipid weight ratio (from 95/5 to 70/30) on nano-emulsions with a 40/60 of oil/surfactant ratio was investigated as shown in **Table 5.1**. Similarly, the nano-emulsion formations were identified and their appearances were recorded. Consequently, nano-emulsions (from the translucent-bluish appearance) were found in the region of oil/surfactant ratio of 40/60 and Crem EL/Gly ratios of 95/5, 90/10, 85/15, 80/20 and 70/30. Following this identification, their droplet size and stability were further investigated by 3D-PCS, Stability Analyzer and Cryo-TEM.

Table 5.1: Summary of different mixing ratios between water/Crem EL/Gly/MCT oil at 25.0 °C. The branched-chain glycolipids used were 2-HDG and 2-HDM.

W / (O/S) Ratio	O/S Ratio	Crem EL/Gly Ratio	Physical Appearance
90/10	60/40	95/5	Opaque/Milky
90/10	60/40	90/10	Opaque/Milky
90/10	50/50	95/5	Opaque/Milky
90/10	50/50	90/10	Opaque/Milky
90/10	40/60	95/5	Translucent-bluish
90/10	40/60	90/10	Translucent-bluish
90/10	40/60	85/15	Translucent-bluish
90/10	40/60	80/20	Translucent-bluish
90/10	40/60	70/30	Translucent-bluish
90/10	40/60	60/40	Opaque/Milky
90/10	40/60	50/50	Opaque/Milky

Based on the preliminary observations, further investigations to determine their droplets sizes and stabilities were conducted for those nano-emulsions containing O/S ratio of 40/60, and Crem EL/Gly of 95/5, 90/10, 85/15, 80/20 and 70/30. The droplets size distribution of the nano-emulsions was determined by 3D-photon correlation spectroscopy. From dynamic light scattering (DLS) measurement, the droplets size distribution of MCT Oil/Crem EL (O/S) with ratio 40/60 was around 110 nm. It was significantly influenced by 2-HDG, showing an increase in size at low 2-HDG concentration. However, increasing 2-HDG concentration, decreased the size, where the smallest size observed at a Crem EL/2-HDG ratio of 85/15 which is around 70 nm (**Figure 5.7**). Finally, a further increase in 2-HDG (20 and 30 wt%) in the surfactant mixture, the size was increased again. It has to be mentioned that Crem EL/2-HDG nano-emulsions with a ratio of higher than 80/20 were not stable and destabilization was observed shortly after the preparation.

When using 2-HDM instead of 2-HDG, as the second surfactant, the emulsions appeared more turbid and its presence did not influence significantly the physical appearance and the droplets size of nano-emulsion for Crem EL/2-HDM up to the 80/20 ratio. The nano-emulsion droplets size obtained from O/S ratio of 40/60 and Crem EL/2-HDM of 85/15 was around 110 nm (**Figure 5.8**). At the ratio of 70/30 for Crem EL/2-HDM, the droplets size of the nano-emulsions increased rapidly after the preparation which can be attributed to their low stability due to the formation of bigger droplets size.

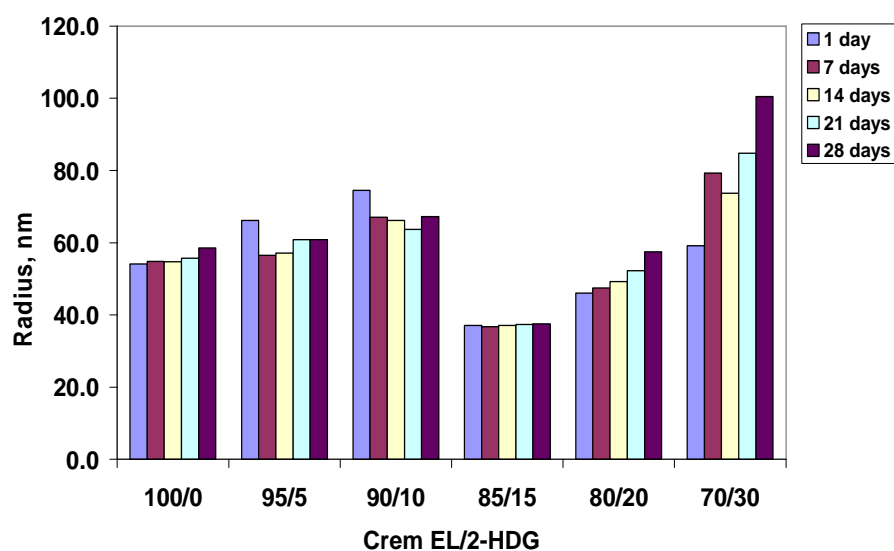
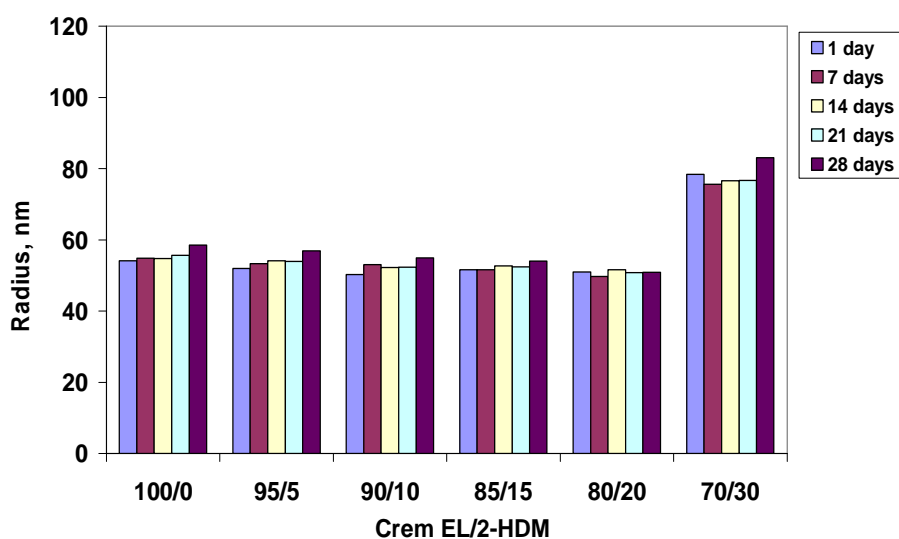


Figure 5.7: Comparison of nano-emulsion droplets radii between water/Crem EL/2-HDG/MCT oil to the reference system of water/Crem EL/MCT oil as a function of Crem EL/2-HDG ratios at 25.0 °C. Water content was fixed at 90 wt%, whereas the oil/surfactant ratio was selected at 40/60.



dilution = 20 wt% of nano-emulsion in water

Figure 5.8: Comparison of nano-emulsion droplets radii between water/Crem EL/2-HDM/MCT oil to the reference system of water/Crem EL/MCT oil as a function of Crem EL/2-HDM ratios at 25.0 °C. Water content was fixed at 90 wt%, whereas the oil/surfactant ratio was selected at 40/60.

5.5.2 Nano-emulsion Stability – Dynamic Light Scattering

Nano-emulsions with 85/15 ratio of Crem EL/Glycolipid (2-HDG/2-HDM) were chosen for further stability tests, based on the above results. Since a significant reduction of oil droplet radius could be observed from Crem EL/2-HDG nano-emulsion system, an increase in stability was expected. To investigate the influence of the branched-chain glycolipids on the nano-emulsion system, the effect of temperature during preparation and storage of the nano-emulsions was also tested.

The optimum nano-emulsions in term of lowest droplet size, with a 85/15 of Crem EL/Glycolipid ratio were therefore prepared at 25.0 °C and 70.0 °C. The storage temperature was fixed at room temperature (25.0 °C) and also at body temperature (37.0 °C) to study the suitability for pharmaceutical applications. 12 samples were prepared and their details (surfactants compositions, preparation and storage temperatures) are listed in **Table 5.2**. Further, the nano-emulsions droplets radii were determined by 3D-PCS (DLS) at 25.0 °C and 37.0 °C.

Table 5.2: Lists of nano-emulsion compositions as well as of their preparation and storage temperatures. Water content was fixed to 90 wt%, whereas the oil/surfactant ratio was 40/60 and the Crem EL/Glycolipid ratio was selected to be 85/15.

Nano-emulsion	T_{preparation}, °C	T_{storage}, °C	% Crem EL	% 2-HDG	% 2-HDM
1A	25	25	100		
1B	25	37	100		
1C	70	25	100		
1D	70	37	100		
2A	25	25	85	15	
2B	25	37	85	15	
2C	70	25	85	15	
2D	70	37	85	15	
3A	25	25	85		15
3B	25	37	85		15
3C	70	25	85		15
3D	70	37	85		15

The nano-emulsion systems were inspected visually and were found to possess translucent-bluish appearance. **Figure 5.9** shows **1A-1D**, **2A-2D** and **3A-3D** nano-emulsions at 1 day (24 hours), 1 week and 1 month of storage in water bath at 25.0 °C and 37.0 °C. As can be seen, the **2A-2D** nano-emulsions, which are based on Crem EL/2-HDG, are more translucent-bluish than those of nano-emulsions based on Crem EL only and Crem EL/2-HDM. The more translucent-bluish aspect usually indicates a smaller droplets size. The nano-emulsions became more turbid after 1 month storage time, which indicates an increase in droplets size. The higher the storage temperature (37.0 °C), the more turbid the samples became and therefore it is not

suitable for the Crem EL/2-HDG nano-emulsion. However, nano-emulsions based on Crem EL only and Crem EL/2-HDM were less affected in their physical aspects up to 1 month storage at 25.0 °C. They also became more turbid at higher storage temperature (37.0 °C) similar to those of Crem EL/2-HDG nano-emulsion.

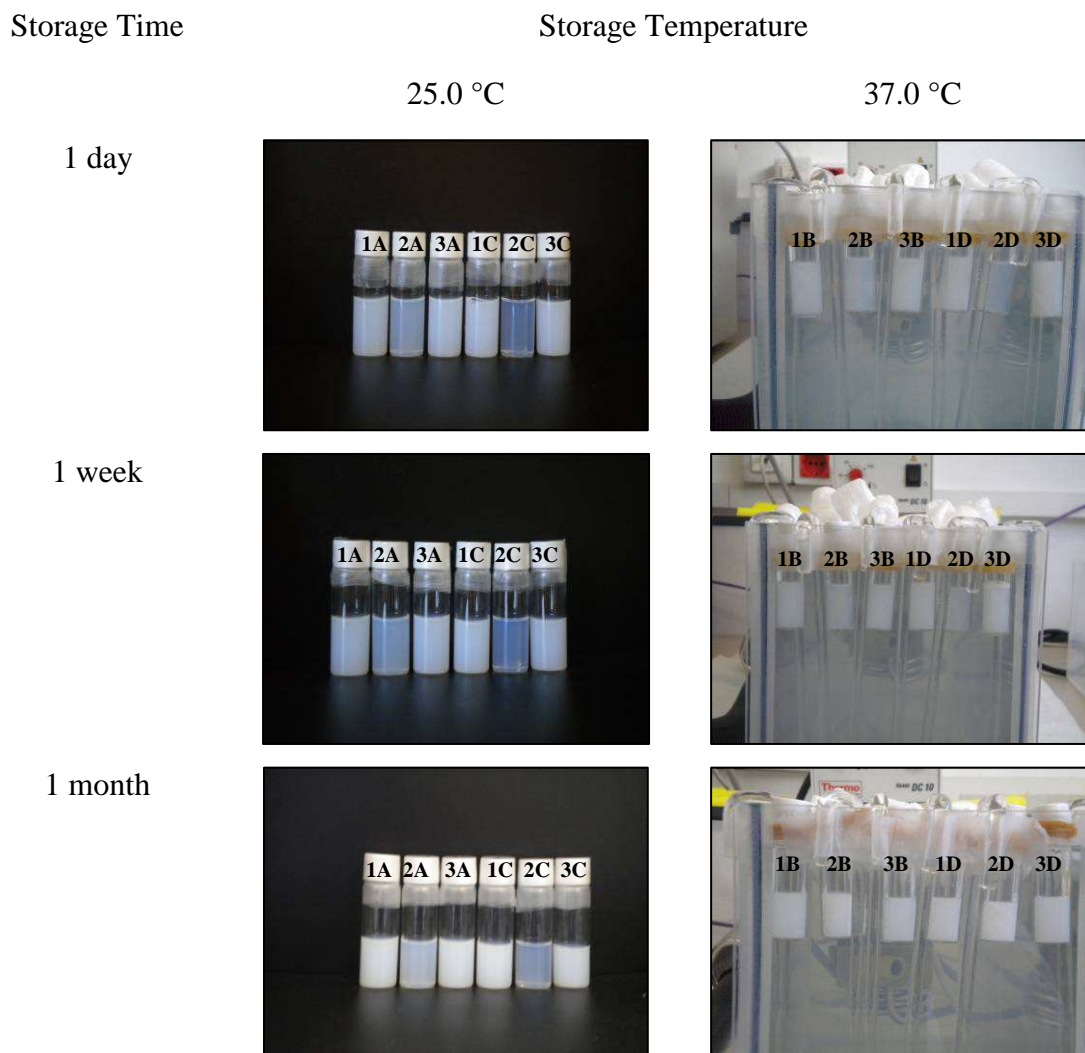
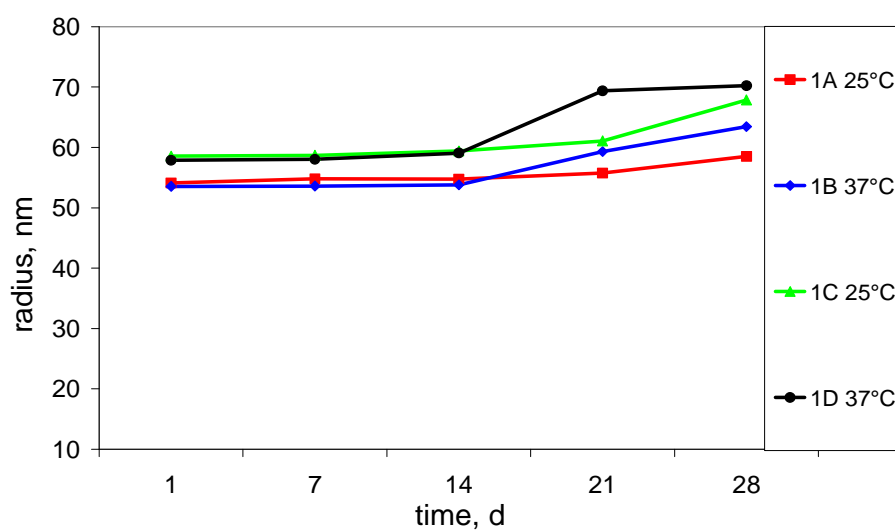
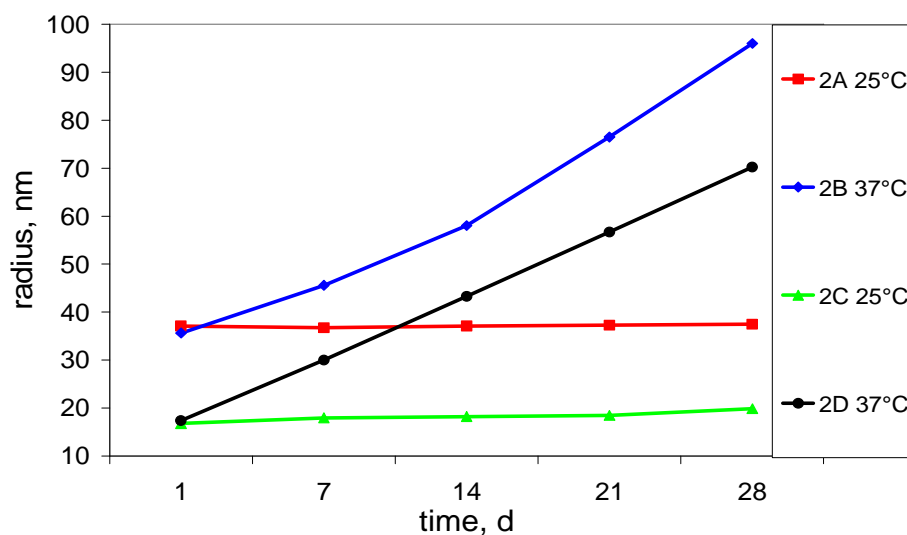


Figure 5.9: Nano-emulsions physical appearance of Crem EL only (1A-1D), 85/15 of Crem EL/2-HDG (2A-2D) and 85/15 of Crem EL/2-HDM (3A-3D) at 1 day, 1 week and 1 month of storage time in water bath at 25.0 °C and 37.0 °C. Refer to Table 5.2 for the nano-emulsion compositions.

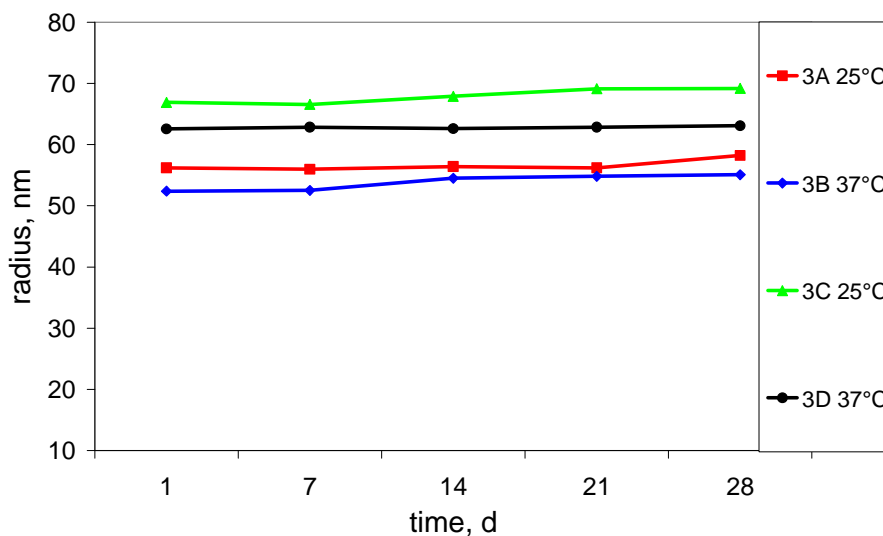
Subsequently, the nano-emulsions were studied quantitatively by dynamic light scattering (DLS) to determine their oil droplets radii as a function of times and to confirm the visual observations (**Figure 5.10**).



(a)



(b)



(c)

Figure 5.10: Nano-emulsion droplet radius (nm) of (a) Crem EL only (1A-1D), (b) 85/15 of Crem EL/2-HDG (2A-2D) and (c) 85/15 of Crem EL/2-HDM (3A-3D) as a function of storage time and temperatures of 25.0 °C and 37.0 °C. Preparation temperatures are 25.0 °C (A, B) and 70.0 °C (C, D). Refer to Table 5.2 for the nano-emulsion compositions.

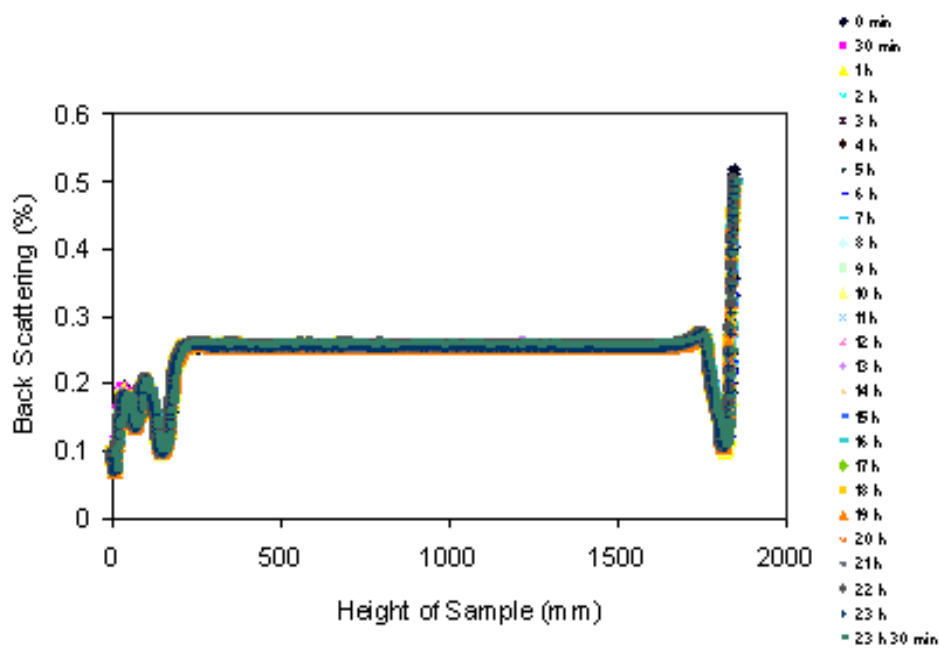
Figure 5.10 shows the oil droplet radius of (a) Crem EL, (b) Crem EL/2-HDG and (c) Crem EL/2-HDM nano-emulsions as a function of time for the two preparation temperatures (A, B: 25.0 °C and C, D: 70.0 °C) and the two storage temperatures (25.0 °C and 37.0 °C). The nano-emulsions of the reference system (**Figure 5.10a**), without glycolipid surfactant, were not significantly influenced either by the preparation or the storage temperature. After 14 days, a small increased of droplet radius could be observed in all nano-emulsions, being the most stable that was prepared at 25.0 °C and stored at 25.0 °C (1A).

Compared to the other nano-emulsion systems, Crem EL/2-HDG (**Figure 5.10b**) exhibited the smallest initial droplet radius. Moreover, we observed a significant temperature effect on the prepared nano-emulsions. Nano-emulsions prepared at 70.0 °C (2C-2D) possessed an initial oil droplet radius of about 15 nm, whereas those prepared at 25.0 °C (2A-2B) were twice bigger (35-37 nm). The storage temperature had also influenced on the stability of Crem EL/2-HDG nano-emulsions. The size of nano-emulsions stored at 25.0 °C (2A and 2C) did not change within the experimental observation period of 4 weeks, while the nano-emulsions stored at 37.0 °C (2B and 2D), showed a rapid increase in size. This might be because of 2-HDG is more lipophilic and does not stabilize the nano-emulsions at higher temperatures. Another possible explanation is due to the destabilizing effect of the surfactant layer at the water-oil interface at higher temperature. The thinner the surfactant layer, the easier the oil droplets can change the radius by Ostwald's ripening or coalescence mechanisms. However, due to small droplets size, the nano-emulsions are stable against creaming or sedimentation [14,18,122].

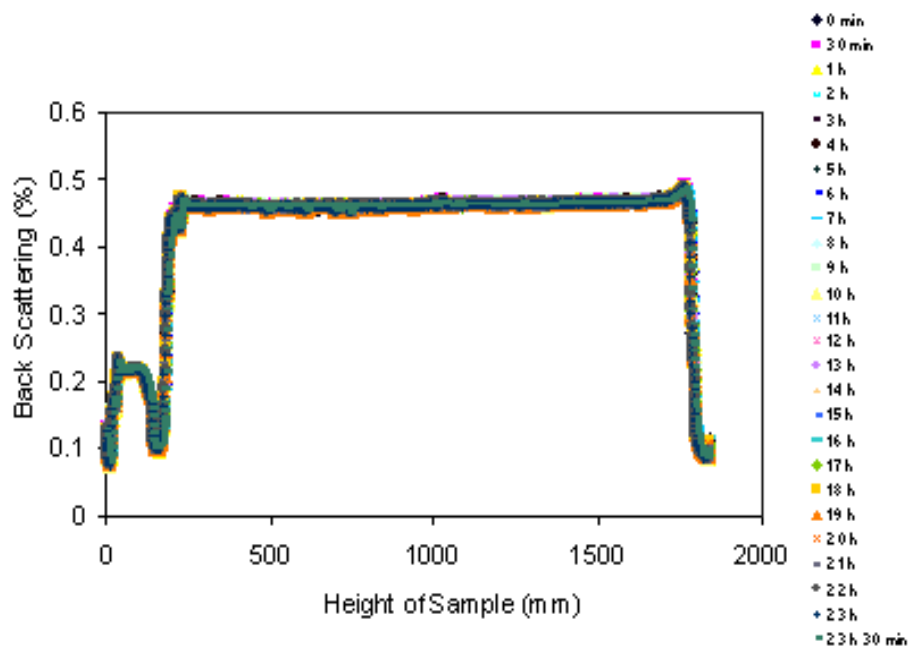
On the other hand, the droplet size and stability of Crem EL/2-HDM nano-emulsions (**Figure 5.10c**) are less dependent on preparation and storage temperatures, and these slightly increased within 4 weeks. Thus, Crem EL/2-HDM nano-emulsions are stable upon storage time. This might be due to the molecular properties of 2-HDM which is more polar (hydrophilic), and make the nano-emulsions more stable in any conditions in 90 wt% of aqueous medium. Nevertheless, the nano-emulsions prepared at 70.0 °C (3C-3D) gave slightly bigger droplet radius than those prepared at 25.0 °C (3A-3B) and a slight increase in size after 28 days was observed.

5.5.3 Nano-emulsion Stability – Light Backscattering

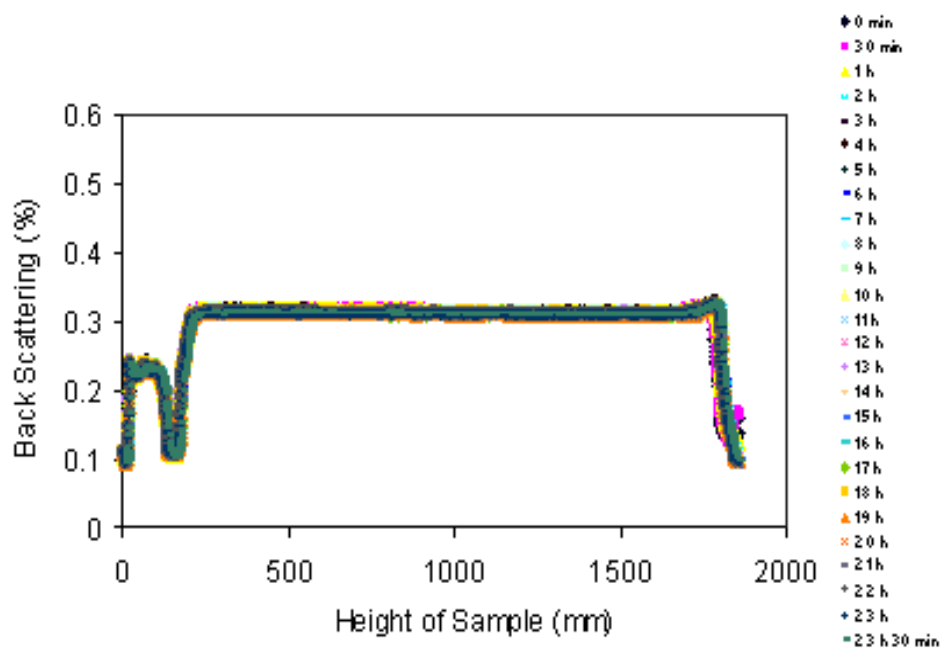
The stabilities of the three nano-emulsions prepared and stored at 25.0 °C were also investigated by light backscattering measurements (Turbiscan analysis). In all the three nano-emulsion samples, Crem EL only (1A), Crem EL/2-HDG (2A) and Crem EL/2-HDM (3A), the backscattering signal did not change during 24 h. **Figure 5.11** shows the backscattering measurement (in backscattering intensity, %) of (a) Crem EL nano-emulsion, (b) Crem EL/2-HDG nano-emulsion and (c) Crem EL/2-HDM nano-emulsion as a function of sample height. The fact that no changes could be observed implies that the droplets radius and droplets number did not change during 24 h. Moreover, since changes of the backscattered light intensity can be detected also for particle migration (creaming or sedimentation), which is not yet visible for the naked eye, the complete overlap of the backscattering curves in **Figure 5.10** over 24 h indicates a long term stability.



(a)



(b)



(c)

Figure 5.11: Back Scattering (%) of (a) Water/Crem EL/MCT oil, (b) Water/Crem EL/2-HDG/MCT oil and (c) Water/Crem EL/2-HDM/MCT oil nano-emulsions as a function of sample height (mm) at 25.0 °C. Data are given for different period of time up to 24 h. Water content was fixed at 90 wt%, whereas oil/surfactant ratio was 40/60 and Crem EL/Glycolipid ratio was 85/15.

For better visualization, the backscattering at a fixed sample height of 1000 nm was plotted as a function of time (**Figure 5.12**). The backscattering remained constant over the whole measurement period for all nano-emulsion systems. The differences in backscattering intensity can be explained by the differences in oil droplet size. Principally, backscattering uses multiple scattering. Therefore, the more particles are in the sample, the higher the backscattering intensity. The composition of the three nano-emulsions tested by light backscattering was identical except for the surfactant, and as mentioned above, the oil droplet size of Crem EL/2-HDG nano-emulsion is much smaller than the other two. Consequently, for the same oil volume fraction, the number of oil droplets must be higher for Crem EL/2-HDG nano-emulsion and indicated by the higher backscattering intensity. Therefore, the backscattering intensity in **Figure 5.12** confirms the results obtained by DLS. Indeed, there is no change in the physical appearance of all nano-emulsions samples after 24 h measurements as shown in **Figure 5.13**.

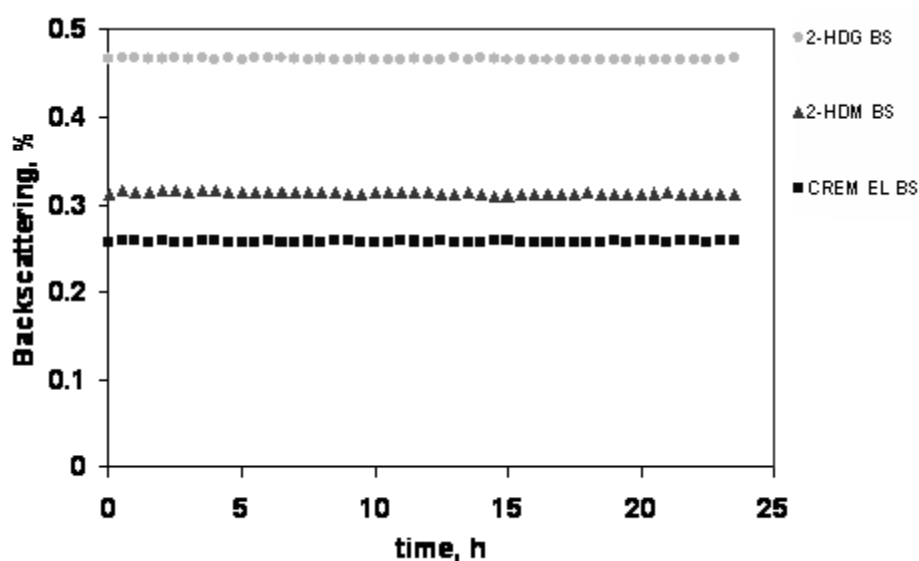


Figure 5.12: Backscattering (%) at a fixed sample height (1000 nm) of Crem EL (1A), Crem EL/2-HDG (2A) and Crem EL/2-HDM (3A) nano-emulsions as a function of measurement time.

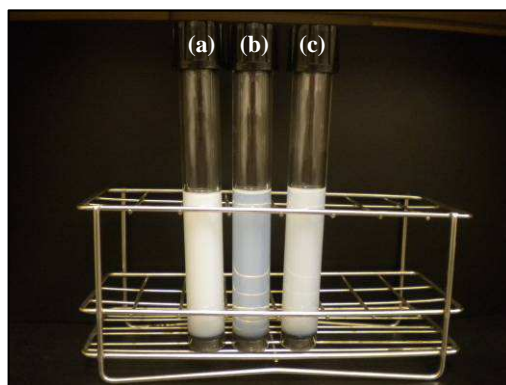


Figure 5.13: Nano-emulsion samples of (a) Water/Crem EL/MCT oil, (b) Water/Crem EL/2-HDG/MCT oil and (c) Water/Crem EL/2-HDM/MCT oil after 24 h measurements. Water content was fixed to 90 wt%, whereas oil/surfactant ratio was 40/60 and Crem EL/Glycolipid ratio was 85/15.

5.5.4 Nano-emulsion Characterization

Cryo-TEM micrographs were used for visualization of the nano-emulsions prepared and stored at 25.0 °C. **Figure 5.14** shows the electron micrographs and the corresponding size distribution obtained by statistical analysis of the nano-emulsions with Crem EL only (1A), Crem EL/2-HDG (2A) and Crem EL/2-HDM (3A). The mixed Crem EL/glycolipid ratio was 85/15. A more homogeneous character of the Crem EL/2-HDG (2A) nano-emulsion in comparison with the Crem EL (1A) and Crem EL/2-HDM (3A) nano-emulsions is observed. This is reflected by a narrower size distribution. In addition, the number of droplets in the Crem EL/2-HDG nano-emulsion seems to be higher than that in the Crem EL and Crem EL/2-HDM nano-emulsions, which is in agreement with the results obtained by light backscattering measurements.

The mean droplet radius of the nano-emulsion based on Crem EL only is about 12-13 nm, while those of Crem EL/2-HDG and Crem EL/2-HDM nano-emulsions are about 8-9 nm and 13-14 nm respectively. This reflects the same tendency of droplet radius obtained by light scattering. Crem EL/2-HDG nano-emulsion possessed the smallest oil droplets radii, whereas those of Crem EL and Crem EL/2-HDM nano-emulsions have nearly similar radii. Moreover, the size distribution of Crem EL nano-emulsion is wider than Crem EL/2-HDM. This explains the slightly lower long term stability, since higher polydispersity (wide distribution) enhances particles' agglomeration and Ostwald ripening process [186]. As expected, the mean oil droplets radii obtained from Cryo-TEM are smaller (**Figure 5.14**) compared to that obtained by dynamic light scattering (**Figure 5.10**). This is reasonable, since droplet sizes obtained from PCS measurements are hydrodynamic radii, i.e. the actual object radius plus a strongly bound water shell, which moves with the object through the bulk phase. As a consequence, the hydrodynamic radius measured by 3D-PCS is usually bigger than the actual radius observed by electron micrographs. Moreover, it cannot be excluded that the freezing of the sample, even rapidly performed (from an aqueous diluted state to a dried and highly concentrated state), shrank the oil droplets leading also to smaller droplets radii.

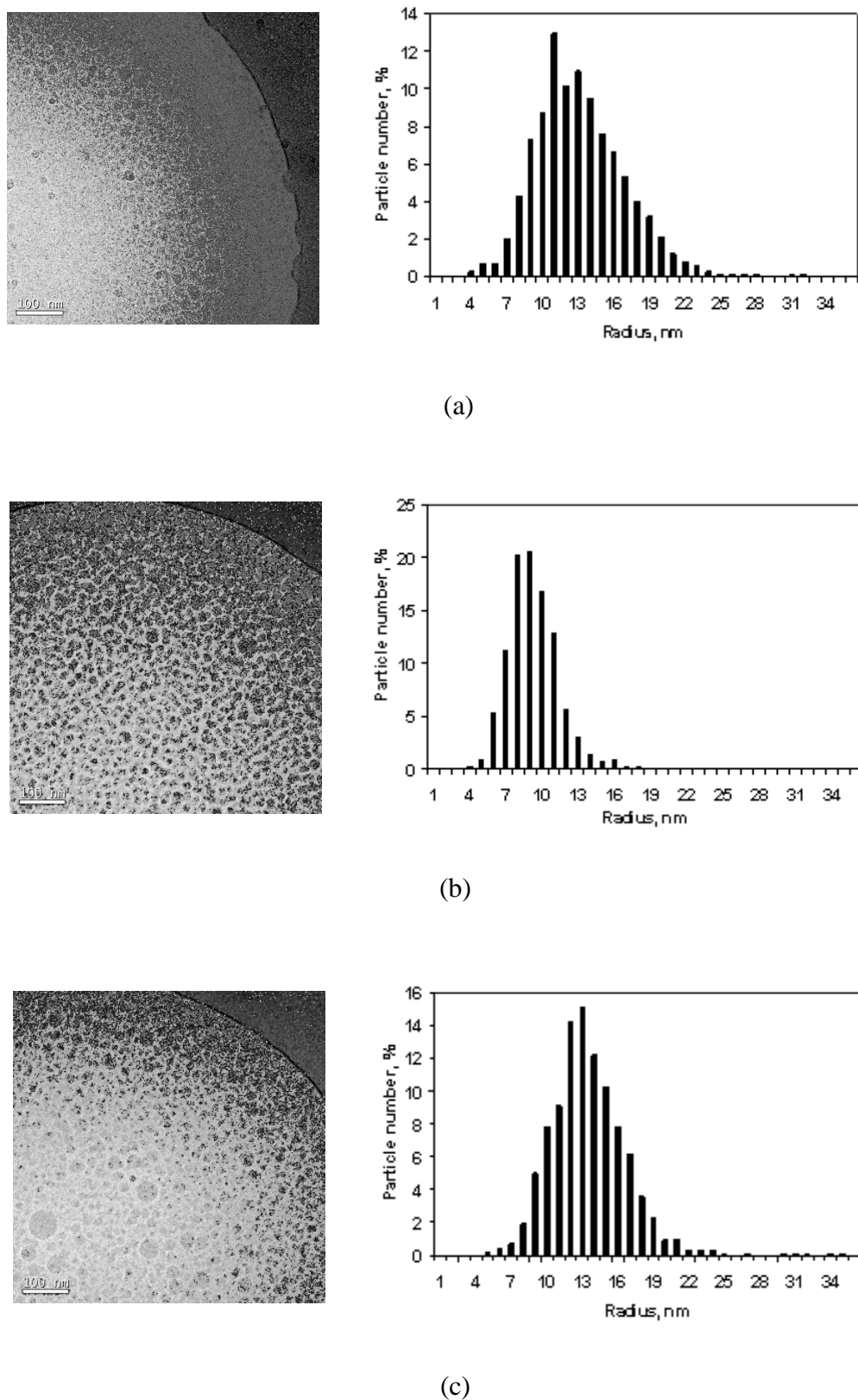


Figure 5.14: Nano-emulsion droplets size images under cryo-TEM and the size distributions of ternary (a) Water/Crem EL/MCT oil (b) Water/Crem EL/2-HDG/MCT oil and (c) Water/Crem EL/2-HDM/MCT oil at 25.0 °C.

5.5.5 Drug Delivery Study

5.5.5.1 Drug Incorporated-Nano-emulsion

The optimized percentage of drug incorporated was determined by the stability of drug in the nano-emulsion against precipitation. The amount of drug to be incorporated into nano-emulsion was chosen by taking into account the maximum solubility of drug in the dispersed phase and the accomplishment of sink conditions in the receptor solution during the release experiments. Accordingly, the amount of ketoprofen (KT) incorporated into the nano-emulsions was 0.50 wt% in the final composition. From observation, the drug was unstable in the nano-emulsion system and precipitated after few hours, when the percentage is higher than this amount.

5.5.5.2 *In-Vitro* Drug Release Study

The release of ketoprofen (KT) from the selected three nano-emulsions to the receptor solution was determined as a function of time during 24 h at 25.0 °C by dialysis bag method. Although dialysis membranes might influence the release behaviour of molecules [187-188], it is not likely to occur in this study, since the chosen membrane molecular weight cut-off is much higher (12,000-14,000 Da) than the molecular weight of ketoprofen (254.28 g mol⁻¹). Additionally, the pH of receptor solution was selected at pH 7.4 considering the pH of blood.

The release profiles of the ketoprofen from the medium chain triglyceride oil solution and those from three nano-emulsions are shown in **Figure 5.15**.

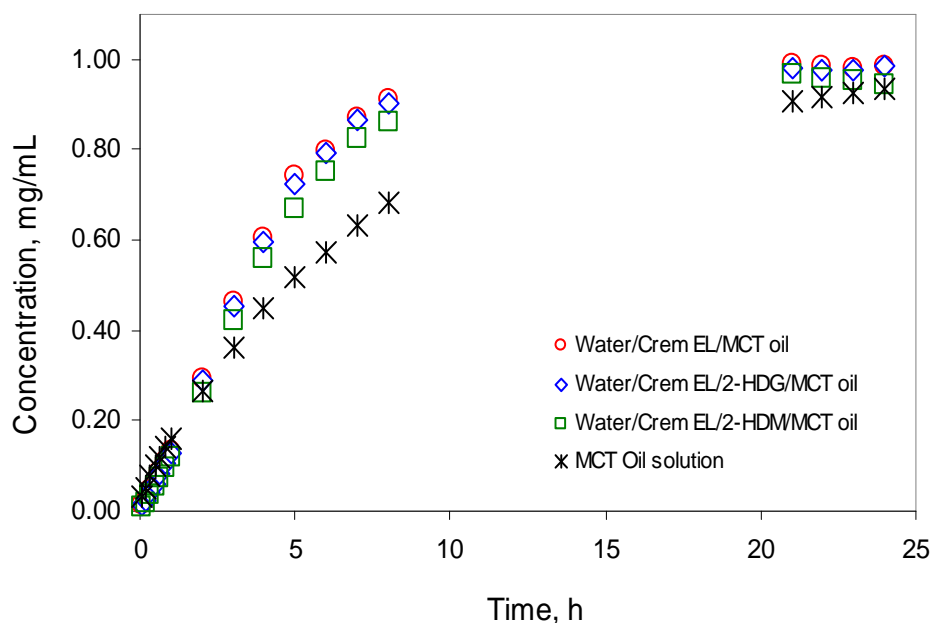


Figure 5.15: Release profile of ketoprofen from the MCT oil solution and from the three nano-emulsions: water/Crem EL/MCT oil, water/Crem EL/2-HDG/MCT oil and water/Crem EL/2-HDM/MCT oil as a function of time at 25.0 °C. The nano-emulsion composition was 90 wt% water content, whereas O/S and Crem EL/Glycolipid ratios of 40/60 and 85/15 respectively.

Three qualitative observations can be drawn from these release profiles. Firstly, at shorter times, the release profiles were approximately the same for all nano-emulsions and MCT oil solution. Secondly, the release of ketoprofen is faster from the nano-emulsions compared to from the MCT oil solution at longer times (from 3 h to 24 h). Thirdly, there is no significant difference in the release of drug between the three nano-emulsions. Hence, although these novel glycosides influenced the oil droplets size and enhanced the stability, they did not affect the drug release from the nano-emulsions.

Table 5.3 shows the amount of ketoprofen released after 24 h from the systems under studied. The release of ketoprofen was almost 100% by a fast mechanism from these nano-emulsions. Compared to the MCT oil solution, the release is faster and therefore is enhanced. As a consequence, these novel nano-emulsions can be considered as promising drug delivery systems, for oral or topical administration of drugs (anaesthetic or analgesic), where a fast response is required.

Table 5.3: Amount of ketoprofen (KT) released after 24 h.

System	KT Released (%)
Water/Crem EL/MCT oil	98.4
Water/Crem EL/2-HDG/MCT oil	98.6
Water/Crem EL/2-HDM/MCT oil	94.5
MCT oil solution	93.3

In order to understand the release mechanism, the experimental results were first compared with theoretical curves, using simulation based on Fick's second law. Neither the ketoprofen oil solution nor the nano-emulsion simulated values matched the experimental points, which indicate that the lipophilic drug does not release according to a pure Fickian diffusion but through a more complex drug transport mechanism.

Besides Fick's law, other mathematical functions were used, such as zero order [136-137] and first order [138-139] as well as Higuchi's law [140-141], Weibull [142-145] and Korsmeyer-Peppas models [146-149]. Examination of the linearization of the release curves with the above mentioned theories revealed that the best results were obtained with the Weibull's distribution function (**Table 5.4**). Determination coefficients, R^2 are higher than 0.98 and could be obtained for all three nano-emulsions.

Table 5.4: Determination Coefficients (R^2) of Weibull Model.

System	Replicate 1	Replicate 2	Replicate 3
MCT oil solution	0.99358	0.99724	0.99715
Water/Crem EL/MCT oil	0.98748	0.98472	0.98663
Water/Crem EL/2-HDG/MCT oil	0.98243	0.98510	0.98515
Water/Crem EL/2-HDM/MCT oil	0.98306	0.98290	0.98358

Weibull's distribution is based on an empirical model, not deduced from any kinetic fundamental and is related with drug dissolution kinetic properties. This model permits the characterization of the drug-release process through the shape parameter β obtained from the fitting of the experimental release results [142-145,188]. In this work the values of β were in the range of 0.75 – 1.01, which according to this model indicates a combined complex release mechanism, where other processes, in addition to diffusion, are also important.

5.6 CONCLUSIONS

The effect of two new synthetic branched-chain glycolipids (2-HDG and 2-HDM) on nano-emulsions of Water/Cremophor[®] EL/Medium chain triglyceride oil system was studied by replacing partially Cremophor[®] EL with the glycolipids. In summary, 2-HDG possesses a higher impact on droplet radius, leading to smaller droplets and higher stability at storage temperature of 25.0 °C than the reference system. On the other hand, 2-HDM slightly improved the properties of the reference nano-emulsion in terms of droplet size and storage time stability.

The release pattern for ketoprofen from nano-emulsions of the reference Water/Cremophor[®] EL/Medium chain triglyceride oil system to a receptor solution was not influenced by the presence of 2-HDG and 2-HDM. However, ketoprofen release was faster from all nano-emulsions compared to a standard medium chain triglyceride solution. Fast release is desirable for drugs, which are used for analgesic and antipyretic applications. Thus, these glycolipids stabilized nano-emulsions are interesting candidates for potential pharmaceutical applications.

CHAPTER 6:
CONCLUSIONS

6.1 CONCLUSIONS

The present PhD research describes the **Physico-chemical Characterization of Branched-chain Glycolipids for Drug Delivery System**, comprising four main research categories. The first is Synthesis of Branched-chain Glycolipids, the second Physico-chemical Characterization of Branched-chain Glycolipids, followed by Binary Phase Behaviour of Branched-chain Glycolipids/Water System towards Formation of Hexosomes and Vesicles, and finally, the Influence of Branched-chain Glycolipids on Ternary Nano-emulsion as Drug Delivery Systems.

Natural and synthetic glycolipids have drawn much attention due to their nonionic, non-toxic, biocompatible and biodegradable properties. Because of the high cost of producing pure natural glycolipids, synthetic substitutes are always in demand. Therefore, new nature-mimic branched-chain glycolipids were synthesized, namely 2-hexyldecyl- β /(α)-D-glucoside (2-HDG) and 2-hexyldecyl- β /(α)-D-maltoside (2-HDM), whose structures are closely related to glyceroglycolipids. Both 2-HDG and 2-HDM have identical carbon numbers in the hydrophobic chains (C_{16}) but differ in their head group polarity, thus differing also in hydrophilic-lipophilic balance (HLB).

2-HDG and 2-HDM are two new nature-like branched-chain glycolipids with interesting and rich phase behaviours. In a thermotropic study, the more hydrophobic surfactant 2-HDG was characterized by a columnar phase, whereas the more hydrophilic surfactant 2-HDM exhibited a smectic A phase. In a lyotropic study (from high to low water gradient), 2-HDG showed two phase transitions, namely isotropic phase (L) \rightarrow inverted hexagonal phase (H_{II}), whereas 2-HDM showed three phase transitions, namely isotropic phase (L) \rightarrow lamellar phase (L_{α}) \rightarrow smectic A phase (SmA). X-ray scattering confirmed the OPM results in which 2-HDG was characterized

by hexagonal phase in the dried and hydrated form, whereas 2-HDM exhibited a lamellar phase in the hydrated form.

In glycolipids/water dispersion, the more hydrophobic surfactant 2-HDG formed an inverted hexagonal liquid crystalline dispersion called hexosomes, whereas the more hydrophilic surfactant 2-HDM with more balanced hydrophilic-lipophilic properties formed lamellar liquid crystalline dispersion which led to the formation of multilamellar vesicles (MLVs). Additions of AOT and SDS to the 2-HDM dispersion induced the formation of unilamellar vesicles with higher stability.

In continuation, ternary phase behaviour was investigated. The behaviour of 2-HDG and 2-HDM in nano-emulsions of a ternary water/nonionic surfactant/oil system was studied with the inclusion of an active ingredient (ketoprofen). In this work, nano-emulsions were prepared by low energy emulsification method: phase inversion composition (PIC). The preparation method involve keeping the temperature constant, but changing the composition during the emulsification process. The effect of these two synthetic branched-chain glycolipids on the reference O/W nano-emulsion of Water/Cremophor[®] EL/Medium chain triglyceride oil system was studied by partially replacing Cremophor[®] EL with the glycolipids. As a result, the optimum nano-emulsion formulation with small droplet size and higher stability is the system with oil/surfactant and Cremophor[®] EL/Glycolipid ratios of 40/60 and 85/15 respectively in 90 wt% of water. 2-HDG possessed a higher impact on droplet radius, leading to smaller droplets and higher stability at storage temperature of 25.0 °C than in the case of the reference system. On the other hand, 2-HDM slightly improved the properties of the reference nano-emulsion in terms of droplet size and storage time stability.

The release pattern for ketoprofen from nano-emulsions of the reference Water/Cremophor[®] EL/Medium chain triglyceride oil system to a receptor solution was not influenced by the presence of 2-HDG and 2-HDM. However, ketoprofen release was faster from all nano-emulsions compared to a standard medium chain triglyceride solution. Fast release is desirable for drugs, which are used for analgesic and antipyretic applications. Thus, these glycolipids stabilized nano-emulsions are interesting candidates for potential pharmaceutical applications.

In conclusion, both branched-chain glycolipids not only provided alternative nonionic surfactants with rich phase behaviour and versatile nano-structures (hexosomes, vesicles and nano-emulsions), but also could be used as new drug carrier systems in the future and are also suitable as nano-emulsion stabilizing agents.

6.2 MOTIVATION FOR FUTURE WORK

Sugar-based surfactants have recently drawn much attention owing to their nonionic and bio-based surfactant properties [50] and of these glycolipids are amongst the most popularly used because they can be found in nature [51] or synthesized from cheap natural resources (e.g. APG) [53].

This future research is designed to synthesis branched-chain alkyl glycosides for surfactant functions [49] whose structures closely mimic many cell wall materials (e.g. ceramides). They are also designed to characterize the physico-chemical properties and binary and ternary phase behaviours for cosmeceutical and pharmaceutical applications. We will focus on several glycosides such as glucoside, galactoside, maltoside and lactoside.

A set of fundamental investigations can be conducted in order to understand their physico-chemical properties which are important in the formulation of hexosomes [87-88], cubosomes [87] nano-vesicles [159], nano-emulsions [122,150] and emulsion [4,189]. These include the measurements of their thermal properties, structural patterns and textures in thermotropic and lyotropic phases, critical aggregation concentrations (CAC), phase behaviours and their stability upon storage time for drug delivery applications.

This research will further explore the formation and stability of glycolipid emulsion creams. The kinetic stability of the emulsion systems will be assessed by measuring droplet size and rheological properties as a function of time. A unique feature and innovation important in cosmeceutic formulations (emulsion cream) is the appearance of the final product. This is measured not only by the performance of the active component, but also by the psychological impact (rheological properties) of the product on the consumer.

Besides, we will also further investigate the formation and the stability of nano-emulsions. In this research, nano-emulsions will be prepared by using low-energy emulsification methods. Two techniques will be applied, firstly by changing the compositions at a constant temperature (phase inversion composition) and second by changing temperatures at a constant composition (phase inversion temperature) [122,189]. The kinetic stability of the nano-emulsion systems will be assessed by measuring droplet size as a function of time.

For these reasons, this proposed research will synthesise technical grade branched-chain glycolipids and use them extensively in the formulation together with specialty materials for high-value applications such as drug delivery systems for cosmeceutical and pharmaceutical applications [4,12,150], where the surfactants are biocompatible, biodegradable, nonionic and non-toxic in nature.

REFERENCES

- [1] Fendler, J. H. *Chem. Rev.* **1987**, 87, 877-899.
- [2] Gelbert, W. M., Ben-Shaul, A., Roux, D. *Micelles, Membranes, Microemulsion and Monolayers*, Springer – Verlag, New York, **1994**.
- [3] Yoshikiyo, M. *Micelles: Theoretical and Applied Aspects*, Plenum Publisher, New York, **1992**, 7, 1st Edition, Chapter 2.
- [4] Evans, D. F. Wennerström, H. *The Colloidal Domain: Where Physics, Chemistry, Biology and Technology Meet*, Wiley-VCH Publication, New York, **1999**, 2nd Edition, Chapter 1.
- [5] Hunter, R. J. *Foundation of Colloid Science*, Oxford Science Publications, Oxford, **1991**, 2nd Edition.
- [6] Fendler, J. H. *Membrane Mimetic Chemistry: Characterizations and Applications of Micelles, Microemulsions, Monolayers, Bilayers, Vesicles, Host-guest Systems and Polyions*, John Wiley & Sons, New York, **1982**, 1st Edition.
- [7] Israelachvili, J. N. *Intermolecular and Surface Forces*, Academic Press Ltd, London, **1991**, 2nd Edition.
- [8] Lasic, D. D. *Liposome: From Physics to Application*, Elsevier Science Publishers, Amsterdam, **1993**, 1st Edition.
- [9] Apel, C. L., Deamer, D. W., Mautner, M. N. *Biochem. Biophys. Acta*, **2002**, 1559(1), 1-9.
- [10] McCormack, B., Gregoriadis, G. *J. Drug Targeting* **1994**, 2, 449-454.
- [11] Martins, L. M. S., Mamizuka, E. M., Camero-Ribeiro, A. M. *Langmuir* **1997**, 13(21), 5583-5587.
- [12] Attwood, D., Florence, A. T. *Surfactant System: Their Chemistry, Pharmacy and Biology*, Chapman and Hall, London, **1983**, 1st Edition.
- [13] Mukerjee, P., Mysels, K. J. *Critical Micelle Concentration of Aqueous Surfactant Systems*, National Bureau of Standard, Washington, **1975**, 1st Edition.
- [14] Mayer, D. *Surfaces, Interfaces and Colloids: Principle and Applications*, John-Wiley & Sons-VCH, New York, **1999**, 2nd Edition.

- [15] Griffin, W.C. *J. Soc. Cosmetic Chem.* **1949**, 1, 311-326.
- [16] Schott, H. *J. Colloid Interface Sci.* **1989**, 133(2), 527-529.
- [17] Stig, E., Friberg, P. B. *Microemulsion: Structure and Dynamics*, Boca Raton: CRC, **2000**.
- [18] Holmberg, K., Jönsson, B., Kronberg, B., Lindman, B. *Emulsions and Emulsifiers*, in *Surfactants and Polymers in Aqueous Solution*, John Wiley & Sons, Ltd, West Sussex, **2003**, 451-471.
- [19] Mayer, D. *Surfactant Science and Technology*, VCH, New York, **1992**, 2nd Edition.
- [20] Stegemeyer ed, H. *Topics in Physical Chemistry: Liquid Crystals*, Steinkopff Darmstadt Springer, New York, **1994**.
- [21] Collings, P. J., Hird, M. *Introduction to Liquid Crystal: Chemistry and Physics*, Taylor and Francis Ltd, London, **1997**.
- [22] Priestly, E. B., Wojtowicz, P. J., Sheng, P. *Introduction to Liquid Crystals*, Plenum Press, London, **1974**.
- [23] Baron, M. *Pure and Appl. Chem.* **2001**, 73, 845-895.
- [24] Brown, G. H., Wolken, J. J. *Liquid Crystals and Biological Structures*. Academic Press. New York, **1979**.
- [25] Hamley, I. W. *Introduction to Soft Matter: Polymers, Colloids, Amphiphiles and Liquid Crystals*, John Wiley and Sons Ltd., Chichester, **2000**.
- [26] Gray, G. W. *Thermotropic Liquid Crystals*, John Wiley and Sons, New York, **1987**.
- [27] Dierking, I. *Textures of Liquid Crystals*, Wiley-Vch Verlag, GmbH & Co. KGaA, Weinheim, **2003**.
- [28] Gray, G. W., Goodby, J. W. *Smectic Liquid Crystals: Textures and Structures*, Philadelphia, **1984**.
- [29] Seddon, J. M., Templer, R. H. *Polymorphism of Lipid-Water Systems In: Handbook of Biological Physics*, Lipowsky, R., Sachmann, E., Elsevier Science B.V. **1995**, 1.

- [30] Seddon, J. M., Robinz, J., Gullik-Krzywicki, T., Delacroix, H. *Phys. Chem. Chem. Phys* **2000**, 2, 4485-4493.
- [31] Mitchell, J. D., Ninham, B. W. *J. Chem. Soc., Faraday Trans 2* **1981**, 77, 601-629.
- [32] Israelachvili, J. N. *Intermolecular and Surface Forces*, Academic Press, New York, **1985**.
- [33] Israelachvili, J. N., Mitchell, D. J., Ninham, B. W. *J. Chem. Soc., Faraday Trans. 2* **1976**, 72, 1525-1568.
- [34] Tiddy, G. J. T., Walsh, M. F. *Lyotropic Liquid Crystals In: Aggregation Processes in Solution*, Wyn-Jones, E. and Gormally, J. (Eds.). Elsevier Science Publishing Co., Amsterdam, **1983**, 151-185.
- [35] Tiddy, G. J. T. *Phys. Reports* **1980**, 57(1), 1-46.
- [36] Winsor, P. A. *Chem. Rev.* **1968**, 68(1), 1-40.
- [37] Seddon, J. M. *Biochim. Biophys. Acta* **1990**, 1031, 1-69.
- [38] Barnes, H. A. *Detergents In: Rheometry Industrial Applications*, Walters, K. John Wiley and Sons (eds), New York, **1980**, 33-118.
- [39] Somasundaran, P., Wines, T. H., Metha, S. C., Garti, N., Farinato, R. *Emulsions and Their Behavior, in Surfactants in Personal Care Products and Decorative Cosmetics*, Rhein, L. D., Schlossman, M., O'Lenick, A., Somasundaran, P., CRC Press: New York, **2007**.
- [40] Blandamer, M. J., Briggs, B., Cullis, P. M., Engberts, J. B. F. N., Norman, R. I. *J. Chem. Soc. Faraday Trans.* **1996**, 92, 3163-3164.
- [41] Hoffmann, H., Ulbricht, W. *Recent. Res. Devel. In Physical Chem.* **1997**, 113-118.
- [42] Krog, N., Riison, T. H., Larsson, K. *Applications in the Food Industry: I*, In: *Encyclopedia of Emulsion Technology*. Becher, P. (ed), Marcel Dekker, New York, **1985**, 2, 321-365.
- [43] Larsson, K., Dejmek, P. *Crystal and Liquid Structures of Lipids*. In: *Food Emulsions*, Larsson, K., Friberg, S. E. (eds), Marcel Dekker, **1990**, 2nd Edition, 97-127.

- [44] Kim, H-H. Y., Baianu, I. C. *Novel Liposome Microencapsulation Techniques for Food Applications. Trends in Food Science and Technology* 2, **1991**, 55-61.
- [45] Pilpel, N., Rabbani, M. E. *J. Colloid Interface Sci.* **1987**, 119, 550-558.
- [46] Kabalnov, A., Tarara, T., Arlauskas, R., Weers, J. J. *J. Coll and Surf. Sci.* **1996**, 184, 227-235.
- [47] Vill, V., Hashim, R. *Curr. Opin. Colloid Interface Sci.* **2002**, 7, 395-409.
- [48] Hashim, R., Sugimura, A., Minamikawa, H., Heidelberg, T. *Liq. Cryst.* **2012**, 39(1), 1-17.
- [49] Hashim, R., Hashim, H. H. A., Rodzi, N. Z. M, Hussien, R. S. D., Heidelberg, T. *Thin Solid Films* **2006**, 509, 27-35.
- [50] Corti, M., Cantù, L., Brocca, P., Del Favero, E. *Curr. Opin. Colloid Interface Sci.* **2007**, 12, 148-154.
- [51] Holmberg, K. *Novel Surfactants: Preparation, Applications and Biodegradability*, Marcel Dekker, Inc., New York, **2003**, 2nd Edition.
- [52] Balzer, D., Lüders, H. H. *Nonionic Surfactants: Alkyl Polyglucosides*, Surfactant Science Series, Marcel Dekker, NewYork, **2000**, 91.
- [53] Hill, K., von Rybinski, W., Stoll, G., *Alkyl Polyglycosides: Technology, Properties and Applications*, VCH: Weinheim, **1997**.
- [54] Nilsson, F., Söderman, O. *Langmuir* **1996**, 12, 902-908.
- [55] von Minden, H. M., Brandenburg, K., Seydel, U., Koch, M. H., Garamus, V., Willumeit, R., Vill, V. *Chem. Phys. Lipids* **2000**, 106, 157-179.
- [56] Hato, M., Yamashita, I., Kato, T., Abe, Y. *Langmuir* **2004**, 20, 11366-11373.
- [57] Kitamoto, D., Toma, K., Hato, M. *Glycolipid-Based Bionanomaterials*. In: *Handbook of Nanostructured Biomaterials and Their Applications in Nanobiotechnology*, Nalwa, H. S., Ed., American Scientific: Los Angeles, **2005**, 1, 239-271.
- [58] Ahmad, N., Ramsch, R. Esquena, J., Solans, C., Tajuddin, H. A., Hashim, R. *Langmuir* **2012**, 28(5), 2395-2403.

- [59] Hussen, R. S. D. *PhD Thesis*; Department of Chemistry, Faculty of Science, University of Malaya, Kuala Lumpur, **2010**.
- [60] von Rybinski, W., Hill, K. *Angew. Chem. Int. Ed.* **1998**, *37*, 1328-1345.
- [61] Shah, J. C., Sadhale, Y., Chilukuri, D. M. *Adv. Drug Deliv. Rev.* **2001**, *47*, 229-250.
- [62] Boyd, B. J., Whittaker, D. V., Khoo, S. -M., Davey, G. *Int. J. Pharm.* **2006**, *318*, 154-162.
- [63] Lutton, E.S. *J. Am. Oil Chem. Soc.* **1965**, *42(12)*, 1068-1070.
- [64] Qiu, H., Caffrey, M. *Biomaterials* **2000**, *21*, 223-234.
- [65] Amar-Yuli, I., Garti, N. *Colloids Surf. B* **2005**, *43*, 72-82.
- [66] Larsson, K. *J. Dispers. Sci. Technol.* **1999**, *20(1-2)*, 27-34.
- [67] Nakano, M., Sugita, A., Matsuoka, H., Handa, T. *Langmuir* **2001**, *17(13)*, 3917-3922.
- [68] Nakano, M., Teshigawara, T., Sugita, A. et al. *Langmuir* **2002**, *18(24)*, 9283-9288.
- [69] de Campo, L., Yagmur, A., Sagalowicz, L., Leser, M. E., Watzke, H., Glatter, O. *Langmuir* **2004**, *20(13)*, 5254-5261.
- [70] Mannock, D. A., Collins, M. D., Kreichbaum, M., Harper, P. E., Gruner, S., McElhaney, R. N. *Chem. Phys. Lipids* **2007**, *148*, 26-50.
- [71] Misquitta, Y., Caffrey, M. *Biophys. J.* **2001**, *81*, 1047-1058.
- [72] Rappolt, M., Hickel, A., Bringezu, F., Lohner, K. *Biophys. J.* **2003**, *84*, 3111-3122.
- [73] Epand, R. M., Epand, R. F., Decicco, A., Schwarz, D. *Eur. J. Biochem.* **2000**, *267*, 2909-2915.
- [74] Briggs, J., Caffrey, M. *Biophys. J.* **1994**, *67*, 1594-1602.
- [75] Hartley, P. G., Alderton, M. R., Dawson, R. M., Wells, D. *Bioconjug. Chem.* **2007**, *18*, 152-159.

- [76] Fong, C., Wells, D., Krodkiewska, I., Weerawardeena, A., Booth, J., Hartley, P. G., et al. *J. Phys. Chem. B* **2007**, *111*, 10713-10722.
- [77] Kamo, T., Nakano, M., Leesajakul, W., Sugita, A., Matsuoka, H., Handa, T. *Langmuir* **2003**, *19*, 9191-9195.
- [78] Rappolt, M. *Planar lipid bilayers and liposomes* In: Leitmannova, A. *Elsevier Book Series*, The Netherlands, **2006**, *5*, 253-283.
- [79] Larsson, K. *Lipids - Molecular Organization, Physical Functions and Technical Applications*. Dundee, Scotland: The Oily Press, **1994**.
- [80] Gustafsson, J., Ljusberg-Wahren, H., Almgren, M., Larsson, K. *Langmuir* **1997**, *13*(26), 6964-6971.
- [81] Larsson, K. *Curr Opin Colloid Interface Sci* **2000**, *5*, 64-69.
- [82] Larsson, K. In: *Mesoporous Crystals and Related Nano-Structured Materials*, Proc. Symposium on Mesoporous Crystals and Related Nano-Structured Materials, Teraski, O., Stockholm, Sweden, 1–5 June 2004, Elsevier, **2004**, *148*, 41-51.
- [83] Hyde, S., Andersson, S., Larsson, K., Blum, Z., Landh, T., Lidin, S., et al. *The Language of Shape. The Role of Curvature in Condensed Matter: Physics, Chemistry, Biology.* , Elsevier book series, The Netherlands, **1997**.
- [84] Yaghmur, A., Laggner, P., Sartori, B., Rappolt, M. *PLoS ONE* **2008**, *3*(4), 2072.
- [85] Caffrey, M. *Curr. Opin. Struct. Biol.* **2000**, *10*(4), 486-497.
- [86] Yaghmur, A., Laggner, P., Zhang, S., Rappolt M. *PLoS ONE* **2007**, *2*(5), 479.
- [87] Yaghmur, A., Glatter, O. *Adv. Colloid Interface Sci.* **2009**, *147–148*, 333-342.
- [88] Amar-Yuli, I., Wachtel, E., Shoshan, E. B., Danino, D., Aserin, A. and Garti, N. *Langmuir* **2007**, *23*, 3637-3645.
- [89] Sagalowicz, L., Michel, M., Adrian, M., Frossard, P., Rouvet, M., Watzke, H. J., Yaghmur, A., de Campo, L., Glatter, O., Leser, M. E., *J. Microscopy*, **2006**, *221*(2), 110-121.
- [90] Drummond, C. J., Fong, C. *Curr. Opin. Colloid Interface Sci.* **2000**, *4*, 449-456.

- [91] Lopes, L. B., Collett, J. H., Bently, M. V. L. B. *Eur. J. Pharm. Biopharm* **2005**, *60*, 25-30.
- [92] Abraham, T., Hato, M., Hirai, M. *Biotechnol. Prog.* **2005**, *21*, 255-262.
- [93] Spicer, P. T., Hayden, K. L., Lynch, M. L., Ofori-Boateng, A., Burns, J. L. *Langmuir* **2001**, *17*, 5748-5756.
- [94] Barauskas, J., Johnsson, M., Johnson, F., Tiberg, F. *Langmuir* **2005**, *21*, 2569-2577.
- [95] Almgren, M., Edwards, K., Karlsson, G. *Coll. Surf., A: Physicochem. Eng. Asp.* **2000**, *174(1-2)*, 3-21.
- [96] Neto, C., Aloisi, G., Baglioni, P., Larson, K. *J. Phys. Chem. B*, **1999**, *103*, 3896-3899.
- [97] Monduzzi, M., Ljusberg-Wahren, H., Larsson, H. *Langmuir*, **2000**, *16*, 7355-7358.
- [98] Mariani, P., Rivas, E., Luzzati, V., Delacroix, H. *Biochem.* **1990**, *29*, 6799-6810.
- [99] Luzzati, V. *Curr. Opin. Struct. Biol.* **1997**, *7*, 661-668.
- [100] Caboi, F., Murgia, S., Monduzzi, M., Lazzari, P. *Langmuir* **2002**, *18*, 7916-7922.
- [101] Lopes, L. B., Ferreira, D. A., de Paula, D., Garcia, M. T. J., Thomazini, J. A., Fantini, M. C. A., et al. *Pharm. Res.* **2006**, *23*, 1332-1342.
- [102] Chung, H., Kim, J., Um, J. Y., Kwon, I. C., Jeong, S. Y. *Diabetologia* **2002**, *45(3)*, 448-451.
- [103] Angelova, A., Angelov, B., Papahadjopoulos-Sternberg, B., Ollivon, M., Bourgaux, C. *Langmuir* **2005**, *21*, 4138-4143.
- [104] Angelova, A., Angelov, B., Lesieur, S., Mutafchieva, R., Ollivon, M., Bourgaux, C., et al. *J. Drug Deliv. Sci. Technol.* **2008**, *18*, 41-45.
- [105] Bangham, A. D., Standish, M. M., Watkins, J. C. *J. Mol. Biol.* **1965**, *13*, 238-252.
- [106] Egelhaaf, S. U., Pedersen, J. S., Schurtenberger, PD Dr. P. *Prog. Colloid Polym. Sci.* **1995**, *98*, 224-227.

- [107] Ninham, B. W., Evan, D. F., Wel, G. J. *J. Phys. Chem.* **1983**, *87*, 5020-5025.
- [108] Talmon, Y., Evan, D.F., Ninham, B.W. *Science* **1983**, *221*, 1047-1048.
- [109] Morigaki, K., Walde, P., Misran, M., Robinson, B. H. *Coll. Surf., A: Physicochem. Eng. Asp.* **2003**, *213*, 37-44.
- [110] Hargreaves, W. R., Deamer, D. W. *Biochem.* **1978**, *17*, 3759-3768.
- [111] Walde, P., Wessicken, M., Rädler, U., Berclaz, N., Conde-Frieboes, K., Luisi, P.L. *J. Phys. Chem. B* **1997**, *101*, 7390-7397.
- [112] Koynova, R., Tenchor, B. *Curr. Opin. Colloid Interface Sci.* **2001**, *6*, 277-286.
- [113] Scamehorn, J. F. *Phenomenon in Mixed Surfactant Systems, ACS Symposium Series 311*, ACS Press, Washington DC, **1986**.
- [114] Holland, P. M. In: *Mixed Surfactant Systems*, Holland, P. M., Rubingh, D. N. (Eds.), ACS Symposium Series, Am. Chem. Soc. Washington DC, **1992**, Chapter 2.
- [115] Kozlov, M. M., Andelman, D. *J. Colloid Interface Sci.* **1996**, *1*, 362-366.
- [116] May, S., Ben-Shaul, A. *J. Chem. Phys.* **1995**, *103*(9), 3839-3848.
- [117] Deli, G., Hatziantoniou, S., Nikas, Y., Demetzos, C. *J. Liposome Res.* **2009**, *19*, 180-188.
- [118] Desai, A., Vyas, T., Amiji, M. *J. Pharm. Sci.* **2008**, *97*, 2745-2756.
- [119] Watwe, R. M., Bellare, J. R. *Current Sci.*, **1995**, *68*(7), 715-724.
- [120] Hofland, H. E. J., Bouwastra, J. A., Gooris, G. S., Spies, F., Talsma, H., Junginger, H. E. *J. Colloid and Interface Sci.* **1993**, *161*, 366-376.
- [121] Minami, H., Inoue, T., Shimozawa, R. *J. Colloid Interface Sci.* **1994**, *164*, 9-15.
- [122] Solans, C., Izquierdo, P., Nolla, J., García-Celma, M. J. *Curr. Opin. Colloid Interface Sci.* **2005**, *10*, 102-110.
- [123] Shinoda, K., Saito, H. *J. Colloid Interface Sci.* **1968**, *26*, 70-74.
- [124] Shinoda, K., Saito, H. *J. Colloid Interface Sci.* **1969**, *30*, 258-263.

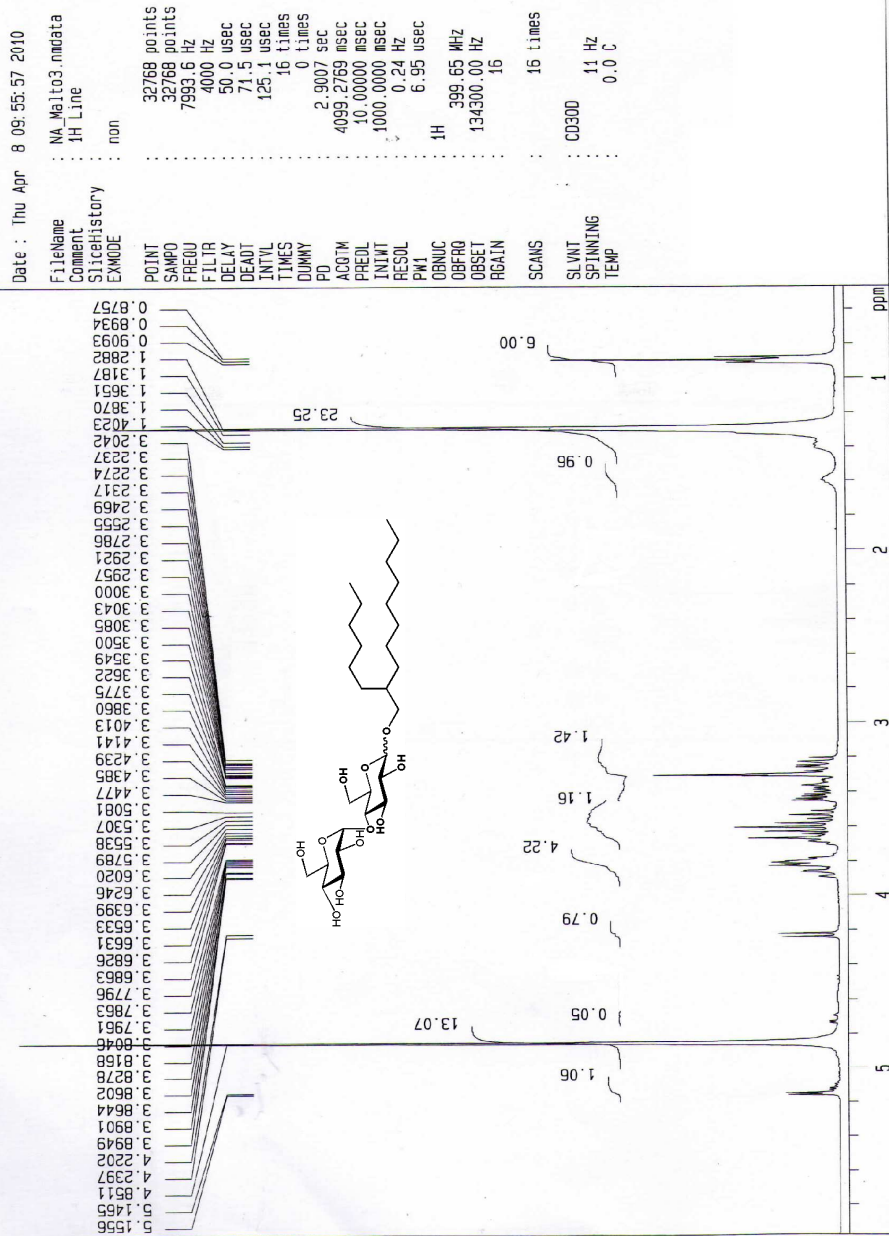
- [125] Gutiérrez, J. M., González, C., Maestro, A., Solè, I., Pey, C. M., Nolla, J. *Curr. Opin. Colloid Interface Sci.* **2008**, *13*, 245-251.
- [126] Tadros, T., Izquierdo, P., Esquena, J., Solans, C. *Adv. Colloid Interface Sci.* **2004**, *108-109*, 303-318.
- [127] Yang, H. J., Cho, W. G., Park, S. N. *J. Industrial Eng. Chem.* **2009**, *15*, 331-335.
- [128] Baluom, M., Friedman, D. I., Rubinstein, A. *Int. J. Pharm.* **1997**, *154*, 235-243.
- [129] Rubinstein, A., Tirosh, B., Baluom, M., Nassar, T., David, A., Radai, R., GlikoKabir, I., Friedman, M. *J. Controlled Release* **1997**, *46*, 59-73.
- [130] Calvo, P., Remuna Lopez, C., Vila Jato, J. L., Alonso, M. J. *Colloid Polym Sci.* **1997**, *275*, 46-53.
- [131] Sznitowska, M., Zurowska-Pryczkowska, K., Dabrowska, E., Janicki, S. *Int. J. Pharm.* **2000**, *202*, 161-164.
- [132] Hatanaka, J., Chikamori, H., Sato, H., Uchida, S., Debari, K., Onoue, S., Yamada, S. *Int. J. Pharm.* **2010**, *396*, 188-193.
- [133] Sonnevile-Aubrun, O., Simonnet, J. T., L'Alloret, F. *Adv. Colloid Interface Sci.* **2004**, *108*, 145-149.
- [134] Friedman, D. I., Schwarz, J. S., Weisspapier, M. *J. Pharm. Sci.* **1995**, *84*, 324-329.
- [135] Izquierdo, P., Wiechers, J. W., Escribano, E., Garcia-Celma, M. J., Tadros, T. F., Esquena, J., Dederen, J. C., Solans, C. *Skin Pharmacol. Phys.* **2007**, *20*, 263-270.
- [136] Donbrow, M., Samuelov, Y. *J. Pharm. Pharmacol.* **1980**, *32*, 463-470.
- [137] Varelas, C. G., Dixon, D. G., Steiner, C. A. *J. Controlled Release* **1995**, *34*, 185-192.
- [138] Gibaldi, M., Feldman, S. *J. Pharm. Sci.* **1967**, *56*, 1238-1242.
- [139] Wagner, J. G. *J. Pharm. Sci.* **1969**, *58*, 1253-1257.
- [140] Higuchi, T. *J. Pharm. Sci.* **1961**, *50*, 874-875.

- [141] Higuchi, T. *J. Soc. Cosmetic Chem.* **1960**, *11*, 85-97.
- [142] Langenbucher, F. *J. Pharm. Pharmacol.* **1972**, *24*, 979-981.
- [143] Costa, P., Manuel, J., Lobo, S. *Eur. J. Pharm. Sci.* **2001**, *13*, 123-133.
- [144] Kosmidis, K., Argyrakis, P., Macheras, P. *Pharm. Res.* **2003**, *20*, 988-995.
- [145] Schreiner, T., Schaefer, U. F., Loth, H. *J. Pharm. Sci.* **2005**, *94*, 120-133.
- [146] Korsmeyer, R. W., Peppas, N. A. *Macro-Molecular and Modeling Aspects of Swelling-Controlled Systems*. In *Controlled Release Delivery Systems*; Marcel Dekker, New York, **1983**.
- [147] Korsmeyer, R. W., Gurny, R., Doelker, E., Buri, P., Peppas, N. A. *Int. J. Pharm.* **1983**, *15*, 25-35.
- [148] Peppas, N. A. *Pharm. Acta Helv.* **1985**, *60*, 110-111.
- [149] Harland, R. S., Gazzaniga, A., Sangalli, M. E., Colombo, P., Peppas, N. A. *Pharm. Res.* **1988**, *5*, 488-494.
- [150] Sadurni, N., Solans, C., Azemar, N., Garcia-Celma, M. J. *Eur. J. Pharm. Sci.* **2005**, *26*, 438-445.
- [151] Kitamoto, D., Morita, T., Fukuoka, T., Konishi, M., Imura, T. *Curr. Opin. Colloid Interface Sci.* **2009**, *14*, 315-328.
- [152] Vill, V., Bocker, T., Thiem, J., Fischer, F. *Liq. Cryst.* **1989**, *6*, 349-356.
- [153] Goodby, J. W., Goërtz, V., Cowling, S. J., Mackenzie, G., Martin, P., Plusquellec, D., Benvegna, T., Boullanger, P., Lafont, D., Queneau, Y., Chambert, S., Fitremann, J. *Chem. Soc. Rev.*, **2007**, *36*, 1971-2032.
- [154] Mannock, D. A., Akiyama, M., Lewis, R. N., McElhaney, R. N. *Biochim. Biophys. Acta, Biomembr.* **2000**, *1509*, 203-215.
- [155] Hato, M., Minamikawa, H., Tamada, K., Baba, T., Tanabe, Y. *Adv. Colloid Interface Sci.* **1999**, *80*, 233-270.
- [156] Hato, M., Minamikawa, H., Seguer, J. B. *J. Phys. Chem. B* **1998**, *102*, 11035-11042.

- [157] Brooks, N. J., Hamid, H. A. A., Hashim, R., Heidelberg, T., Seddon, J. M. *Liq. Cryst.* **2011**, 38(11-12), 1725-1734.
- [158] Howe, J., von Minden, M., Gutschmann, T., Koch, M. H., Wulf, M., Gerber, S., Milkereit, G., Vill, V., Brandenburg, K. *Chem. Phys. Lipids* **2007**, 149, 52-58.
- [159] Mishra, A., Panda, J. J., Basu, A., Chauhan, V. S. *Langmuir* **2008**, 24, 4571-4576.
- [160] Soussan, E., Cassel, S., Blanzat, M., Rico-Lattes, I. *Angew. Chem., Int. Ed. Engl.* **2009**, 48, 274-288.
- [161] Hirlekar, R., Jain, S., Patel, M., Garse, H., Kadam, V. *Curr. Drug Deliv.* **2010**, 7, 28-35.
- [162] Gradzielski, M. *J. Phys. Condens. Matter*, **2003**, 15, 655-697.
- [163] Johnson, S., Bangham, A. *Biochim. Biophys. Acta (BBA) – Biomembr.* **1969**, 193, 82-91.
- [164] Johnson, S., Bangham, A., Hill, M., Korn, E. *Biochim. Biophys. Acta (BBA) – Biomembr.* **1971**, 233, 820-826.
- [165] Diat, O., Roux, D. *J. Phys. II* **1993**, 3, 9-14.
- [166] Gentile, L., Rossi, C. O., Olsson, U., Ranieri, G. A. *Langmuir* **2011**, 27, 2088-2092.
- [167] Bulut, S., Zackrisson Oskolkova, M., Schweins, R., Wennerström, H., Olsson, U. *Langmuir* **2010**, 26, 5421-5427.
- [168] Albino, J. D., Nambi, I. M. *Funct. Sens. Mater.* **2010**, 93-94.
- [169] Arutchelvi, J., Bhaduri, S., Uppara, P., Doble, M. *J. Industrial Microbiol. Biotechnol.* **2008**, 35, 1559-1570; 10.1007/s10295-008-0460-4.
- [170] Bednarski, W., Adamczak, M., Tomasik, J., Plaszczyk, M. *Bioresource Technol.* **2004**, 95, 15-18.
- [171] Brown, M. J. *Int. J. Cosmetic Sci.* **1991**, 13, 61-64.
- [172] Donnelly, M. J., Bu'Lock, J. D. *J. Chem. Technol. Biotechnol.* **1994**, 61, 187-195.

- [173] Faivre, V., Rosilio, V. *Expert Opin. Drug Delivery* **2010**, *7*, 1031-1048.
- [174] Franzetti, A., Gandolfi, I., Bestetti, G., Smyth, T. J. P., Banat, I. M. B. *Eur. J. Lipid Sci. Technol.* **2010**, *112*, 617-627.
- [175] Garti, N. *Coll. Surf., A: Physicochem. Eng. Asp.* **1999**, *152*, 125-146.
- [176] Imura, T., Morita, T., Fukuoka, T., Kitamoto, D. *Chem. – Eur. J. Microscopy* **2006**, *231*, 2434–2440; 231st National Meeting of the American-Chemical-Society, Atlanta, GA, March 26-30, 2006.
- [177] Kitamoto, D., Ghosh, S., Nakatani, Y. *Chem. Commun.* **2000**, *10*, 861-862.
- [178] Kitamoto, D., Isoda, H., Nakahara, T. *J. Biosci. Bioeng.* **2002**, *94*, 187-201.
- [179] Kralova, I., Sjoblom, J. *J. Dispersion Sci. Technol.* **2009**, *30*, 1363-1383.
- [180] Krasowska, A. *Postepy Hig. Med. Dosw.* **2010**, *64*, 310-313.
- [181] Tuleva, B., Christova, N., Cohen, R., Stoev, G., Stoineva, I. *J. Appl. Microbiol.* **2008**, *104*, 1703-1710.
- [182] Clogston, J. D., Patri, A. K. *Methods Mol. Biol.* **2011**, *697*, 109-117.
- [183] Hatziantoniou, S., Deli, G., Nikas, Y., Demetzos, C., Papaioannou, G. In: *Microscopy in Nanobiotechnology* Mozafari, M. R. Ed. *Micron.* **2007**, *38*, 819-823.
- [184] Yilmaz, E., Borchert, H.-H. *Int. J. Pharm.* **2006**, *307*, 232-238.
- [185] Yilmaz, E., Borchert, H.-H. *Eur. J. Pharm. Biopharm.* **2005**, *60*, 91-98.
- [186] Walkow, J. C., McGinity, J. W. *Int. J. Pharm.* **1987**, *35*, 91-102.
- [187] Clement, P., Laugel, C., Marty, J. P. *J. Controlled Release* **2000**, *66*, 243-254.
- [188] Papadopoulou, V., Kosmidis, K., Vlachou, M., Macheras, P. *Int. J. Pharm.* **2006**, *309*, 44-50.
- [189] Becher, P., *Emulsion (Theory and Practice)*, Reinhold, New York, **1966**, 2nd Edition, 2-36.

1H Line

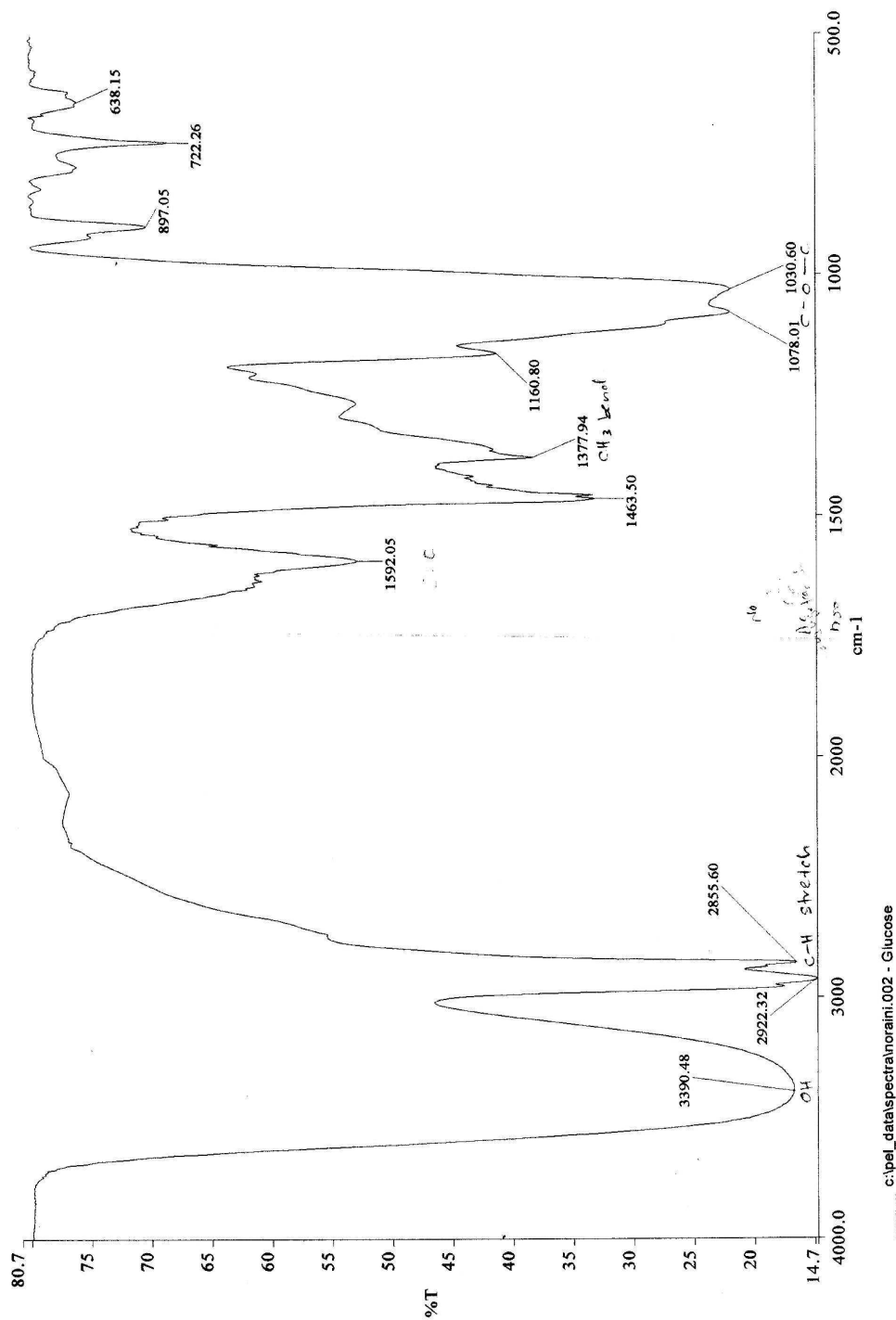


Date : Thu Apr 8 09:55:57 2010
FileName : NA_Malto3.mmdata
Comment : 1H Line
SliceHistory : non
EXMODE : non

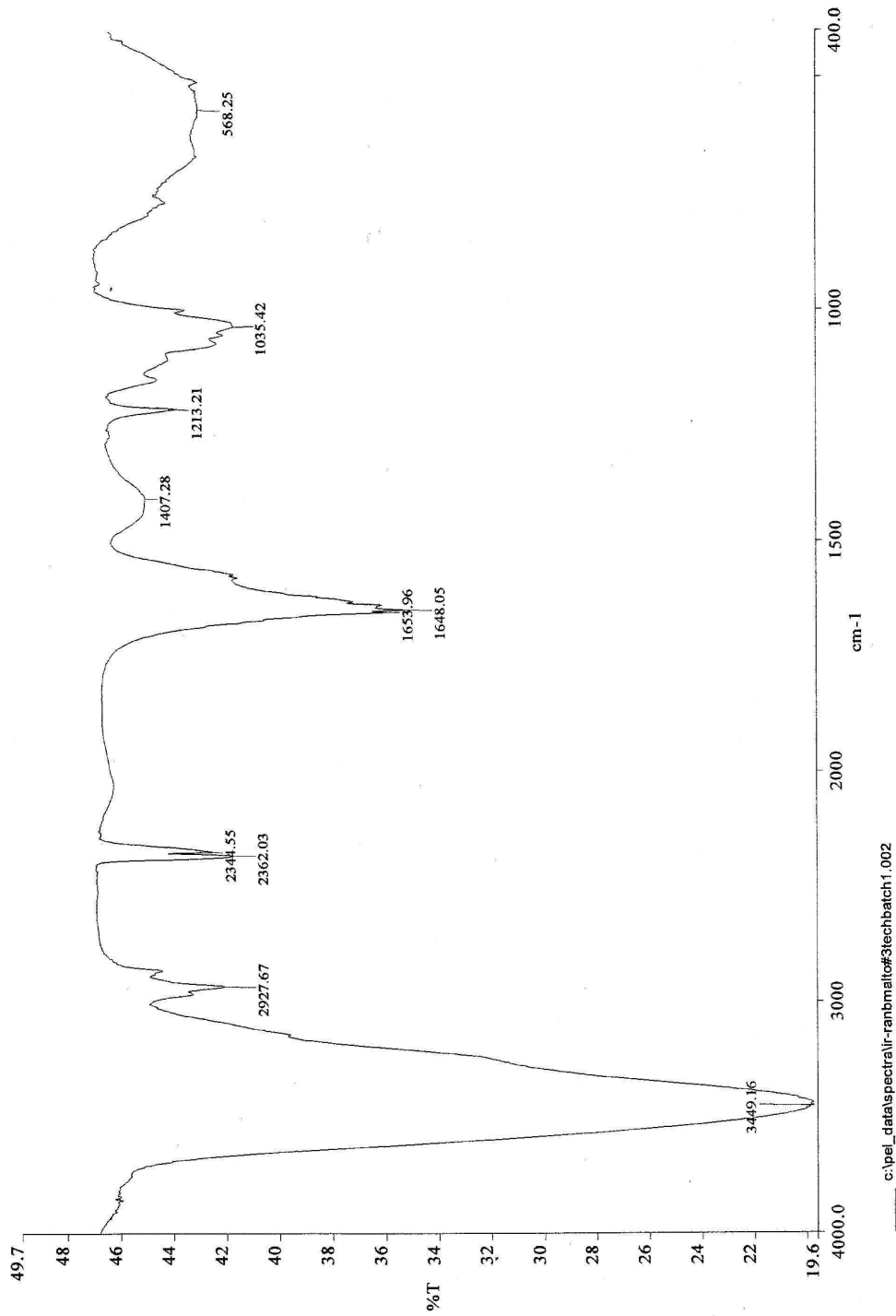
POINT : 32768 points
SAMPD : 32768 points
FREQD : 75933.6 Hz
FILTR : 4000 Hz
DELAY : 50.0 usec
DEADT : 71.5 usec
INYL : 125.1 usec
TIMES : 16 times
DUMMY : 0 times
PD : 2.9007 sec
ACQTM : 4099.2769 msec
PREDL : 10.00000 msec
ININT : 1000.00000 msec
RESOL : 0.24 Hz
PWI : 6.95 usec
ORNUC : 1H
OBFRO : 399.65 MHz
OBSST : 134300.00 Hz
RGAIN : 15
SCANS : 16 times
SLVNT : CD300
SPINNING : 11 Hz
TEMP : 0.0 C

$^1\text{H-NMR}$ spectrum of 2-hexyldecyl- $\beta(1-6)$ -D-maltoside

(B) FTIR Spectra



FTIR spectrum of 2-hexyldecyl- β /(α)-D-glucoside



c:\pel_data\spectra\ir-ranbmalco#3techbatch1.002

FTIR spectrum of 2-hexyldecyl- β /(α)-D-maltoside

APPENDIX 2

(A) PhD PUBLICATIONS

Journal Articles

1. Noraini Ahmad, Roland Ramsch, Jordi Esquena, Conxita Solans, Hairul Anuar Tajuddin, Rauzah Hashim, *Physico-Chemical Characterization of Natural-Like Branched-Chain Glycosides Towards Formation of Hexosomes and Vesicles*, *Langmuir*, **2012**, 28 (5), 2395–2403.
2. Ahmad, N., Ramsch, R., Llinas, M., Solans, C., Hashim, R. and Tajuddin, H. A., *Influence of Branched-Chain Alkyl Glycosides on Nano-Emulsions of a Ternary System for Pharmaceutical Applications*, *Colloid and Polymer Science*, **2012**, submitted.

Proceeding Papers

1. Noraini Ahmad, Roland Ramsch, Meritxell Llinàs, Conxita Solans, Rauzah Hashim and Hairul Anuar Tajuddin, *Influence Of Branched-Chain Glycolipids On Nano-Emulsion For Drug Delivery System*, *International Conference on Nanotechnology – Research and Commercialization (ICONT2011)*, **2011**.
2. Ramsch, R., Ahmad, N., Hashim, R., Tajuddin, H. A., Esquena, J., Solans, C., *Nature-Like Synthetic Glycolipids Exhibiting A Rich Phase Behavior*, *CED 41 Meetings – Detergency & Cosmetics*, **2011**.

(B) PROCEEDINGS OF CONFERENCE/SEMINAR/WORKSHOP

1. **Title** : Physico-Chemical Characterization of Hexosomes and Vesicles from Nature-Like Branched-Chain Glycolipids

Date : 27 May – 1 June 2012

Activity: Nanoformulation 2012 Conference (International)

Venue : Barcelona, Spain

Role : Poster presenter

2. **Title** : Characterization of Ternary Water/Oil/Branched-Chain Glycosides Systems for Pharmaceutical Applications

Date : 28 February 2012

Activity: Fundamental Sciences Of Self-Assembly Seminar 2012 (FSSA 2012) (International)

Venue : Chancellery Building, University of Malaya

Role : Poster presenter

3. **Title** : Influence of Branched-Chain Glycolipids on Nano-Emulsion for Drug Delivery System

Date : 13 October 2011

Activity: UM–A*STAR Meetings (International)

Venue : Jurong Island, Singapore

Role : Oral presenter

4. **Title** : Characterization of Ternary Water/Oil/Branched-Chain Glycosides
Systems for Pharmaceutical Applications
- Date** : 26 June – 1 July 2011
- Activity:** Nanoformulation2011 Conference (International)
- Venue** : Suntec City Convention Centre, Singapore
- Role** : Poster presenter
5. **Title** : Influence of Branched-Chain Glycolipids on Nano-Emulsion for Drug
Delivery System
- Date** : 6-9 June 2011
- Activity:** International Conference on Nanotechnology – Research and
Commercialization (ICONT2011) (International)
- Venue** : Kota Kinabalu, Sabah
- Role** : Oral presenter
6. **Title** : Physico-Chemical Characterization of Hexosomes and Vesicles from
Natural-Like Branched-Chain Glycolipids
- Date** : 30 May – 1 June 2011
- Activity:** Advanced Concepts and Applications on Functional Materials
Workshop (University)
- Venue** : Department of Chemistry, University of Malaya
- Role** : Oral Presenter

7. **Title** : Natural-Like Synthetic Glycolipids Exhibiting a Rich Phase Behavior
Date : 6-7 April 2011
Activity: CED 41 Meetings – Detergency & Cosmetics (International)
Venue : Barcelona, Spain
Role : Poster Presenter
8. **Title** : Branched Glycolipids – Biomimetic Amphiphilic Molecules for Promising Drug-Carriers
Date : 30 March – 1 April 2011
Activity: Colloid Workshop of COST Action D43 Functionalized Materials and Interfaces (International)
Venue : Universidad Complutense de Madrid, Spain
Role : Participant (Supervisor in Spain Presenting My Research as Oral Presenter)
9. **Title** : Physico-chemical Characterizations of Branched-chain Alkyl Glycosides Nano-structured for Pharmaceutical Applications
Date : 3 September 2010
Activity: Colloid and Interfacial Chemistry Group Seminar (International)
Venue : IQAC-CSIC, Barcelona, Spain
Role : Oral presenter

10. **Title** : Characterization of Branched-chain Glycosides for Nano-emulsion Applications
Date : 9-11 June 2010
Activity: Nanoformulations2010 Conference (International)
Venue : Stockholm University, Stockholm, Sweden
Role : Poster presenter
11. **Title** : Formulation of Branched-chain Alkyl Glycosides Emulsion
Date : 10 February 2010
Activity: Glycolipids Science and Technology Group Seminar (University)
Venue : Department of Chemistry, University of Malaya
Role : Oral presenter
12. **Title** : Branched-chain Glycoside in Ternary Water-Paraffin-Surfactant System
Date : 13-15 January 2010
Activity: InForm Connect 2010 Seminar (International)
Venue : Rimba Ilmu, University of Malaya
Role : Poster presenter
13. **Title** : Synthesis of Branched-chain Alkyl Glycosides
Date : 16 April 2009
Activity: Liquid Crystal Group Seminar (UM, USM and UTAR) (National)
Venue : Department of Chemistry, University of Malaya
Role : Oral presenter

(C) RESEARCH GRANT

Grant : Postgraduate Research Fund – *Peruntukan Penyelidikan Pascasiswazah (PPP)*, University of Malaya

Project number: PS242 / 2009A

(D) AWARD

Name of Award : Travel Grant to Participate Nanoformulation 2011
Conference, Singapore

Awarding Institution: Integrating Nanomaterials in Formulations (Inform),
European Union FP7

Award : Certificate and money

(E) ATTACHMENTS

- Program** : Researcher Exchange Programme

Host Institution : Instituto de Química Avanzada de Cataluña (IQAC)
Consejo Superior de Investigaciones Científicas (CSIC)

Host Country : Barcelona, Spain

Duration of Visit : 26 May – 9 June 2012

Sponsor/Financier: Integrating Nanomaterials in Formulations (InForm),
European Union FP7

2. **Program** : Overseas Research Programme
- Host Institution** : Instituto de Química Avanzada de Cataluña (IQAC)
Consejo Superior de Investigaciones Científicas (CSIC)
- Host Country** : Barcelona, Spain
- Duration of Visit** : 29 January – 3 April 2011
- Sponsor/Financier:** Ministry of Higher Education Malaysia (MOHE)
-
3. **Program** : Researcher Exchange Programme
- Host Institution** : Instituto de Química Avanzada de Cataluña (IQAC)
Consejo Superior de Investigaciones Científicas (CSIC)
- Host Country** : Barcelona, Spain
- Duration of Visit** : 3 May – 15 September 2010
- Sponsor/Financier:** Integrating Nanomaterials in Formulations (InForm),
European Union FP7